EVALUATION OF LASER EXCITED ATOMIC FLUORESCENCE SPECTROMETRY WITH GRAPHITE TUBE ELECTROTHERMAL ATOMIZERS AS AN ANALYTICAL TOOL FOR ULTRATRACE ANALYSIS

By

JORGE A. VERA

A DISSERTATION PRESENTED TO THE GRADUATE SCHOOL
OF THE UNIVERSITY OF FLORIDA IN PARTIAL FULFILLMENT
OF THE REQUIREMENTS FOR THE DEGREE OF
DOCTOR OF PHILOSOPHY

UNIVERSITY OF FLORIDA

1989

Dedicated to my wife, Nelly, and my son, Carlos David, for their love and support. In memory of my mother who will always be in my heart.

ACKNOWLEDGMENTS

I gratefully acknowledge the support of Dr. Benjamin Smith, Dr. Jose A. Lanauze, and Dr. Nicolo Omenetto, whose knowledge, enthusiasm, and helpful suggestions were a continuing source of inspiration.

I would like to thank the members of Dr. Winefordner's research group for their help and friendship. I wish to express my deepest appreciation to Dr. Moi Leong, Giuseppe Petrucci, Chris Stevenson, and Joe Simeonsson for their contribution to this work.

I would like to sincerely thank Dr. James D. Winefordner for his continual guidance and patient encouragement during the course of this work. It has been both a great learning experience and a great joy to work with such a distinguished and friendly individual.

TABLE OF CONTENTS

LIST OF TABLES

LIST OF FIGURES

Abstract of Dissertation Presented to the
Graduate School of the University of Florida in
Partial Fulfillment of the Requirements for
the Degree of Doctor of Philosophy

EVALUATION OF LASER EXCITED ATOMIC FLUORESCENCE SPECTROMETRY WITH GRAPHITE TUBE ELECTROTHERMAL ATOMIZERS AS AN ANALYTICAL TOOL FOR ULTRATRACE ANALYSIS

By

Jorge A. Vera

May, 1989

Chairman: James D. Winefordner
Major Department: Chemistry

Laser excited atomic fluorescence spectrometry combined with graphite tube electrothermal atomization is evaluated with respect to sensitivity and limits of detection. Three different pulsed, tunable dye laser systems are considered, in which the dye is pumped by an Nd:YAG laser, an N_2 laser and a Copper (Cu) vapor laser. Three spectrometric systems are studied and used to evaluate the analytical capabilities of the laser atomic fluorescence technique for the detection of lead. The fluorescence is excited and observed longitudinally in a graphite tube electrothermal atomizer. In addition, results are presented for the

determination of thallium, iridium, gallium, and iron. Finally, a comparison is given between the experimental detection limits obtained for lead and those calculated under the assumption that the limiting noise is due to the intrinsic error in the signal itself (intrinsic detection limit). It is shown that the detection limits obtained are greater than the calculated intrinsic ones by a factor ranging from 79 to 1.3×10^4, depending upon the laser system. Several approaches that can be used to improve the experimental detection limit for the laser fluorescence method are extensively discussed.

CHAPTER 1
INTRODUCTION

Our modern society has developed an increased need for the ultrasensitive determination of trace metals mainly due to the technological advances in the last two decades. Progress in materials science research over the past twenty years has led to the preparation and characterization of a variety of high purity materials. Compositional characterization of high purity materials is being carried out regularly by analyzing for impurities at parts per billion (ppb) to sub-ppb levels. In a continual effort to achieve lower detection limits, the analyst has been forced to contemplate more complex, costly and time-consuming techniques to achieve his goal. In addition to the needs of the high purity materials industry, there has been a realization of the importance of trace element chemistry in biological systems. This awareness has been stimulated by the rising concern in industrialized nations of man's impact on his environment and its biological effect on him. Also, in this area, the analytical chemist has been obligated to look for new techniques that will allow him to provide the

information that life scientists need to understand the beneficial or harmful effects of trace elements on the biochemistry of man.

Need for High Sensitivity Methods

In order to understand and justify the need for the development of new and extremely sensitive atomic spectroscopic methods, several examples could be presented. An excellent first example [1] comes from the study of the effect of impurities during the production of silicon solar-cells. The presence of such impurities can influence the properties of solar cells in a variety of ways, namely, (a) crystal growth can be perturbed resulting in defects, inclusions, precipitates or polycrystalline structure; (b) the bulk properties of silicon may be altered by electrically active impurity centers which reduce the minority-carrier diffusion length; and (c) impurities may induce contact degradation as well as contact interface degradation, series- or shunt-resistance effects. The elements that can be present as impurities include Al, B, C, Ca, Co, Mo, V, Zn, and others. The concentration of the impurities in the silicon melt ranges from 10^{12} atoms $\cdot$ cm^{-3} to values as high as 10^{17} atoms $\cdot$ cm^{-3} corresponding to required detection limits of from 0.02 parts per billion to 2000 parts per

billion [2, 3]. Another example of the need of extreme sensitivity comes from the production of optical glass fibers [4] where ultratrace concentrations of certain transition elements cause unacceptable attenuation of transmitted light. During the fabrication of these fibers, it is necessary to determine if metallic impurities are causative factors for the periodic production of high-loss fibers and to determine the maximum levels that can be tolerated without noticeable optical effects. Also, in this case, detection limits in the sub-parts per billion range are essential. Although it has been demonstrated that the need for elemental trace analysis in the biological materials field are almost completely covered with the development of graphite furnace-atomic absorption spectrometry, there are some instances in which ultrahigh sensitivity is certainly a must. For example, a toxicological study of thallium poisoning in rat brains [5] presented the need for a technique that will avoid the use of the preconcentration step required by a more conventional method.

All the examples given above have a common link; that is, the average sensitivity needed ranges from 1 part in 10^{10} to 1 part in 10^{13} or from 0.1 ng/g to 0.1 pg/g. A dissolution of 1 g of sample in 100 ml of solution to be

analyzed would then require the use of a method whose concentrational detection limit encompasses the range 1 pg/ml to 1 fg/ml. In addition, assuming that 1 mg of solid can be sampled with sufficient accuracy (assuming homogenous material), absolute detection limits from 0.1 pg to 0.1 fg (10^{-15} g) would be required [6]. Refer to Figure 1-1.

Taking a closer look to the offerings, in terms of detection limits of several atomic spectrometric techniques [7-10], indicates that, while the above mentioned upper limit is definitively approached for several elements by the technique of atomic absorption and atomic fluorescence with electrothermal atomization and atomic emission with the combination of inductively coupled plasma and mass spectrometry [11, 12] the lower limit is still far from being reached. As a result, the analyst is forced to contemplate other techniques, irrespective of complexity cost,and time consumption.

Laser-based atomic spectroscopic methods represent the only viable approach that will permit the analyst to cover the lower limit of concentrations with the added advantage of a very large increase in selectivity. The advent of laser sources, especially dye lasers, has set up the

Figure 1-1. Average Sensitivity Needed in Ultratrace Chemical Analysis.

Requirements:

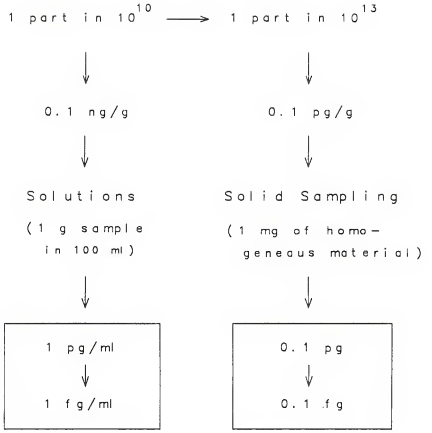

framework upon which the so called single atom detection (SAD) techniques have developed [13-16]. These techniques have been able to reach the ultimate goal of chemical analysis; that is, the detection of one single atom present in the observation region during a single probing interval [17, 18]. The concept of a single atom detection is a very restricted one in as much as it refers to the atoms in the probing region and not in the sample. Nevertheless, the utilization of laser-based approaches that may in principle achieve the SAD limit have been the road taken by many researchers in order to obtain increased sensitivity for the determination of trace elements even if one atom detection is not their final goal.

Classification of Detection Techniques

A broad but simple classification divides detection techniques into three main groups: viz., optical, electrical, and mechanical. Mechanical detection is based upon a change in the trajectory of motion of an atom as a result of its interaction with an optical field. This category encompasses laser-induced beam deflection technique [19, 20] and optoacoustic spectroscopy (OAS) [21]. While the former method seems rather exotic for analytical chemists, the latter has been shown to be primarily useful for the

determination of molecular species where the sensitivity, although impressive in some experiments performed, will always be limited by the typically low absorption cross sections of molecular spectral lines (see Figure 1-2).

Electrical detection techniques can be subdivided into optogalvanic, photoionization, and field ionization techniques. The optogalvanic effect can be defined as a perturbation of the state of ionization in a plasma in response to the absorption of optical radiation, which changes the relative level populations of atomic or molecular constituents of the plasma. Ionization from the laser-excited state is brought about by inelastic collisions with electrons or other particles in the plasma. When this approach is carried out in flames, the term laser-enhanced ionization spectroscopy (LEIS) is commonly used, and over the last twelve years several groups around the world [22-25] have been able to demonstrate the applicability of LEIS for trace-element analysis. A large increase in sensitivity could be obtained if a high-lying level from the ground state is excited by multistep process using multiple laser beams tuned at consecutive atomic transitions [24]. A more recent development is an attempt to observe LEIS using a graphite furnace atomizer [26], but the method seems to be limited mainly by

Figure 1-2. Laser Spectral Methods of Detection of Atoms.

(a) Absorption method based on light transmission measurement.

(b) Fluorescence method.

(c) Resonant deflection method.

(d) Stepwise resonant photoionization method.

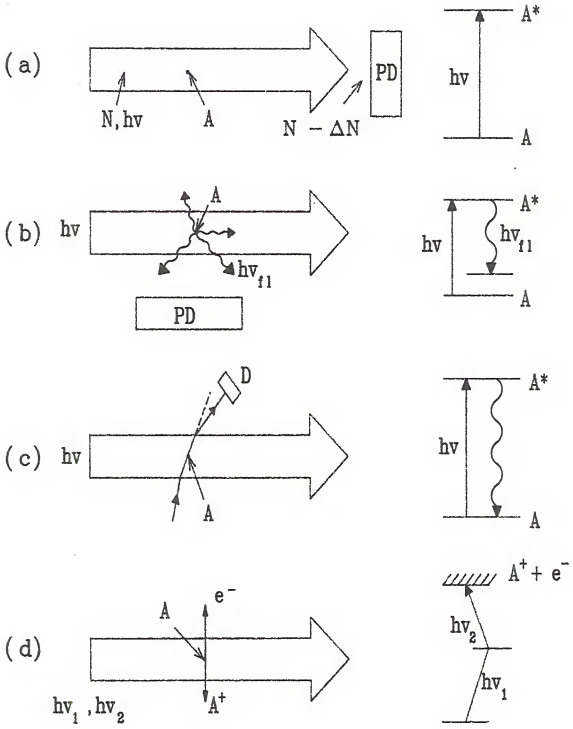
(a)
N, hν
A
PD
N − ΔN
A*
hν
A
(b)
hν
A
hν_f1
PD
A*
hν
hν_f1
A
(c)
hν
D
A
A*
hν
A
(d)
A
e⁻
hν_1 , hν_2
A⁺
A⁺ + e⁻
hν_2
hν_1

the thermionic emission from the heated graphite tube. All of the reported experiments in LEIS have shown that, even in the best cases, this technique will only reach the upper end of the concentrational detection limits range stated above.

In the photoionization technique, the atoms after being excited by absorption of one or more laser photons, with the same or different frequencies, are transferred to the ionization continuum by non-resonant absorption of another laser photon. This transfer may, occasionally, also proceed via an unstable autoionizing state excited by resonant photon absorption from a level below the ionization continuum. With this technique, collisions are not needed, and the presence of a buffer gas is not essential. In the field ionization technique, the atoms are first raised by a multistep or a multiphoton process to Rydberg or autoionization levels lying near the ionization continuum. Atoms in Rydberg levels have a long lifetime in the absence of quenching collisions. By applying a pulsed electric dc field shortly after the excitation pulse, the Rydberg atom can spontaneously ionize before it has a chance to decay to a lower-lying level. No additional energy is needed here in the ionization step. The autoionization process is brought about by the reduction of the potential energy experienced

by the excited valence electron when moving in a direction opposite to the electric field vector. Both photoionization and the field ionization technique work best with atomic beams in vacuo, as Letokhov [27, 28] and Hurst and Payne [29] have amply demonstrated. By using pulsed laser pumped dye lasers [Nitrogen (N_2), Neodymium:YAG (Nd:YAG) and Cu vapor lasers] to probe an atomic beam, produced by an electrothermal graphite or tantalum atomizer, via a multistep optical process, it is possible to determine traces of elements in the low parts per trillion range. A diverse number of applications have been reported where elements such as B, Ga, Yb, Rh, Ru and Al were determined. At the same time, it was shown that various research areas can benefit from the use of laser photoionization spectroscopy (LPIS), such as oceanography, cosmochemistry, geochemistry, and nuclear sciences, in addition to the already mentioned areas of high purity materials and biological materials. It is also worthy to note that recently a continuous wave (CW) pumped dye laser system [30, 31] was used for the determination of barium isotopes using a multistep resonance excitation scheme and an instrumental set-up very similar to the one used with pulsed laser systems. Although CW laser systems are limited by the wavelength range that they cover,

it is possible to achieve extreme sensitivity as shown in these cases where an instrumental detection limit of 10 ag was reported (see Figure 1-3).

Optical detection techniques include methods based on any optical phenomenon--such as fluorescence, absorption, stimulated emission, polarization, Raman scattering, birefringence, anomalous dispersion, and anomalous refraction--that can be induced or detected by laser radiation. Up to now, only fluorescence and absorption techniques have been capable of achieving the extreme sensitivity desired for ultratrace element analysis. Absorption methods (laser) are carried out by two main variants, intracavity absorption spectroscopy (ICAS) and saturated absorption spectroscopy. The former one consists of placing the absorption cell inside the dye laser cavity where laser photons pass a large number of times through the atomic vapor before they are coupled out. Meanwhile, in the latter approach, a pump laser (high intensity) is used to saturate an atomic transition and this saturation is monitored by absorption spectroscopy with a relative weak probe laser. Laser absorption techniques are limited mainly by fluctuations in the laser power and by the own nature of an absorption measurement where a very small signal is obtained from the difference

Figure 1-3. Comparison of Quantum Transition Schemes for (a) Resonant Photoionization Spectroscopy and (b) Optogalvanic Spectroscopy.

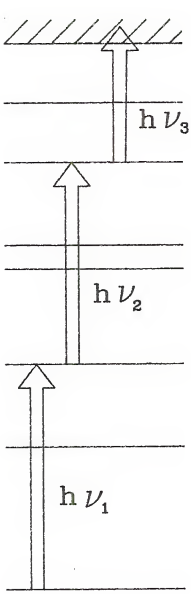

(a)

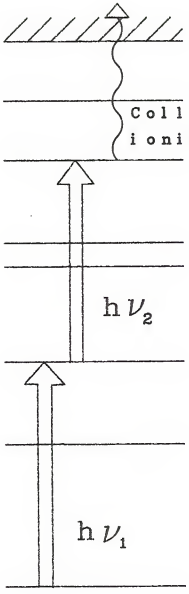

(b)

between two large signals.

Atomic fluorescence spectroscopy can be subdivided into resonance fluorescence (RF) and nonresonance fluorescence (NRF) techniques. The basic operation of these methods consists of the optical excitation of atoms to an excited state which subsequently undergo radiational deexcitation over a short period of time. If the frequency of the fluorescent photon is the same as the excitation frequency, it is called RF, or otherwise it is called NRF. The main practical advantage of using NRF instead of RF is that laser background scattering can be more easily rejected. The use of resonance fluorescence spectroscopy must face the problem of reducing laser background scattering. In order to improve detection efficiency, the analyst is forced to use CW pumped dye lasers because of their excellent beam collimation and increased duty factors, but their reduced range of wavelengths and their low efficiency for second harmonic generation (SHG) limits the number of elements that could be determined. So far, only a few experiments have been reported where RF was used. It is important to note that the main purpose of these previous studies was to achieve SAD; it is unlikely that they will be applicable to any kind of "dirty" chemical samples. Non-resonance atomic fluorescence

spectroscopy, especially when it is combined with electrothermal graphite atomizers, allows the analyst to carry out extremely sensitive determinations. This happens largely because pulsed laser pumped dye laser systems can now be employed, which bring about a distinct number of advantages. First, a large increase in source spectral irradiance which will allow saturation conditions in most cases; saturation means that the populations of an atom's upper and lower state are equalized, and as a result, the excited-state population is determined entirely by the atom's intrinsic properties and is relatively independent of the atomic environment. Second, a wide range of wavelengths can now be covered because of the several dyes that can be used and the use of the nonlinear methods such as second harmonic generation (SHG), sum frequency generation (SFG) and Raman shifting techniques. Third, temporal resolutions (narrow) could now be achieved. NRF does not present the rigorous baffling and alignment procedures related to RF experiments, and for this reason the possibility of using conventional small atom reservoirs, such as graphite furnace atomizers, now exist. A short review of the number of publications reported since 1973 reveals that the combination of laser excited atomic fluorescence spectroscopy (LEAFS) with electrothermal

atomization can certainly achieve limits of detection within the span needed for ultrahigh sensitivity [32-36].

Intent of Dissertation

The present work was intended to evaluate and characterize laser excited atomic fluorescence spectroscopy when used in combination with electrothermal graphite tube atomizers. Three different laser systems combined with different atomization and detection apparatuses were used to complete this evaluation.

CHAPTER 2
THEORETICAL CONSIDERATIONS

Atomic Fluorescence Spectroscopy Historical Background

The re-emission by an atom of radiation as fluorescence after the absorption of light from a suitable source was first reported in 1905 when Wood [37, 38] succeeded in exciting atomic fluorescence of the D lines of sodium vapor. He used an evacuated test tube containing sodium vapor as the atom reservoir and a gas flame containing sodium chloride as the illuminating source. Wood termed this fluorescence "resonance radiation" and the name is still encountered today for the atomic fluorescence of resonance lines such as the D lines. Similar work was carried out with other readily volatile elements, enclosed cells again being used to contain the atomic vapor, and was mainly concerned with fundamental studies of atomic spectra. This work has been described in some detail by Mitchell and Zemansky [39] and by Pringsheim [40].

The fluorescence of atoms in flames was first reported in 1923 by Nichols and Howes [41, 42] for calcium, strontium, barium, lithium and sodium in a Bunsen flame.

Similar observations were also reported by Badger [43] and by Mannkopff [44] for a number of other volatile elements. Further interest in the subject then appears to have lapsed until the use of atomic fluorescence spectrometry in 1956 by Boers, Alkemade, and Smit [45] to study quenching processes in flames. Following this, a further report was given by Alkemade [46] in 1962 on sodium fluorescence in flames together with the suggestion that it might have analytical possibilities. This suggestion was followed by Winefordner, Vickers and Staab [47-49], who reported the first successful analytical application of atomic fluorescence spectrometry with the determination of zinc, cadmium, and mercury. These initial studies were carried out using turbulent flames as atomizers and low intensity metal vapor discharge lamps as sources to produce atomic fluorescence. The atomic fluorescence was observed in those studies with a single channel, high luminosity, inexpensive monochromator-photomultiplier detector and dc electronic processing. Since those early studies, acetylene flames (separated and not-separated), chamber type nebulizers, electrothermal furnace atomizers, higher intensity sources, including electrodeless discharge lamps (EDL), pulsed and cw; hollow cathode discharge lamps (HCL), pulsed and cw; dye lasers, pulsed and cw;

multichannel TV image detectors; rapid scan spectrometers; and phase sensitive (lock in), boxcar, and photon counting measurement systems have been used. A more detailed discussion of the principles, methodologies, and applications of atomic fluorescence spectrometry is available in the monographs by Winefordner, Schulman, and O'Haver [50], Sychra, Svoboda, and Rubeska [51], and Kirkbright and Sargent [52]. In addition, a very large number of reviews covering this topic [53-69] have appeared in literature.

Absorption Process

The processes of atomic absorption that precede the evolution of atomic fluorescence are well documented and the theoretical principles of atomic absorption are well discussed in several excellent monographs, notably the comprehensive treatment of L'Vov [70] plus a review by Piepmeier [71] and various chapters in the monograph by Alkemade et al. [72]. The absorption process is, of course, quantized, and in fluorescence one has to bear in mind that the restriction of line-width in the source is not essential for fluorescence work as it is in absorption. Indeed some line broadening in the source-line to give a good fit over the entire profile of the absorption line of the atomic species is desirable since this allows the maximum energy to be

transferred to the atoms to be excited. The treatment, therefore, depends on the type of light source used (e.g., line-source or continuum). It also depends on the type of fluorescence that is being measured [73].

Fluorescence Transitions

There are four main types of atomic fluorescence, resonance, direct line, stepwise, and thermally assisted fluorescence. A fifth type, namely sensitized fluorescence, is when one atomic species is excited at the appropriate wavelength and transmits its energy to a second chemical species which thus becomes excited and emits its characteristic radiation subsequently. Since sensitized fluorescence is seldom used in analytical studies, it will not be discussed any further.

Resonance Fluorescence (Figure 2-1a) occurs when radiation of a given frequency ν_j excites an electron from its ground state E_o to an excited state E_j. Subsequently the excited electron transits back from E_j to E_o and emits energy of the same frequency ν_j. Thus, the excitation (absorbed) and the fluoresced energy have the same frequency (wavelength). Normally, a lesser number of photons are emitted than absorbed because of deactivating collisions undergone by the excited atom in the atom reservoir during

Figure 2-1. Types of Atomic Fluorescence.
(a) Resonance.
(b) Excited state resonance.
(c) Stokes direct-line.
(d) Excited state Stokes direct-line.
(e) Anti-Stokes direct-line.
(f) Excited state anti-Stokes direct-line.
(g) Stokes stepwise line.
(h) Excited state Stokes stepwise line.
(i) Anti-Stokes stepwise line.
(j) Excited state anti-Stokes stepwise line.
(k) Thermally assisted Stokes or anti-Stokes stepwise line (depending upon whether the absorbed radiation has shorter or longer wavelengths, respectively, than the fluorescence radiation).
(l) Excited state thermally assisted Stokes or anti-Stokes stepwise line (depending upon whether the absorbed radiation has shorter or longer wavelengths, respectively, than the fluorescence radiation).
(m) Sensitized (D = donor, D^* = excited donor, A = acceptor, A^* = excited acceptor, $h\omega_e$ = exciting radiation, $h\omega_f$ = fluorescence radiation.
(n) Two-photon excitation via a virtual level.
(o) Two-photon excitation via a real level.

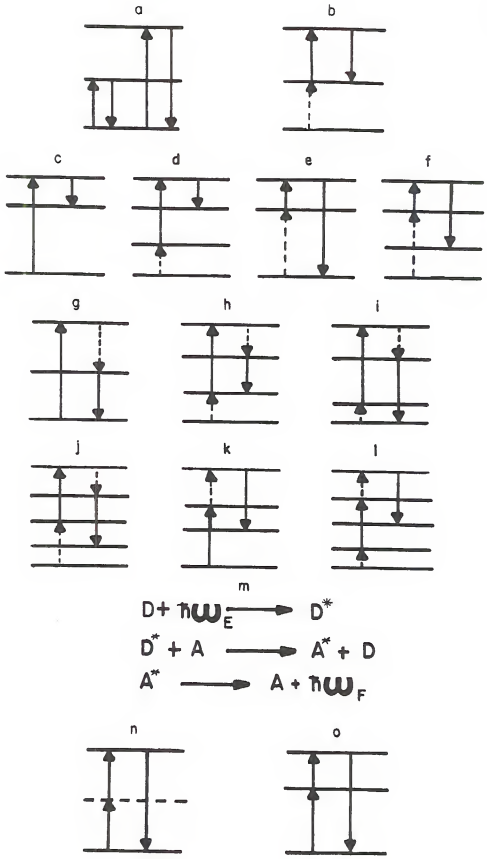
a
b
c
d
e
f
g
h
i
j
k
l
m
$D + \hbar\omega_E \longrightarrow D^*$
$D^* + A \longrightarrow A^* + D$
$A^* \longrightarrow A + \hbar\omega_F$
n
o

its lifetime. This diminution in the total quantity of energy is denoted by the quantum efficiency coefficient Y and is defined by

$$Y = \frac{\text{number of photons emitted, } s^{-1}}{\text{number of photons absorbed, } s^{-1}} \qquad (2.1)$$

Direct Line Fluorescence (Figure 2-1, c-f) involves a transition between a radiatively excited state E_j and an intermediate state E_i above the ground state E_o. Quite commonly E_i may be the first excited state. In the process, radiation of frequency ν_k is evolved. It is axiomatic that $\nu_k < \nu_j$ since less energy is involved in the intermediate transition than in the absorption one. In other words, the wavelength of the fluorescent line radiation is longer than that of the excitation line radiation.

This is particularly useful when dealing with analyte solutions that contain matrix material likely to cause scatter of source radiation or when source-induced scatter from the cell windows or atomizer walls has been observed by the detector.

Stepwise fluorescence (Figure 2-1, g-l) occurs when an atom is radiatively excited to a level (say) E_j from which

the electron passes to an intermediate level E_i by nonradiative processes after which it transits back to a lower (usually ground) state E_o by an emissive process involving fluorescence of energy of frequency ν_i. The nonradiative processes that take the electron from E_j to E_i commonly involve deactivation by collision with other entities in the atom reservoir or intersystem crossing. Again, it is apparent that $\nu_i < \nu_j$ because of the energy loss that has occurred by nonradiative processes in the production of the fluorescence.

Thermally assisted fluorescence (Figure 2-1, k-l) involves a component of nonradiative augmentation in the excitation process. The electron is promoted to an excited state E_j by absorption of radiation of frequency ν_i from the source. The electron is then further promoted to a nearby intermediate level E_j+ by "thermal" excitation from the flame or plasma. It then transits back to a lower level E_i by evolution of fluorescence of frequency ν_n.

Fluorescence Radiance Expressions

In the treatment that follows, it is assumed that the atom under consideration had only two levels (i.e., ground, 1, and first excited state, 2) excited states (the higher, 3, 4, . . . energy levels) are assumed not to influence the

population of state 1; the atoms are evenly distributed in the atomizer; the atomizer has a uniform temperature, T, and all species are in thermodynamic equilibrium; the light source radiation impinging upon the gaseous species does not affect the energy distribution, the velocity distribution, or the atomizer temperature; the analyte atoms are present as a trace component in the atomizer; the radiation density of the source is spatially uniform and constant while traversing the atomizer; and finally polarization and coherence effects are negligible.

The basic fluorescence radiance expression is given by

$$B_F = \left\langle \frac{l}{4\pi} \right\rangle \; Y_{21} \; E_{\nu_{12}} \int_0^\infty k_\nu d\nu \qquad (2.2)$$

where

l = path length in direction of detection system, m

4π = number of steradians in a sphere (fluorescence is isotropic), sr

Y_{21} = fluorescence power (quantum) efficiency, W fluoresced/W absorbed

$E_{\nu_{12}}$ = spectral irradiance of exciting radiation at absorption line, ν_{12}, W m^{-2} Hz^{-1}

$\int_0^\infty k_\nu d\nu$ = integrated absorption coefficient over absorption line, m^{-1} Hz

The product $E_{\nu_{12}} \int_0^\infty k_\nu d\nu$ is the power absorbed (W) from the source radiation by the analyte atoms per unit volume (m^3) of atomizer species. The product of Y_{21} and $E_{\nu_{12}} \int_0^\infty k_\nu d\nu$ converts the power absorbed per unit volume to power fluoresced per unit volume. The product of 1 and Y_{21} $E_{\nu_{12}} \int_0^\infty k_\nu d\nu$ converts the power fluoresced per unit volume to power fluoresced per unit area of the atomizer. Finally, dividing by 4π (sr) gives the power (W) fluoresced per unit area (m^2) per unit solid angle (sr). The integrated absorption coefficient is given by

$$\int_0^\infty k_\nu d\nu = n_1 \left\langle \frac{h\nu_{12}}{c} \right\rangle B_{12} \left[1 - \left[\frac{g_1 n_2}{g_2 n_1} \right] \right], \ m^{-1} \text{ Hz} \qquad (2.3)$$

where

n_1 = concentration of analyte atoms, m^{-3}

$h\nu_{12}$ = energy of the exciting photon, J

c = speed of light, m s^{-1}

B_{12} = Einstein coefficient of induced absorption; $m^3 J^{-1} s^{-1} Hz$

g_1, g_2 = statistical weights of states 1 and 2, respectively, dimensionless

n_1, n_2 = concentration of states 1 and 2, respectively, m^{-3} (note that $n_1 + n_2 = n_T$, the total concentration of atoms in all states).

Utilizing the steady state approach, where the excitation rate equals the de-excitation rate, that is

$$\left\langle k_{12} + \frac{B_{12} E_{\nu 12}}{c} \right\rangle n_1 = \left\langle k_{21} + A_{21} + \frac{B_{21} E_{\nu 12}}{c} \right\rangle n_2 \qquad (2.4)$$

where

k_{12}, k_{21} = excitation and de-excitation nonradiational (collisional) rate constants, s^{-1}

A_{21} = Einstein coefficient of spontaneous emission, s^{-1}

B_{21} = Einstein coefficient of induced (stimulated) emission; $m^3 J s^{-1} Hz$

B_{12} = Einstein coefficient of induced absorption, $m^3 J s^{-1} Hz$

n_1, n_2 = concentration of electronic states 1 and 2, m^{-3}

c = speed of light, m s^{-1}

The fluorescence power (quantum) efficiency Y_{21} is defined as

$$Y_{21} = \frac{A_{21}}{A_{21} + k_{21}} \tag{2.5}$$

and A_{21} is related to B_{21} and B_{12} by

$$A_{21} = \left\langle \frac{8\pi h\nu_{12}^3}{c^3} \right\rangle B_{21} = \left\langle \frac{8\pi h\nu_{12}^3}{c^3} \right\rangle \left\langle \frac{g_1}{g_2} \right\rangle B_{12} \tag{2.6}$$

where h is the Planck constant. Combining expressions, B_F for a two level atom core is given by

$$B_F = \left\langle \frac{1}{4\pi} \right\rangle Y_{21} E_{\nu_{12}} \left[n_1 \left\langle \frac{h\nu_{12}}{c} \right\rangle B_{12} \left\langle \frac{E^*_{\nu_{12}}}{E^*_{\nu_{12}} + E_{\nu_{12}}} \right\rangle \right] \tag{2.7}$$

where

$$E^*_{\nu_{12}} = \frac{c\, A_{21}}{B_{21}\, Y_{21}} \tag{2.8}$$

and in terms of the saturation spectral irradiance, $E^s_{\nu_{12}}$, that is, the source irradiance which results in a fluorescence radiance 50% of the maximum possible value.

$$E^s_{\nu_{12}} = E^*_{\nu_{12}} \left\langle \frac{g_1}{g_1 + g_2} \right\rangle \tag{2.9}$$

and substituting for n_1 in terms of n_T, B_F is given by

$$B_F = \left\langle \frac{1}{4\pi} \right\rangle Y_{21}\, E_{\nu_{12}}\, n_T \left\langle \frac{h\nu_{12}}{c} \right\rangle \left[\frac{B_{12}}{1 + E_{\nu_{12}}/E^s_{\nu_{12}}} \right] \tag{2.10}$$

Several conclusions can be made concerning the fluorescence radiance B_F:

1. B_F is linear with n_T as long as the optical density is low, (i.e. $k_\nu l \geq 0.05$).

2. B_F is linearly dependent upon the source irradiance and the fluorescence quantum efficiency if

$$E_{\nu_{12}} << E^{s}_{\nu_{12}} \text{ , that is,}$$

$$B_F = \left\langle \frac{1}{4\pi} \right\rangle Y_{21} E_{\nu_{12}} n_T \left\langle \frac{h\nu_{12}}{c} \right\rangle B_{12} \qquad (2.11)$$

which is the case for excitation by conventional sources.

3. B_F is independent of the source irradiance and the fluorescence quantum power if $E_{\nu_{12}} > E^{s}_{\nu_{12}}$. There is saturation of the upper state.

$$B_F = \left\langle \frac{1}{4\pi} \right\rangle Y_{21} E^{s}_{\nu_{12}} n_T \left\langle \frac{h\nu_{12}}{c} \right\rangle B_{12} \qquad (2.12)$$

or substituting for $E^{s}_{\nu_{12}}$

$$B_F = \left\langle \frac{1}{4\pi} \right\rangle h\nu_{12} A_{21} n_T \left\langle \frac{g_1}{g_1 + g_2} \right\rangle \qquad (2.13)$$

4. If the concentration n_T is increased greatly, then B_F does not follow the expressions above but rather is related to the $\sqrt{n_T}$ [74].

5. If a narrow line source [75, 76] is used for excitation and if all other assumptions given above are valid, then the exact expression for B_F is more complex than those listed above but is, in general, similar; for example, B_F is still linearly related to n_T, but now the source irradiance absorbed is determined by the width and profile of the exciting line, the velocity distribution of the absorbers, and the broadening mechanism for the absorbers.

Basics of lasers

A laser consists of a medium in which there is a greater population in an excited state than in some lower state and a reflecting structure that traps light within it [77]. A medium that has a population inversion will cause a net increase in the intensity of light that passes through

it because the stimulated emission caused by relaxation of the higher excited state exceeds the absorption from the lower state. It acts as an amplifier for light at a frequency that corresponds to the energy difference between the two levels that have the population inversion. Light emitted by the laser medium perpendicular to the cavity mirrors, be it simple fluorescence or stimulated emission, is trapped in an optical cavity so it is fed back through the amplifier for further amplification. Lasing develops as the spontaneous emission is amplified by stimulated emission.

Laser radiation is characterized by extremely high values of the following properties: directionality, monochromaticity, coherence, and radiance [78].

Directionality. This property results because the active material (medium) is placed in a resonant cavity formed by two plane parallel mirrors. Only a wave propagating along the direction normal to the mirrors can oscillate.

Monochromaticity. The monochromaticity of laser radiation is mainly due to the following effects: first, the resonant character of the interaction between the electromagnetic radiation and the matter, with gain in the active medium; and second, the presence of the resonant cavity

formed by the mirrors, which allows oscillation of only characteristic frequencies.

Coherence. Coherence can be distinguished as spatial coherence and temporal coherence. To define spatial coherence, let us consider two points P_1 and P_2 of the wave examined which, at $t = 0$, are on the same wavefront. By definition, the phases of the electric (or magnetic) fields are the same (at $t = 0$) at the two points. If the phases remain equal for $t > 0$, the two points are said to be coherent.

To define temporal coherence, let us consider the electric field of the wave at a given point and at two successive instants t and $t + \tau$. If the phase difference remains constant for a given value of τ and any t, and if this continues to be true for any value of τ, the wave is said to have a perfect temporal coherence.

Radiance. For an elementary radiation source with emitting surface dS (cm^2), the radiant power dP emitted in the solid angle $d\Omega$ (sr), at an angle θ with the surface normal, is given by

$$dP = B \cos \theta \, dS \, d\Omega \qquad (2.14)$$

The coefficient B is called the radiance of the source along the direction considered. If B is independent of θ and dS, the source is isotropic. The radiance of the laser is much higher (by four to ten orders of magnitude) than the radiance of the best incoherent sources. This is a consequence of the high power, and most important the high directionality of the laser radiation.

Lasers can operate in four different modes: (a) continuous wave (cw), (b) pulsed, (c) Q-switched (repetitive or single pulse), and (d) mode-locked (repetitive or pulsed). Excellent discussions on the technological aspects of laser operation are given in the monographs by Svelto [79], Demtröder [80] and Siegman [81].

Pulsed lasers have proven to be the most reliable sources of coherent radiation available to the analytical spectroscopist. Of all the different types of pulsed lasers, three of them stand out, mostly because of their versatility as optical pumps for dye lasers. These are the nitrogen, excimer, and Nd:YAG lasers, and a fourth type that is becoming the choice of some analysts, the Cu vapor laser.

The Nd:YAG (where YAG represents yttrium aluminum garnet) laser has become very popular recently because of its very high output energies, repetition rates, and

wavelength outputs. In this laser, Nd^{3+} ions are doped in a host crystal such as YAG. A simplified scheme of the energy levels of the Nd:YAG crystal can be seen in Figure 2-2. The pump transitions $^4I_{9/2} \rightarrow (^4F_{5/2}, {}^2H_{9/2})$ and $^4I_{9/2} \rightarrow (^4S_{3/2}, {}^4F_{7/2})$ are in the red region of the spectrum while the laser transition $^4F_{3/2} \rightarrow {}^4I_{11/2}$ occurs in the near infrared (λ = 1.06 μm). An Nd:YAG rod is placed within an elliptical cavity where flashlamps excite the already stated transitions. The gain of the Nd:YAG laser is sufficiently high that it is often operated with an unstable resonator configuration that can extract energy from the sides of the rod as well as the center [82]. An unstable resonator can be defined as an optical cavity with no closed ray paths; any ray eventually "walks" out of the resonator, around one (or both) of the mirrors or outside the limiting aperture. Unlike Gaussian beam profiles generated by low-gain stable oscillators, the unstable-resonators mode is not described by a simple analytical expression. In a near field, unstable-resonator beam the energy is distributed in an annular ring about the central beam axis. The oscillator is often Q-switched to obtain very high, reproducible peak powers that can be efficiently frequency doubled, tripled, and quadrupled. An amplifier can boost the output powers so that ca. 700 mJ of

Figure 2-2. Simplified Energy Levels in Nd:YAG.

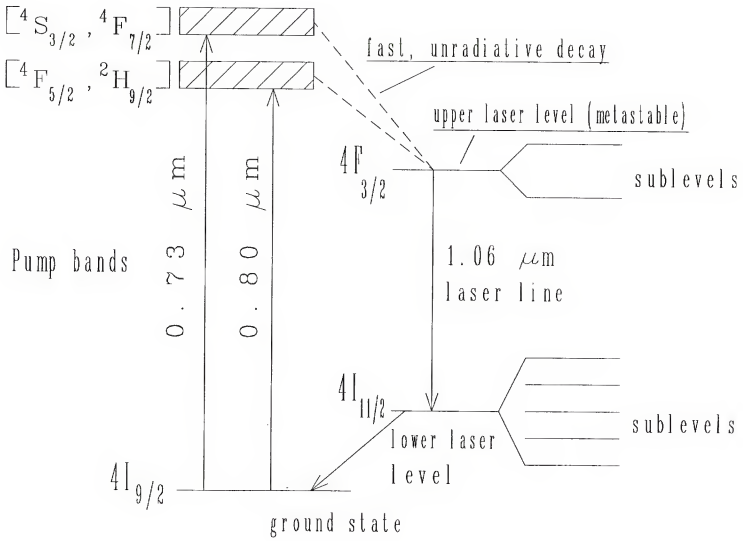
$[^4S_{3/2}, {}^4F_{7/2}]$
$[^4F_{5/2}, {}^2H_{9/2}]$
fast, unradiative decay
upper laser level (metastable)
$4F_{3/2}$
sublevels
Pump bands
0.73 μm
0.80 μm
1.06 μm
laser line
$4I_{11/2}$
sublevels
lower laser
level
$4I_{9/2}$
ground state

energy is available at 1.06 μm. If the output is passed through a series of nonlinear crystals installed on commercial lasers, one obtains 200 mJ at 532 nm, 100 mJ at 355 nm, and 50 mJ at 266 nm. These characteristics are almost ideal for a number of applications.

In the nitrogen (N_2) laser system, laser action takes place in the so called second positive system, that is, in the transition from the $C^3\Pi_u$ state (henceforth called C state) to the $B^3\Pi_g$ state (B state). The excitation of the C state is believed to arise from electron-impact collisions with ground-state N_2 molecules. Since both C and B states are triplet states, transitions from the ground state are spin-forbidden. The lifetime (radiative) of the C state is 40 ns, while the lifetime of the B state is 10 μs. Therefore, the laser can be operated in a pulsed mode provided that the electrical pulse is appreciably shorter than 40 μs. Laser action takes place predominately on several rotational lines of the $v''(o) \rightarrow v'(o)$ transition (λ = 337.1 nm). Besides being favored by the pumping process, this transition, in fact, exhibits the largest Franck-Condon factor (see Figure 2-3).

The configuration necessary to operate an N_2 laser requires a discharge channel with electrodes mounted along the

Figure 2-3. Energy Levels of the N_2 Molecule Involved in the Lasing Process.

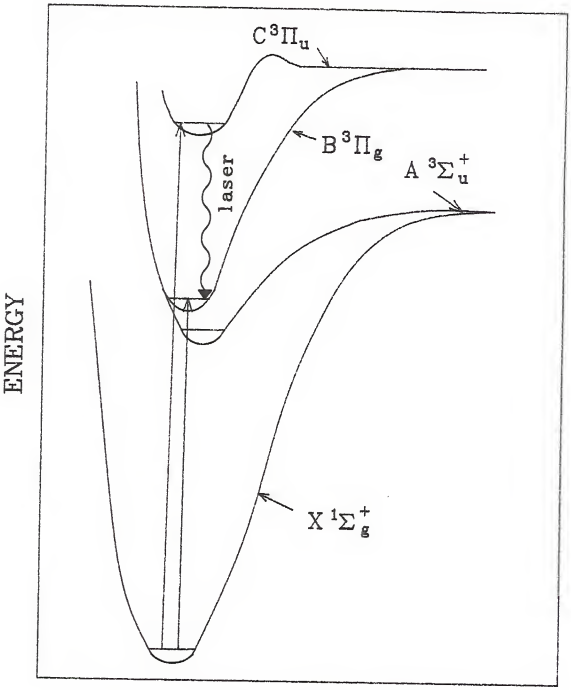
$C^3\Pi_u$
$B^3\Pi_g$
$A\ ^3\Sigma_u^+$
laser
$X\ ^1\Sigma_g^+$
ENERGY
DISTANCE

entire length. As a flow of N_2 gas passes through the channel at ca. 40 torr, a high voltage supply charges a capacitor C_1 to a voltage of 20-30 kV and a thyratron then is triggered to rapidly charge a second capacitor C_2. The laser electrodes are in parallel with C_2 and will break down as C_2 charges. The energy in C_2 (dumping capacitor) is then transferred into a spark discharge where electronic excitation of N_2 occurs. Light emitted along the discharge path will be amplified as it travels down the laser tube (channel). A mirror located at one end will add a second pass for the light while an uncoated window defines the other end of the cavity. The laser pulse widths are only 5-10 ns. The energy of each pulse is ca. 1-10 mJ, resulting in peak power of 100 kW - 1.5 MW.

Excimer lasers are quite similar to nitrogen lasers in construction [83]. A gas mixture of helium, fluorine (or hydrogen chloride), and one of the rare gases--argon, krypton or xenon--is flowed through the discharge channel where the gas is electronically excited. The inert gas in its excited state, combines F_2 to form a XeF, KrF, or ArF excimer (a molecule stable only in the excited state), similarly Xe gas can combine with HCl to form a XeCl excimer, which is probably the most used type of excimer today.

Since the excimer ground state is unstable, relaxation results in the rapid dissociation of the molecule. Thus, there is a population inversion while the excimer exists and lasing can be achieved. The excimer laser produces high energy pulses in the UV - XeF lases at ca. 351 nm with ca. 50 mJ, XeCl at 308 nm with ca. 100 mJ, KrF at 248 nm with ca. 150 mJ, and ArF at 193 nm with ca. 50 mJ. The output pulse widths are ca. 10-25 ns and the lasers are typically operated at repetitive rates of 10-500 Hz (see Figure 2-4).

Metal vapor lasers became commercially available in the last four years even if their development can be traced back to the mid-1960s. Several metals can be induced to produce laser radiation, among them Pb, Cu, Au, Ca, Sr, and Mn. Of these, the most important at present is the Cu vapor laser which oscillates in the green (510.5 nm) where efficiency is quite high (> 1%) and in the yellow, at 578.2 nm. All metal lasers are self-terminating and are, therefore, operated in a pulsed regime. A general scheme for the relevant energy levels of the Cu vapor laser is shown in Figure 2-5. The $3d^{10}\ 4s\ ^2S$ (ground state) $\rightarrow$ $3d^{10}\ 4p\ ^2P$ (excited 2) transition is allowed while the $3d^{10}\ 4s\ ^2S$ (ground state) $\rightarrow$ $3d^9\ 4s^2\ ^2D$ (excited 1) is forbidden by electric-dipole interaction. Under the Born approximation, it is thus expected that the

Figure 2-4. Potential Energy Diagram of the $XeCl^*$ Excimer.

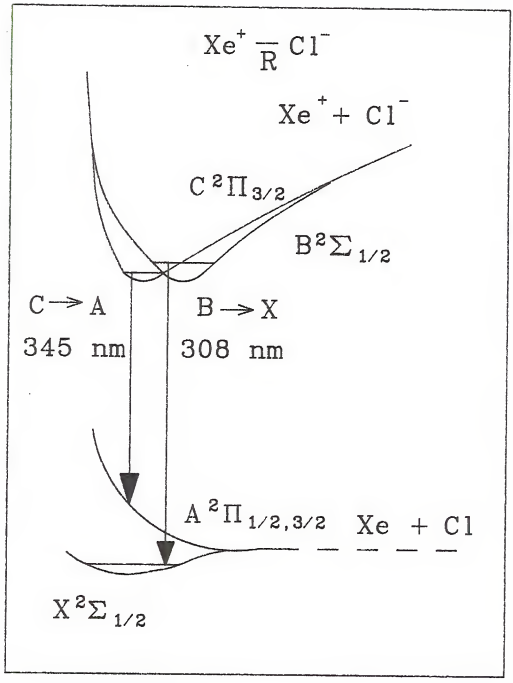
Xe+ Cl−
R
Xe+ + Cl−
C 2Π3/2
B2Σ1/2
C → A
345 nm
B → X
308 nm
A 2Π1/2,3/2
Xe + Cl
X2Σ1/2
ENERGY
DISTANCE

Figure 2-5. Lasing Diagram for a Cu Vapor Laser.

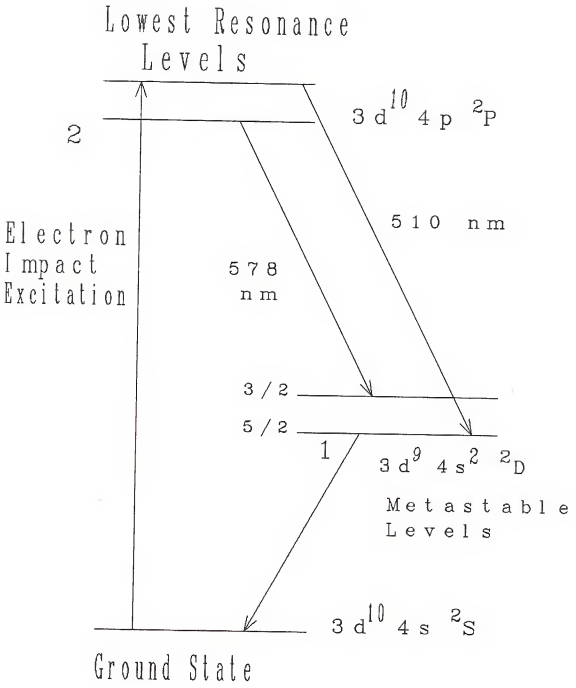
Lowest Resonance Levels
2
$3d^{10}\,4p\,{}^2P$
510 nm
578 nm
Electron Impact Excitation
3/2
5/2
1
$3d^9\,4s^2\,{}^2D$
Metastable Levels
$3d^{10}\,4s\,{}^2S$
Ground State

electron impact cross section of the (ground state) → (excited 2) transition to be appreciably larger than that of the (ground state) → (excited 1) transition. To accumulate sufficient population in the upper laser level, the (excited 2) → (ground state) radiative transition rate, which would usually be fast, must be slowed down to a value comparable to the (excited 2) → (excited 1) radiative rate. This means that a sufficient atomic density must be present to produce radiation trapping on the (excited 2) → (ground state) transition. Note that since the (excited 1) → (ground state) transition is forbidden, the laser can only operate on a pulsed basis with pulse duration of the order of or shorter than the lifetime of level 2. In order to oscillate, a Cu vapor laser needs high vapor densities, as already mentioned; for this reason it must be operated at high temperatures (≈ 1500°C). The laser tube is therefore usually made of alumina and the central region is held in an oven. A few torr of He is also added to the laser tube to prevent deposition of copper on the (cold) end windows. Cu vapor lasers have been operated with average powers of 20-100 W and repetition rates of 4-15 kHz.

The most important lasers from an analytical viewpoint are the dye lasers. A dye solution will lase at wavelengths

controlled by its fluorescence spectrum, typically a 30-100 nm region. Different dyes allow lasing from ca. 340 nm - 1 μm. There are many different kinds of dye lasers with widely differing characteristics [84]. They differ from each other primarily in the method of optical pumping and wavelength selection. There are three major classes: N_2, excimer, Nd:YAG, and Cu vapor pumped; flashlamp pumped; and CW dye lasers pumped by argon or krypton ion lasers. For the sake of completeness, only the first class will be discussed here; excellent reviews of the other two major classes are readily available [84, 85].

In pulsed laser pumped dye lasers, the exciting laser is focused along an axis perpendicular to the dye laser axis (transverse pumping) with a cylindrical lens so that a thin line of fluorescence appears across the front of the dye cell as shown in Figure 2-6. Dye concentrations are chosen so the excitation light is totally absorbed within a short distance of entering the solution. The excitation lasers are so intense during their pulse that a nearly total population inversion can be obtained for the dye molecules within that small excited region. A grating diffracts light at a specific wavelength determined by the angle of the grating back through the excitation region of the dye cell.

Figure 2-6. Construction of a High-Power Tunable Dye Laser.

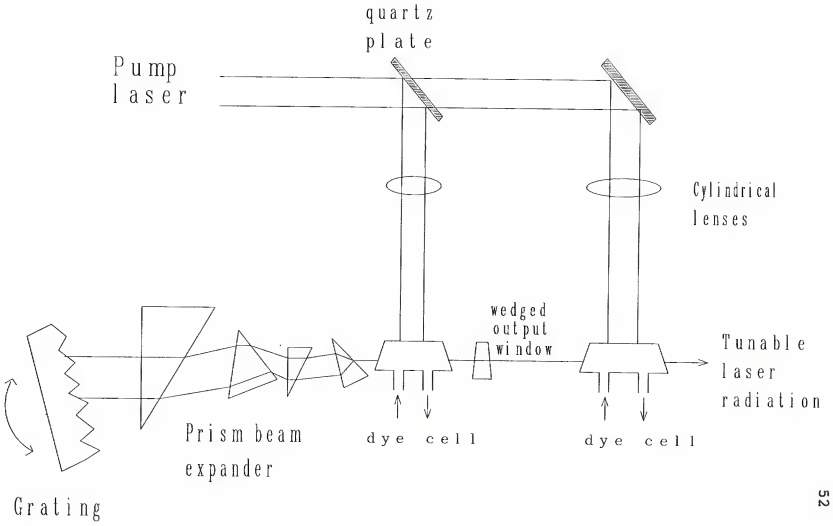
quartz
plate
Pump
laser
Cylindrical
lenses
wedged
output
window
Tunable
laser
radiation
Prism beam
expander
dye cell
dye cell
Grating

A beam expander is used between the grating and the dye cell to decrease the bandwidth of the laser by magnifying the angles of diffraction leaving the grating and filling the grating. Either a set of prisms or a Galilean telescope is used to expand the beam [86, 87]. An etalon can be placed between the beam expander and the grating if a very narrow bandwidth is desired. The bandwidth of a typical dye laser is 0.01 nm with just the grating and the beam expander but reduces to 0.001 nm with etalon. The other end of the cavity is an uncoated glass or quartz wedge. Since most pump lasers have so much power available, the oscillator in many cases saturates. Under these conditions, a second dye cell (and in some cases a third) is added as an amplifier, and the major portion of the pump beam is directed through this (these) cell(s) along with the output of the oscillator.

Laser Atomic Fluorescence Spectrometry

Laser excited fluorescence has gained a firm reputation as one of the most attractive tools for studying the complicated dynamics of combustion processes [63, 72, 88]. In fact, like all "scattering" methods (e.g., Raman techniques), it is intrinsically characterized by high spatial resolution, thus providing local data without the necessity

of sometimes inaccurate Abel inversion procedures. In addition, with pulsed laser excitation, temporal resolution is possible as already mentioned.

From an analytical point of view, the technique of laser induced fluorescence has been applied to atomizers such as atmospheric pressure flames [89-94], graphite furnaces [33-36, 95-97], inductively coupled plasma [98-100], and other types of atom cells [101, 102]. In flame and plasma work, some of the early results, as well as some of the recent ones, are of rather discontinous quality, the detection limits being in several cases inferior to those given with the same or similar experimental facilities by either atomic emission or atomic absorption. On the other hand, the results from the laboratories of Bolshov [35, 97, 103-106], Tilch [34, 107-108], Michel [36, 109-111], and Omenetto [112, 113], for electrothermal atomization and pulsed laser excitation represent the best detection limits obtained so far for the elements investigated. Nevertheless some recent reports [114, 115] have demonstrated that flames and plasmas can still be successfully used as atomizers and are both capable of providing detection limits that for many elements are sufficient to allow their direct determination in the sample solution without any prior chemical treatment.

It is also important to note that increased selectivity and sensitivity can be achieved by applying stepwise excitation schemes (double resonance) [32, 113].

However, electrothermal atomization provides unprecedented sensitivities for all the elements so far investigated, showing that this must be the only method of choice in all those cases where the available sample size is limited and the elements to be determined are below the limit of determination of the other spectrometric methods.

Electrothermal Atomization

After Walsh [116] and Alkemade and Milatz [117, 118] developed atomic absorption spectrometry, the problem of developing absolute methods of analysis captivated the interest of L'Vov who four years later demonstrated the approach of using a high temperature graphite cuvette to produce atomic vapors [70, 119-122]. Early publications stated a very high sensitivity for most of the elements measured by atomic absorption spectrometry (AAS) but also indicated an apparent freedom from matrix effects based on the results obtained. This led to great interest in the technique and consequently many researchers studied the processes involved.

Some of this work included characterization of atomic absorption signals and various methods of their measurement [123, 124], the influence of the rate of heating of the atomizer on the analytical sensitivity [125-127], the effects of atomizer geometry and construction material on the signal [128-132], the mechanism of atom formation [133-136], the interferences due to compound formation and composition of the matrix [137-139], calculation of diffusion coefficients in tube atomizers [140-142], and the supply and removal of sample vapor from the atomizer [143-147].

Some of the advantages that electrothermal atomization (ETA) has over flame or plasma techniques [123, 148] are as follows:

1. ETA requires only a few microliters of sample per analysis.
2. Difficult to nebulize liquids can be conveniently handled.
3. The efficiency of the vaporization process is generally better than in a flame or plasma, due to the faster heating rate.
4. The efficiency of the atomization process is usually better than in a flame but not as high as in a plasma.

5. Enhancements in the signal to noise ratios in the electrothermal atomizer are a result of the smaller sample volume, the absence of analyte dilution and the increased lifetime of the atomic vapor within the analytical volume.
6. The chemical and thermal environment can be better controlled in ETA.
7. The capability of direct solid sampling exists.

Principles of Operation and Optimum Design

Electrothermal atomizers are resistively heated devices that generally employ a three-stage heating program to dry, char (ash), and atomize the sample. Power is provided from a low-voltage (≈ 10 V), high current source capable of delivering up to 500 A. The temperature of the atomizer is a complicated function of time and various other factors, such as the input power, the mass of the atomizer, and its heat losses by convection, conduction, and radiation.

Some considerations that should be important in the design and operation of an electrothermal atomizer are: (a) the atomizer should be tubular to contain the atomic (or molecular) vapor. This improves vapor-tube wall thermal equilibration and increases the vapor temperature, thus promoting molecular dissociation; (b) the atomizer should be

constructed of pyrolytic graphite. This material has the desirable properties of low permeability to gases, low porosity, high purity, a high sublimation temperature, a high resistance to oxidation, and a high thermal conductivity; (c) the atomizer should be capable of achieving high rates of heating. This maximizes the rate of analyte evaporation and the rate of molecular dissociation; (d) the maximum temperature attained by the atomizer must be made independent of its rate of heating. This allows an optimum steady-state temperature to be set for each element preventing vapor condensation; (e) temporal and spatial non-isothermality of the atomizer must be minimized; (f) the atomizer should be as long as possible, its upper length being limited by the requirements of higher power consumption and maintaining isothermality, but note that in fluorescence measurements, the length will also affect the solid angle of collection; and (g) the atomizer should be of minimal mass to maximize its rate of heating.

Theoretical Aspects of the Atomization Process

The atomization processes occurring with electrothermal atomizers would seem to be simpler than the complex interactions occurring with flame atomization [72, 149]. Thermodynamic theories can be postulated which incorporate

the dissociation of metal oxides, and other species, and the reduction of metal oxides. However, when the required calculations are carried out for these, and other processes, it becomes apparent that the theoretical results obtained do not always fit readily with results obtained experimentally. Because of this problem, other approaches have concentrated on kinetic theories to obtain information on atomization. While this second approach is probably more helpful analytically, since it can give rise to information that is analytically useful, it is not easy to interpret the experimental results, apart from the simplest cases. It is inevitable, therefore, that a complete understanding of the situation will come from a combination of both the thermodynamic and kinetic approaches.

Thermodynamic Model

For a better understanding of the thermodynamic approach, it is necessary to be aware of the various reactions which can occur in an atomizer. To simplify the problem, it will be assumed that the metal salts obtained in an atomizer, after drying the sample solutions, are relatively unstable and, therefore, are decomposed to their metal oxides prior to any significant atomization occurring. Possible reactions can then be summarized as follows:

1. Evaporation of the Metal Oxide Prior to Atomization.

Some metal oxides have high vapor pressures at the temperatures at which atomization is first observed to occur, (e.g., SbO_3 and SiO_2). Assuming the simple gas-law equation is valid, it is possible to show that the vapor pressure exerted by, for example, 1 ng of metal oxide (molecular weight = 100), completely vaporized in a volume of 0.1 ml, at T K, would be 6×10^{-6} mm Hg. If the vapor pressure of the metal oxide is greater than this value, at the minimum atomization temperature, then significant losses of the metal oxide, due to molecular evaporation, would be expected to occur prior to atomization. This problem would be much greater if volatile metal halides were present in the atomizer. A typical example of this situation occurs in the determination of Pb in seawater [150].

2. Thermal Dissociation of the Metal Oxide.

The degree of dissociation of metal oxides, α, can be calculated from the following equations

$$-\Delta G = RT \ln K_p \qquad (2.15)$$

$$\alpha = K_p / [K_p + \sqrt{P(O_2)}] \qquad (2.16)$$

where $P(O_2)$ is the partial pressure of oxygen, ΔG is the free energy, and K_p is the equilibrium constant for the dissociation of the metal oxide MO as shown in the next equation

$$MO \leftrightarrows M + \frac{1}{2} O_2 \qquad (2.17)$$

Values of ΔG at various temperatures can be obtained for many metal oxides from tables of thermodynamic data. For carbon atomizers, two additional controlling factors are the equilibria existing between oxygen and carbon

$$2\ C + O_2 \leftrightarrows 2\ CO \qquad (2.18)$$

$$2\ CO + O_2 \leftrightarrows 2\ CO_2 \qquad (2.19)$$

These equilibria effectively control the value of $P(O_2)$.

3. Reduction of the Metal Oxide.

Reduction of the oxide by either carbon, or the metal from the atomizer is an extension of the theory of dissociation of metal oxides. In this case, the dependence of the metal oxide decomposition on the carbon/oxygen equilibria is more apparent. The theory is described here in terms of carbon reduction, although most of the conclusions are equally valid for metal atomizers (e.g., tantalum and tungsten).

The reduction process can be described by the equation

$$MO(s/l) + C(s) \leftrightarrows M(g) + CO(g) \qquad (2.20)$$

The free-energy change for the reaction, ΔG°, can be obtained from the difference of the sum of the free energies of formation of the products and reactants. In this calculation, it is essential to use ΔG values which correspond to the correct physical state of each component. By using the various free-energy values for reactants and products over a range of temperatures, it is possible to calculate the temperature at which

formation of the free gaseous metal becomes feasible (i.e., ΔG^{o}, becomes negative).

It is sometimes easier to use Ellingham diagrams [151] for these calculations, where the thermodynamic information is presented graphically. These diagrams were originally used for studying metallurgical reduction processes, so they require modification to incorporate the added criterion for the formation of gaseous metal atoms.

The difficulty in using this thermodynamic model for atomization is in relating theoretically derived values with results obtained experimentally. The problem arises for two reasons: (a) the thermodynamic calculation of the minimum atomization temperature ($\Delta G^{o} = 0$) is dependent on an equilibrium reaction; therefore, some proportion of the metal oxide will be dissociated at all temperatures. The quantity of metal atoms formed will be dependent on the quantity of metal oxide present in the atomizer, that is, the greater the quantity of metal oxide present, the greater the concentration of metal atoms formed at any temperature; (b) the minimum concentration of an element which can be determined is dependent on the detection limit and

also on the analytical technique. Quite different analytical conditions could therefore be used with the result that widely differing values are obtained for the minimum temperatures at which atomization is observed. It is correct to say that almost any temperature could be obtained since the value obtained is solely dependent on the conditions chosen.

4. Carbide Formation.

In the same way that free-energy changes can be calculated for carbon reduction of metal oxides it is possible to calculate the free-energy changes occurring in the formation of stable carbide compounds

$$MO + 2C \leftrightarrows MC + CO \qquad (2.21)$$

Carrying out this calculation frequently shows that the metal oxide decomposes to form a stable carbide at temperatures below that at which carbon reduction of the metal oxide to gaseous metal atoms occurs. This temperature is also often below that at which atomization is first observed.

5. Thermodynamic Theories of Atomization.

From the previous sections, it is apparent that there are five important thermodynamic parameters: (a) H_{MO}, the heat of vaporization of the metal oxide, (b) E_{MO}, the dissociation energy of the metal oxide, (c) H_M, the heat of vaporization of the free metal, (d) E_{MC}, the dissociation energy of the metal carbide, and (e) E_{CO}, the dissociation energy of carbon monoxide.

Several situations can be predicted, therefore, (a) if $H_{MO} < E_{MO}$ and E_{MC}, vaporization of the metal oxide will occur prior to any reaction; (b) if E_{MO} and $E_{MC} < H_M$, then reduction of the metal oxide or carbide will occur rapidly at the atomization temperature, and the rate of atomization will be dependent on H_M; (c) if $H_M < E_{MO}$ and E_{MC}, the rate of atomization will be dependent on E_{MC}; (d) if $H_M < E_{MC} < E_{MO}$, the rate of atomization will be dependent on E_{MO}. While thermodynamic considerations are clearly important in the atomization processes, it is apparent that these processes must also be kinetically controlled to explain the experimental results.

Kinetic Models

The kinetic models which have been proposed vary from the simple to the complex; unfortunately, no more than a brief description of each can be given here. The models are divided into two groups, atomization under increasing temperature first used by L'Vov [70], and atomization under isothermal conditions proposed by Fuller [152]. Neither of these models is entirely satisfactory although each has advantages. L'Vov's model approximates the situation with rod, cup, and filament atomizers and probably for easily atomized elements of high temperatures in a furnace. Fuller's model approaches the situation existing in furnace atomizers, particularly for elements which are difficult to atomize for low temperatures.

Atomization Under Increasing Temperatures. L'Vov proposed an equation for atomization in a furnace, where dN/dt is the rate of change in the number of atoms, N, present in the gaseous state in the atomizer, $n_1(t)$ is the number of atoms entering the system, and $n_2(t)$ is the number of atoms leaving the system. For a constantly increasing atomization temperature, the following equations are valid where τ_1 is the time taken to transfer the total number of atoms, N(o), to the system; hence

$$dN/dt = n_1(t) - n_2(t) \tag{2.22}$$

$$n_1(t) = At \tag{2.23}$$

where A is the atomization factor.

$$\int_{t=0}^{t=\tau_1} n_1(t)dt = N(o) \tag{2.24}$$

Solving the above equation gives

$$n_1(t) = 2\ N(o)\ t/\tau_1^2 \tag{2.25}$$

Assuming that atoms are removed from the system by vapor diffusion, then

$$n_2(t) = N/\tau_2 \tag{2.26}$$

where τ_2 is the average residence time of atoms in the system. By substitution

$$dN/dt = [2\ N(o)\ t/\tau_1^{\,2} - (N/\tau_2)] \qquad (2.27)$$

L'Vov describes two situations when integrating the above equation.

For $t \leq \tau_1$

$$N = 2\ N(o) \cdot \frac{\tau_2^{\,2}}{\tau_1^{\,2}} \left[\langle \frac{t}{\tau_2} \rangle - 1 + \exp \langle \frac{-t}{\tau_2} \rangle \right] \qquad (2.28)$$

and for $t \geq \tau_2$

$$N = 2\ N(o) \cdot \frac{\tau_2^{\,2}}{\tau_1^{\,2}} \left[\left[\langle \frac{t}{\tau_2} \rangle - 1 + \exp \langle \frac{-t}{\tau_2} \rangle \right] \cdot \exp \left[\langle \tau_1 - t \rangle / \tau_2 \right] \right] \qquad (2.29)$$

These two equations describe the number of atoms, N, in the system at time t. From these equations, it can be seen that the signal grows in an exponential manner and also decays away exponentially.

Atomization Under Isothermal Conditions. Fuller [152] measured the variation in atom concentration in a graphite furnace under conditions where the furnace temperature was essentially constant for the greatest part of the atomization process.

With the notation used earlier,

$$dN/dt = n_1(t) - n_2(t) \qquad (2.30)$$

here,

$$n_1(t) = k_1 \, [\, N(o) - N(t) \,] \qquad (2.31)$$

where N(o) is the initial quantity of element introduced to the atomizer and N(t) is the quantity of element atomized up to time t, and k_1 is the rate constant for the atomization process, N(t) can be calculated from

$$N(t) = N(o) \, [\, 1 - \exp(-k_1 t) \,] \qquad (2.32)$$

which on substitution gives

$$n_1(t) = k_1 N(o) \exp(-k_1 t) \qquad (2.33)$$

The rate of loss of atoms from the furnace is controlled by diffusion processes and the velocity of the purge gas passing through the furnace, hence

$$n_2(t) = k_2 N \qquad (2.34)$$

where k_2 is the rate constant for the removal of atoms from the furnace. By substitution in the above equations, and subsequent integration produces an equation that represents the concentration of atoms at any time

$$dN/dt = k_1 N(o) \exp(-k_1 t) - k_2 N \qquad (2.35)$$

$$N = [k_1/(k_2-k_1)] N(o) [\exp(-k_1 t) - \exp(-k_2 t)] \qquad (2.36)$$

The main advantage of the kinetic models is that they are used to produce analytically useful information. This

information can be used to (a) determine when to use peak height or peak area measurements, (b) when to use stopped gas flow conditions, (c) prediction of the optimum conditions for the control of matrix interferences, and (d) determination of reaction mechanisms [70].

Laser Atomic Fluorescence Spectrometry Using Graphite Electrothermal Atomizers

Non-flame atomizers started to be investigated for use in atomic fluorescence in 1968 when Massmann [153] using a heated graphite cup obtained detection limits in the range of 10^{-9} to 10^{-14} g for nine elements. Shortly after this report, the use of carbon filaments, tungsten and platinum loops, and carbon rod atomizers was demonstrated by West and Williams [154], Bratzel et al. [155, 156], and Amos et al. [157], respectively, for both atomic absorption (AA) and atomic fluorescence measurements. Laser atomic fluorescence in a non-flame atomizer [LEAFS-ETA] was demonstrated by Neumann and Kriese [95] in 1974 where a flashlamp-pumped dye laser was used for excitation and the reported detection limit for lead was 0.2 pg. Including Neumann and Kriese's work, all the subsequent applications of LEAFS-ETA [96, 97, 103, 158-160] were carried out using open type atomizers, rods, cups or boats, mainly because the observation at right angle of the fluorescence was very much simplified and it

was thought that blackbody emission from the heated graphite will be very difficult to mask if the more conventional and commercially available tube atomizers were used. It has been mentioned before that the detection limits reported, especially those of Bolshov [161], are the lowest so far obtained for a very diverse group of elements. More recently, the approach of modifying graphite tube atomizers by opening holes across the cylinder [109-111, 162, 163] has produced some excellent data. Finally the last step is the use of an unmodified tube atomizer [164] carried out with an ingenious modification of the optical collection apparatus.

The process of analyte atomization in electrothermal atomizers cannot avoid the problems presented by matrix interferences. The influence of the matrix composition on the analytical signal not only decreases the analytical sensitivity, but also complicates the definition of adequate standards. The analytical potential of the LEAFS-ETA method is based on the extremely high sensitivity that it provides, but in order to achieve that potential this technique needed to prove itself in the world of real samples. Bolshov et al. [35] have started to move in that direction with a great deal of success. Their first real sample analytical application involved the determination of iridium in

industrial acidic solutions. In this case not only was the sensitivity much better than graphite furnace atomic absorption spectrometry but in a parallel determination both methods showed an insignificant statistical difference when the results are compared [104]. In another application involving the determination of cobalt in glass and in quartz, which is very important in the fabrication of optical fibers [35, 106, 165-170], the limit of detection is approximately two orders of magnitude better than that for the traditional techniques. Recently, other workers have shown the versatility of LEAFS-ETA technique as demonstrated by Goforth and Winefordner [171], in the determination of manganese and copper in wheat flour, spinach leaves and steel. Dougherty et al. [172] have reported the determination of thallium in bovine liver and mouse brains at levels that are lower then those achievable by GFAAS. In this case the fluorescence method avoids the use of a preconcentration step needed when the same type of samples are analyzed by the atomic absorption method. It is important to remark that all of these applications were carried out using graphite cup or modified graphite tube electrothermal atomizers which brings about the possibility that the use of unmodified graphite tube atomizers could provide a very large

increase in the number of real sample applications. As shown extensively in the literature [7], graphite tube atomizers are the best option available to the analyst when trace analysis is performed in a very complicated matrix and very high sensitivity is required.

CHAPTER 3
DETERMINATION OF THE OPTIMUM CONDITIONS FOR LEAFS-ETA

When the duration (t_o) of the radiation pulse producing excitation (of an atom) is comparable to, or shorter than, the fluorescence lifetime of the upper state of the transition being observed, the steady-state assumption presented in a previous section does not hold, and the rate of change in population of the excited level cannot be neglected [173-175]. In this non-steady-state situation, the populations of the different levels both during ($0 \geq t \geq t_o$) and after ($t > t_o$) termination of the excitation pulse can be obtained by solving a system of rate equations [176-181].

The determination of the optimum conditions for excitation and recording of fluorescence is very important when LEAFS is considered as the method for the measurement of ultratrace concentrations of elements. For this reason, the analysis of the non-steady-state regime of LEAF is of particular interest since the experiments are carried out with the use of pulsed lasers whose pulse duration is about several nanoseconds.

Laser Fluorescence Spectroscopy of Three-Level Systems

If the spectral width of the laser radiation is far in excess of the width of the atomic absorption line, then the rate equations for a three-level system are

$$\frac{dn_1}{dt} = - n_1 (R_{12} + R_{13}) + n_2 R_{21} + n_3 R_{31}$$

$$\frac{dn_2}{dt} = n_1 R_{12} - n_2 (R_{21} + R_{23}) + n_3 R_{32} \qquad (3.1)$$

$$\frac{dn_3}{dt} = n_1 R_{13} + n_2 R_{23} - n_3 (R_{31} + R_{32})$$

where R_{ij} are the total rates of excitation and deactivation of the appropriate levels including radiative and collisional processes. The system may be solved analytically in a general form for the light-wave field in the form of a step function or a rectangular pulse.

When trace concentrations of elements are measured in nonflame atomizers the atom, as a rule, interacts with the resonance field in an inert atmosphere. In this case, the rates of collisional processes may be of the same order or less than radiative rates. If, in addition, such an atomic system is investigated in which the distances between levels $\Delta E_{ij} >> kT$ (in nonflame atomizers, the temperature in the analytical zone is of the order of several hundreds of °C), one can deliberately neglect the process of collisional excitation of the higher levels.

Consider a three-level model of an atom as shown in Figure 3-1. If the laser frequency is set for the transition 1-3, then with due regard to the above assumptions the constants R_{ij} in the system become

$$R_{12} = R_{23} = 0 \quad ; \quad R_{31} = \rho B_{31} + A_{31} + Z_{31}$$

(3.2)

$$R_{13} = \rho B_{13} \quad ; \quad R_{21} = Z_{21} \quad R_{32} = A_{32} + Z_{32}$$

Figure 3-1. A Three-Level Scheme of an Atom. Statistical weights of the levels are g_1, g_2, g_3; R_{ij} are the rates of excitation of the levels.

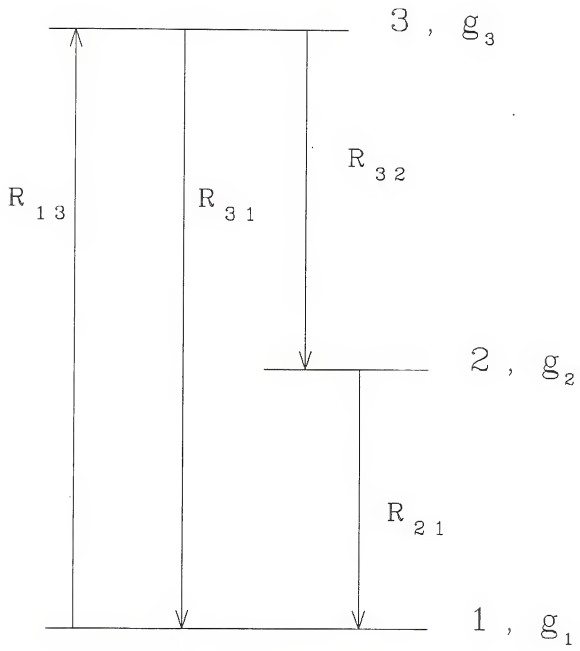
3 , g3
R32
R13
R31
2 , g2
R21
1 , g1

where ρ ($J\ m^{-3}\ Hz^{-1}$ is the spectral density of the laser radiation energy, B_{13} and B_{31} ($J^{-1}\ m^3\ Hz\ s^{-1}$) are the Einstein coefficients of induced absorption and emission, A_{31}, A_{32} (s^{-1}) are Einstein coefficients for spontaneous radiation, Z_{21}, Z_{31}, Z_{32} (s^{-1}) are the rates of collisional deactivation of the appropriate levels. The solution of this system for ρ independent of time and with the initial conditions $n_2(o) = n_3(o) = 0$, $n_1(o) = n_T$ is [175]

$$n_1(t) = n_T \frac{R_{13}}{\xi_2 - \xi_1} \left[-\left\langle 1 - \frac{R_{21} + R_{32}}{\xi_1} \right\rangle \exp(-\xi_1 t) \right.$$

$$\left. + \left\langle 1 - \frac{R_{21} + R_{32}}{\xi_2} \right\rangle \exp(-\xi_2 t) \right]$$

$$+ n_T \frac{R_{21}(R_{31} + R_{32})}{\xi_2 \xi_1}$$

$$n_2(t) = n_T \frac{R_{13}\, R_{32}}{\xi_2 - \xi_1} \left\langle - \frac{1}{\xi_1} \exp(-\xi_1 t) + \frac{1}{\xi_2} \exp(-\xi_2 t) \right.$$

$$\left. + n_T \frac{R_{13}\, R_{32}}{\xi_1\, \xi_2} \right\rangle \qquad (3.3)$$

$$n_3(t) = n_T \frac{R_{13}}{\xi_2 - \xi_1} \left[\left\langle 1 - \frac{R_{21}}{\xi_1} \right\rangle \exp(-\xi_1 t) \right.$$

$$\left. - \left\langle 1 - \frac{R_{21}}{\xi_2} \right\rangle \exp \left\langle - \xi_2 t \right\rangle \right] + n_T \frac{R_{13}\, R_{21}}{\xi_2\, \xi_1}$$

where ξ_1 and ξ_2 are determined by

$$\xi_{1,2} = \frac{X + R_{21}}{2} \mp \left[\left\langle \frac{X + R_{21}}{2} \right\rangle^2 - R_{13}\, R_{32} \right]^{1/2}$$

and (3.4)

$$X \equiv R_{13} + R_{31} + R_{32}$$

The Case of a Metastable Level

Such an approximation is fulfilled rather well, (e.g., for lead) when Pb atoms are excited at the transition $6p^2\ ^3P_o$ - $7s\ ^3P_1^o$ (λ = 283.31 nm) and fluorescence is collected at the transition $7s\ ^3P_1^o$ - $6p^2\ ^3P_2$ (λ = 405.78 nm). At atmospheric pressure and in an argon atmosphere, the lifetime of the level $6p^2\ ^3P_2$ is 1.8×10^{-5}s [182]. The values A_{31} and A_{32} equal, respectively, $0.6 \times 10^8\ s^{-1}$ and $3 \times 10^8\ s^{-1}$ [183] so that the relationship $R_{21} << A_{31}, A_{32}$ is certainly valid.

In the case of $R_{21} = 0$, the solution is simplified. Steady-state values of populations are $n_1(\infty) = n_3(\infty) = n_\tau$, this corresponds to a physically obvious situation, namely, upon the appearance of the laser pulse at the moment t = 0, all the atoms from the ground state will follow the cycle 1-3-2 and accumulate at the metastable level. The temporal behavior of the upper level population is determined now by

$$n_3(t) = n_T \frac{R_{13}}{\xi_2 - \xi_1} \left[\exp(-\xi_1 t) - \exp(\xi_2 t) \right] \qquad (3.5)$$

For ease of further calculation, we assume that the laser pulse is rectangular and has an amplitude ρ and duration τ: $\rho(t) = \rho(0 \leq t \leq \tau)$; $\rho(t) = 0$ $(t > \tau)$. It is well known that the collection of direct line fluorescence considerably simplifies the problem of suppression of the Rayleigh and Mie scattering; therefore, in the system being considered, photons should be recorded at a frequency ν_{32} which corresponds to the transition 3-2. It can also be assumed that the recording system integrates the fluorescence radiation over the time interval from t_1 to t_2, and therefore, the signal value can be taken as the total number of photons with the frequency ν_{32} radiated by a unit volume of the atomic cloud within the time $t_2 - t_1$

$$N_f = \int_{t_1}^{\tau_2} A_{32}\, n_3(t)\, dt \qquad (3.6)$$

The choice of the beginning and the duration of the integration interval $(t_2 - t_1)$ may have a considerable

influence on the experimentally-determined dependence of the fluorescence signal on the value ρ. For ease of calculation, it is assumed that t_1 coincides with the beginning of the laser pulse and t_2 with its end, so that the fluorescence signal is being integrated during the laser pulse [178].

In this case, the value N_f is determined by Equation (3.5)

$$N_f = \int_0^t A_{32}\, n_3(t)\, dt = n_T \frac{A_{32}}{A_{32} + Z_{32}} \cdot$$

(3.7)

$$\left\langle 1 - \frac{\xi_2 \exp(-\xi_1 t) - \xi_1 \exp(-\xi_2 t)}{\xi_2\ \xi_1} \right\rangle$$

For additional calculations, the values $\xi_{1,2}$ will now be expressed in an explicit form in terms of the rates of radiative and collisional transitions. For the case being considered ($R_{21} = 0$) from Equation 3.4, it is possible to obtain approximate expressions for $\xi_{1,2}$ [174, 177]

$$\xi_1 \simeq \frac{R_{13}\,R_{32}}{X} = \frac{\rho B_{13}(A_{32} + Z_{32})}{A_{31} + Z_{31} + A_{32} + Z_{32} + \rho B_{13}(1 + g_1/g_3)} \tag{3.8}$$

$$\xi_2 \simeq X = A_{31} + Z_{31} + A_{32} + \rho B_{13}(1 + g_1/g_3)$$

(Note that $\xi_2 > \xi_1$.) Now going back to Equation 3.7 for N_f, it can easily be shown that when the condition

$$\xi_1 \tau \geq 5 \tag{3.9}$$

is fulfilled, the expression for N_f is transformed with an accuracy of $\leq 3\%$ and Equation 3.7 becomes

$$N_f = n_T \frac{A_{32}}{A_{32} + Z_{32}} \tag{3.10}$$

This relationship shows that during the time τ determined from Equation 3.9, all atoms follow the cycle 1-3-2 and accumulate at the metastable level, and, in this case,

the total of photons N_t is determined by the quantum efficiency of fluorescence in the channel 3-2.

In the case under consideration, a saturation regime of the total fluorescence signal is realized since N_t in Equation 3.10 is independent of ρ. By using Equation 3.8, it is possible to rewrite Equation 3.9 as

$$\left[\frac{\rho B_{13} (A_{32} + Z_{32})}{A + Z + \rho B_{13} g} \right] \tau \geq 5 \qquad (3.11)$$

where the notations $A = A_{31} + A_{32}$, $Z = Z_{31} + Z_{32}$, and $g = 1 + g_1/g_3$ have been introduced. This condition can be fulfilled in various experimental situations.

In the high source intensity case, if the condition

$$\rho B_{13} g >> A + Z \qquad (3.12)$$

is realized, then the case of Equation 3.10 is fulfilled with

$$\tau \geq \frac{5\ g}{A_{32} + Z_{32}} \qquad (3.13)$$

This condition has a distinct physical sense. In a field with high energy density, saturation of the transition 1-3 is obtained so that populations of these levels are maintained in the saturated state ($n_3/n_1 \approx g_3/g_1$). In this situation, the rate of accumulation of the atoms at the metastable level is independent of the radiation power and is determined by the total rate of deactivation of the level 3 in the channel 3-2. In the absence of quenching ($Z_{32} << A_{32}$) the condition stated in Equation 3.13 is fulfilled for Pb at $\tau \geq 20$ ns.

In a weak field where relationship

$$\rho B_{13}\ g << A + Z \qquad (3.14)$$

is realized, the condition stated by Equation 3.11 is fulfilled for τ which satisfies the relation

$$\tau \geq \frac{5}{\rho B_{13}} \left\langle 1 + \frac{A_{31} + Z_{31}}{A_{32} + Z_{32}} \right\rangle \qquad (3.15)$$

Now the accumulation rate of atoms at level 3 is determined by the rate of induced absorption 1-3 and by the ratio of decay probabilities from level 3 in the channels 3-1 and 3-2. In the strong field, signal N_f would be saturated, as it would also be in the case where level 2 had a finite lifetime. In contrast to this, saturation in a weak field is possible only if a metastable level is available.

It can be shown that for Pb-type atom in an inert gas atmosphere and at a laser pulse duration $\tau = 5 \times 10^{-9}$ s, the approximation $\xi_1\tau \leq 1$ and $\xi_2\tau >> 1$ is valid. In this case neglecting exp $(-\xi_2\tau)$ in Equation 3.7 and retaining the first two terms in the expansion exp $(\xi_1\tau)$, the following equation is obtained [175]

$$N_f = n_T \frac{A_{32}}{A_{32} + Z_{32}} \left\langle 1 - \frac{\xi_2(1 - \xi_1\tau)}{\xi_2 - \xi_1} \right\rangle$$

$$\approx n_T \frac{A_{32}}{A_{32} + Z_{32}} \xi_1 \tau \qquad (3.16)$$

$$= n_T \frac{\rho B_{13} A_{32} \tau}{A + Z + \rho B_{13} g}$$

This expression illustrates a well known dependence of the fluorescence signal: the linear growth at small levels of ρ which satisfy Equation 3.14, the slowing down of the growth in the region $\rho B_{13}\, g \approx A + Z$, and saturation in the region of large ρ values satisfying Equation 3.12. The asymptotic value N_f is determined by

$$N_f^{MAX} \approx n_T \frac{A_{32}\, \tau}{g} \qquad (3.17)$$

It is important to note that when a metastable level is available, the atoms will follow the cycle 1-3-2 only once within time τ and when quenching occurs ($Z_{32} \neq 0$) only a part of these atoms will radiate photons of frequency ν_{32}.

The Case of Rapid Decay of Level 2

In this limiting case, a three-level system degenerates into a two-level one in which the upper level may decay with the probabilities A_{32} and A_{31} and emit photons of frequencies ν_{31} and ν_{32}.

Provided that $R_{21} >> R_{13}$, R_{31}, R_{32}, then Equation 3.4 for $\xi_{1,2}$ is transformed to

$$\xi_{1,2} \approx \frac{X + R_{21}}{2} \mp \frac{R_{21} - X}{2} \qquad (3.18)$$

where

$$\xi_1 \approx X \qquad \xi_2 \approx R_2 \qquad \text{and} \qquad \xi_2 >> \xi_1$$

In this case the solution of the system is transformed in such a way that $n_2(t) = 0$ and for $n_1(t)$ and $n_3(t)$ with regard to Equation 3.4

$$n_1(t) = \frac{n_T}{X} \left[R_{13} \exp(-Xt) + R_{31} + R_{32} \right] \qquad (3.19)$$

$$n_3(t) = \frac{n_T R_{13}}{X} \left[1 - \exp(-X\tau) \right]$$

Assuming a rectangular laser pulse the fluorescence signal can now be expressed as

$$N_f = N_T \frac{A_{32} R_{13}}{X} \left\langle \tau - \frac{1}{X} [1 - \exp(-X\tau)] \right\rangle \qquad (3.20)$$

In the case where the condition $X\tau >> 1$ is fulfilled, the above relationship becomes

$$N_T \approx n_T \frac{A_{32} R_{13}}{X} \left\langle \tau - \frac{1}{X} \right\rangle \approx n_T \frac{A_{32} R_{13}}{X} \tau \qquad (3.21)$$

This condition is approached when the system reaches a steady-state regime at which the fluorescence signal becomes

$N_f = n_3^{ss} A_{32} \tau$ where n_3^{ss} is the steady-state value of the population of the upper level.

The above expression coincides exactly with Equation 3.16. At small levels of ρ a linear mode of fluorescence is observed which transits to saturation at $\rho B_{13} g >> A + Z$. In the saturation mode, however, in the contrast to the case of a metastable level, the parameter $A_{32} \tau/g$ may be far in excess of 1, so that $N_f >> n_T$. From the physical viewpoint it indicates the presence of a cyclic interaction of the low-level system with the resonance field in the saturation regime; as a result of this interaction one atom repeatedly radiates photons during the interaction with the resonance field of radiation.

Optimization of Laser Radiation Parameters

Detection of trace concentrations of elements requires that the maximum possible signal-to-noise ratio (S/N) is realized. The methods for increasing and optimizing S/N depend considerably on experimental conditions and on the nature of the background signal in a specific analytical technique. This problem has been analyzed in detail in [184-186].

One of the first parameters that needs to be optimized is laser power. In the case where the background, which restricts the detection limits of the analysis, is not connected with the scattered laser radiation but is determined by the thermal radiation of the atomizer, noise in the recording system, etc., then it is advantageous to operate in the region of fluorescence saturation. In this case, the maximum level of the fluorescence signal is attained, and, consequently, the precision of the analysis is enhanced due to a decreasing contribution of the source fluctuations to the signal ones.

However, in the case where the background level is determined by the scattered radiation (Rayleigh and Mie scattering in the analytical volume, luminescence of the atomizer windows, etc.), there exists an optimum level of the value ρ at which the maximum S/N ratio is achieved. The importance of the optimum value of ρ is explained by the fact that the background increases linearly with increasing ρ, whereas the rate of growth of the signal $N_f(\rho)$ slows down, in the region where near saturation conditions are approached.

By writing the general expression for the fluorescence signal in the form [187]

$$N_f = C_1 \, n_T \frac{\rho}{\rho + \rho_s} \tag{3.22}$$

where C_1 is a constant accounting for the collection and recording of fluorescence and also for the specific model of the atom. In the case of the Poisson distribution of noise photoelectrons for the background fluctuations, which is determined by source induced scatter, one may write $N = C_2 \sqrt{\rho}$ where C_2 is a constant analogous to C_1. The signal-to-noise ratio in this case is

$$S/N = \frac{C_1}{C_2} \left\langle \frac{n_T \sqrt{\rho}}{\rho + \rho_s} \right\rangle \tag{3.23}$$

It can be shown that the maximum of this expression determined from $\partial(S/N)/\partial\rho = 0$ is attained at the optimum energy density

$$\rho^{opt} = \rho^s \tag{3.24}$$

In cases where the laser radiation is sufficiently intense, it will be advantageous to broaden the beam cross section and also increase the analytical volume, maintaining always the density of the excitation energy at the level ρ^{opt}.

Certain requirements arise in relationship to the duration of the laser pulse when trace concentration of Pb-type atoms are determined in nonflame atomizers. In this situation, when the power of laser radiation is close to the saturating one, the majority of atoms accumulate at the metastable level during a laser pulse, as it has been already established. In fact, in experiments with Pb atoms in an Ar atmosphere, it was found that with an intensity of laser radiation of about 10 kW cm^{-2} during a 5 ns pulse approximately 40% of the atoms are transferred into the metastable level [175]. Increasing the duration of the pulse at a fixed energy density ρ would lead to a decrease in the S/N ratio (e.g., the background grows in proportion to the pulse duration and the growth rate of the fluorescence signal decreases due to depletion of the ground state).

By using Equation 3.7, the number of signal photoelectrons recorded per single laser pulse can be written as

$$s = C_1 \left(1 - \frac{\xi_2 \exp(-\xi_1 \tau) - \xi_1 \exp(-\xi_2 \tau)}{\xi_2 - \xi_1} \right) \qquad (3.25)$$

where C_1 is a constant accounting for certain parameters of the atomic system and other collection parameters (solid angle, volume, efficiency of the photomultiplier tube, etc.). During the total time of evaporation of the sample, Δt, the total number of signal photoelectrons, S, is

$$S = s \, \Delta t \, f \qquad (3.26)$$

where f is the laser repetition frequency. The total number of background photoelectrons within the same time is

$$N = (C_1 n_b + n_d) \tau \, \Delta t \, f \qquad (3.27)$$

where n_d is the number of dark photoelectrons per second and n_b is the number of background photoelectrons due to scattering of laser radiation and to the thermal radiation of the atomizer. Assuming again Poisson statistics of the background photoelectrons, we write an expression for S/N ratio as follows

$$S/N = K \sqrt{\Delta t f}\, \sqrt{\tau} \left\langle 1 - \frac{\xi_2 \exp(-\xi_1 \tau) - \xi_1 \exp(-\xi_2 \tau)}{\xi_2 - \xi_1} \right\rangle \tag{3.28}$$

In experiments with Pb [175], it has been shown that the maximum value of S/N is attained at

$$\tau_{opt} = \frac{1}{\xi_1} + \frac{2}{\xi_2} \tag{3.29}$$

Introducing values for ξ_1 and ξ_2 calculated from typical parameters produces a $\tau_{opt} \approx 7$ ns when $\xi_1 = 2 \times 10^8\ s^{-1}$ and $\xi_2 = 2.8 \times 10^9\ s^{-1}$.

A third laser parameter that may improve the detection limit is the laser repetition frequency, f. The value of f^{opt} can be reasonably increased up to values of the order of τ_o^{-1}, where τ_o is the smallest of two times: the lifetime of the atom at the metastable level or the time of residence of the atom in the analytical volume. For Pb, the lifetime of the level 7s $^3P_1^\circ$ at atmospheric pressure was given previously as 1.8×10^{-5} s. The residence time of the atom in an

analytical volume of diameter 1 cm (assuming that a graphite cup is used) at thermal velocities 10^5 cm/s is also $\approx 10^{-5}$ s.

Thus, in an experiment where Pb atoms are being determined, the optimal repetition frequency is of the order of 10^5 Hz. A dye laser excited by a Cu vapor laser can work in the kHz range. A frequency increase up to 10 kHz can enhance the sensitivity by at least 10 times.

It is also worth noting that by decreasing the laser linewidth to a value of the order of the absorption linewidth ($\Delta\lambda \approx 0.003$ nm) while maintaining the same spectral brightness could also provide a small increase in sensitivity owing to the fact that the background radiation level would decrease.

The previous discussion has pointed out a number of considerations that the analyst faces when choosing an appropriate laser system to be used as a source for LEAFS in nonflame atomizers. Experiments where all of the predicted optimization parameters are used or at least closely approached need to be performed.

Optimization of Atomization Efficiencies

In addition to the optimization of the laser spectrometer system, it is very important for the efficiency of atomization to be optimized to improve the overall

performance of the analytical method. Considering the maximum analyte atom density during the transient signal that is delivered by electrothermal atomizers (ETA), the atomization efficiency at this moment may be defined as

$$\eta_{ap} = \frac{N_{ap}}{N_{ai}} = f_{sl}\,(t_p, \tau_1, \tau_2)\,\eta_t\,\beta(T) \qquad (3.30)$$

where N_{ap}, and N_{ai} are the number of analyte atoms within the observation volume at the peak maximum and the number of analyte atoms which is introduced, respectively; f_{sl} is the supply-loss function depending on time t, volatilization time τ_1, and residence τ_2; η_t is the fraction of sample transported into the atomizer itself, which in most cases is assumed to be unity; $\beta(T)$ is the fraction of the analyte in the atomic form and is assumed to be unity for further considerations (i.e., molecule formation and ionization will be ignored) [188, 189].

Now, using these assumptions the atomizer efficiency can be expressed as

$$\eta_{ap} = f_{sl} = \left[1 - \exp \left\langle \frac{-\tau_1}{\tau_2} \right\rangle \right] \frac{\tau_2}{\tau_1} \qquad (3.31)$$

The residence time, τ_2, can be calculated using a relatively simple model formulated by L'Vov et al. [141]. For gas-stop conditions

$$\tau_2 = l^2/8D \qquad (3.32)$$

where l is the tube length and D is the diffusion coefficient ($m^2\ s^{-1}$) which is inversely proportional to the gas pressure and is temperature dependent. The atomic number density within a tube atomizer then becomes

$$n_a = \frac{C_a V_s N_a \tau_2}{l r^2 M \tau_1} \left[1 - \exp \left\langle \frac{-\tau_1}{\tau_2} \right\rangle \right] \qquad (3.33)$$

where C_a and V_a are the analyte concentration and the sample volume, respectively, N_a is Avogadro's number, r is the tube radius, and M is the molar mass of the analyte.

A cup atomizer is usually operated with a purge gas flow to minimize oxidization. When the residence time of the analyte within the observation zone is short compared with the volatilization time, then the atomic density can be expressed as

$$N_a = \frac{C_a V_s N_a}{S_a M \tau_1 \bar{V}_a} \tag{3.35}$$

where S_a is the cross section of the atom cloud perpendicular to the direction of the gas flow, and $\bar{V}_a$ is the average velocity of analyte atoms within the observation zone.

The atomic density within the atomizer can be determined by measuring the atomic-absorption signal or the fluorescence signal. A very good example of this is given in the work at L'Vov et al. [190] and Slavin and Carnrick [191] for the case of atomic absorption spectrometry. The important issue from the fluorescence point of view is that by calculating the atomic density in the atomizer, the atomization efficiency can be calculated. With this data and additional data on diffusion coefficients [189, 192,

193], the residence time of the atoms can be obtained. The residence time of the atoms is a very important parameter to optimize especially when the atomic number density in the atomizer is very small and the fluorescent signal can be enhanced by giving the probing laser beam the chance to interrogate the vapor cloud for a much longer time.

CHAPTER 4
EXPERIMENTAL

The general experimental system used for all experiments is shown in Figure 4-1. The basic setup can be divided into three parts: the laser system, the furnace system, and the detection. Since in this work three different laser systems, three different furnace systems, and three different detection systems were used, it is justified to divide the experimental discussion into three parts.

Nitrogen Pumped Dye Laser System

Laser System

The nitrogen-pumped dye laser (Model DL-II dye laser, Molectron; UV-24 nitrogen laser, Molectron, Palo Alto, CA) was operated at 20 Hz. The dye laser output had a spectral linewidth of 0.015 nm (full width half maximum, FWHM), a pulse width of 5 ns, and a typical pulse energy of 0.8-1.1 mJ in the region (520-620 nm) where the laser was used. In addition, several non-linear crystals were used to produce second harmonic generation (SHG). A total of four cells in a single unit, each cell containing a different potassium dihydrogen phosphate (KDP) crystal (e.g., cut at a different

Figure 4-1. General Experimental Block Diagram for the Laser Excited Atomic Fluorescence Experiments.

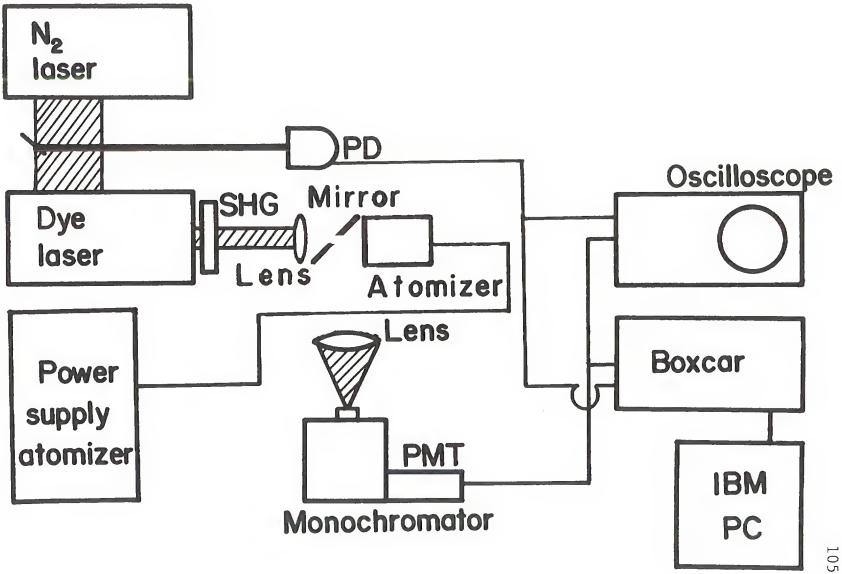
N_2 laser
PD
Oscilloscope
Dye laser
SHG
Mirror
Lens
Atomizer
Power supply atomizer
Lens
Boxcar
PMT
IBM PC
Monochromator

angle) was used to cover the range of 265-310 nm (Model 562-126, INRAD, Northvale, NJ). Finally, it is important to note that a copper mesh shield is used to enclose the N_2 pump laser to prevent radiofrequency interferences in the electronic detection system.

The dye laser was operated according to the manufacturer's instructions. Static dye cuvettes were used every time. Although this dye laser system is equipped with a flowing dye system, the use of the static cuvettes proved to be as effective not only in terms of laser output power but in terms of photochemical deterioration of the dye solutions. More specifically, the dye laser performed for more than seven hours before any noticeable reduction in power occurred. The three dyes (Exciton, Dayton, OH) used during these experiments are given in Table 4-1. In the case of the lead experiments, it was necessary to shift the maximum wavelength of emission for the Coumarin 540A dye. This process was achieved by the addition of a couple of drops of Rhodamine 6G dye solution as reported by Drullinger [194]. The addition of this dye shifted the maximum emission wavelength of C540A by about 10-12 nm.

In order to improve the second harmonic generation process (also known as frequency doubling), the visible

TABLE 4-1. WAVELENGTH COVERAGE PROVIDED BY THE DIFFERENT DYE SOLUTIONS USED IN THE LEAFS-ETA EXPERIMENTS

Laser System	Laser Dye	Wavelength Range (nm)	Solvent	Concentration (molar)
N_2	Coumarin 540 A	515-583	ethanol	1×10^{-2}
N_2	Rhodamine 590	568-605	ethanol	5×10^{-3}
Nd:YAG	Rhodamine 590	552-584	methanol	2.5×10^{-4} [a] 1×10^{-4} [b]
Cu Vapor	Rhodamine 590	555-584	methanol	4×10^{-4}
Cu Vapor	Rhodamine 590	559-606	methanol	1×10^{-3}
Cu Vapor	Rhodamine 590 & Kiton Red	575-614	methanol	8.8×10^{-4} [c] 2.1×10^{-4} [c]

[a] oscillator cell
[b] amplifier cell
[c] laser dye mixture

output from the dye laser was passed through a focusing lens (150 mm focal length). The non-linear crystal was carefully aligned with this beam and positioned at an intermediate distance before the focal point of the lens. In fact, to avoid optical damage, it is important not to focus the laser beam inside the crystal. By doing this the output energy per pulse increases greatly, producing enhancements of 3-6 times as compared with no focusing at all and the typical pulse energies in the UV region ranges from 15-60 μJ. A color filter (UG-11, Corion Corp., Holliston, MA) is used to separate the UV light from the visible output.

Furnace System

Two different graphite tube atomizer systems were used. The first furnace system (Figure 4-2) was a homemade version of any typical, commercially available, Massman type graphite tube furnace (e.g., Perkin Elmer, Model 2100, Perkin-Elmer Corp., Norwalk, CT). It consisted of a pair of brass blocks mounted on top of a square phenolic block. The two brass blocks are machined to fit a pair of graphite contact rings that contain the graphite tube. By using this configuration, it is possible to maintain different flows of inert gas (Ar) inside of the graphite tube and outside of the tube. To achieve good electrical contact a fastener is

Figure 4-2. Graphite Tube Electrothermal Atomizer (Homemade Version).

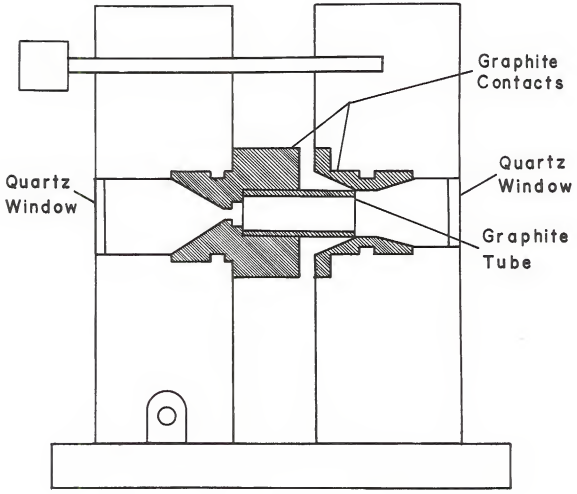

Graphite Tube Furnace

placed between the two brass blocks and with the help of a metal spring the graphite tube stays in position during the experiment. Quartz windows are set on each side of the graphite tube atomizers, but they are not required for its operation. The heating power is provided by a pair of SCR power supplies (SCR 20-250, Electronics Measurements, Neptune, NJ) connected in series and the flow of inert argon gas was controlled by a pair of flowmeters (Matheson Gas Prod., Secaucus, NJ).

The heating rate and the final temperature of the graphite tube were controlled by the voltage setting on the power supply and also by a timing circuit. The power supply was programmed so that the output is linear with the resistance in the controlling circuits [195], with 100 Ω corresponding to full power. The length of heating time was controlled by a timer chip (555, Texas Instruments, Dallas, TX) which controls a relay (W171 DIP-12, Magnecraft, Chicago, IL). The normally closed (NC) relay pins were parallel with a 100 Ω resistor. This parallel circuit was in a series with a 0-25 Ω variable resistor. The circuit was then connected to two programming imputs on the power supply.

With the switch of the relay in its normally closed position, there was no significant resistance in the controlling circuit. The drying cycle was controlled manually by the 0-25 Ω variable resistor. After drying, a pushbutton was used to initiate the atomization cycle. When the 555 timer was started, it sent a signal activating the relay. The normally closed switch was opened, causing the 100 Ω resistance in the controlling wires of the power supply, and thus initiating the set maximum output power on the power supply. The amount of time the system was activated was controlled by a timing capacitor (10 μF), and a timing resistor (0-5 MΩ). A variable resistor was used so that the atomization time could be varied between 0 and 5 s. By setting the maximum output voltage on the power supply and also setting the atomization time with the timing resistor and capacitor, the graphite tube could be reproducibly heated up to any specified temperature. The temperature of the graphite furnace was measured with an optical pyrometer (Model 87C, Pyro, Bergenfield, NJ).

The second atomization system used is an HGA-2200 (Perkin-Elmer Corp., Norwalk, CT) which operation is described in [196]. This system provides three main advantages over the homemade version. First, all the heating steps

(drying, ashing, atomization and cleaning) are controlled by the internal electronics in the power supply; second, the atomization temperature is easily measured with a calibrated photodiode installed on the atomizer and also controlled by the electronics of the power supply; and third, the operator can choose between two different rates of atomization depending on the type of element being determined.

Detection Electronics

The laser beam is directed through the furnace tube and into an air-acetylene flame which served the purpose of tuning the laser to the appropriate transition by aspirating into it a relatively high concentration solution of the elements sought and recording the resulting fluorescence signals. The fluorescence light is collected with a medium luminosity monochromator (Model EU-70, Heath, Acton, MA), and converted into an electrical signal by using a photomultiplier tube wired for pulsed operation (Model R1414, Hamamatsu, Bridgewater, NJ). The output from the photomultiplier tube was converted to a voltage with a 1 KΩ resistor amplified via an Evans voltage amplifier and sent into a boxcar integrator (Stanford Research Corporation, Palo Alto, CA). The output of the boxcar integrator was inputed to an analog-to-digital converter which was interfaced with a

computer for data acquisition, analysis, and storage. A chart recorder was also used, mainly during the optimization of the analytical measurement system.

As shown in Figure 4-3, the laser beam was axially directed along the furnace tube and the resulting fluorescence collected with a plane mirror which had a hole (ϕ = 3 mm) in the center to allow the exciting of the laser beam and which was positioned at 45° with respect to the excitation axis. A lens was used to image the center of the tube at the entrance slit of the fluorescence monochromator. A slight demagnification factor assured the matching of the monochromator and the fluorescence collection solid angles. Another lens is used to focus the laser beam just beyond the hole drilled in the plane mirror so that direct reflection of laser photons into the direction of the monochromator could be minimized. Nevertheless, some photons (due to diffraction effects as well as scattering from the optical components) will always find their way into the detection system. This negates any possibility of measuring resonance fluorescence with the present optical arrangement. The use of color filters, such as LG370 and WG320, (Corion Corp., Holliston, MA) in the fluorescence optical path was therefore compulsory in order to isolate the fluorescence

Figure 4-3. Detailed Scheme of the Excitation-Detection Arrangement. The laser beam is focused by the lens at the central hole of the plane mirror.

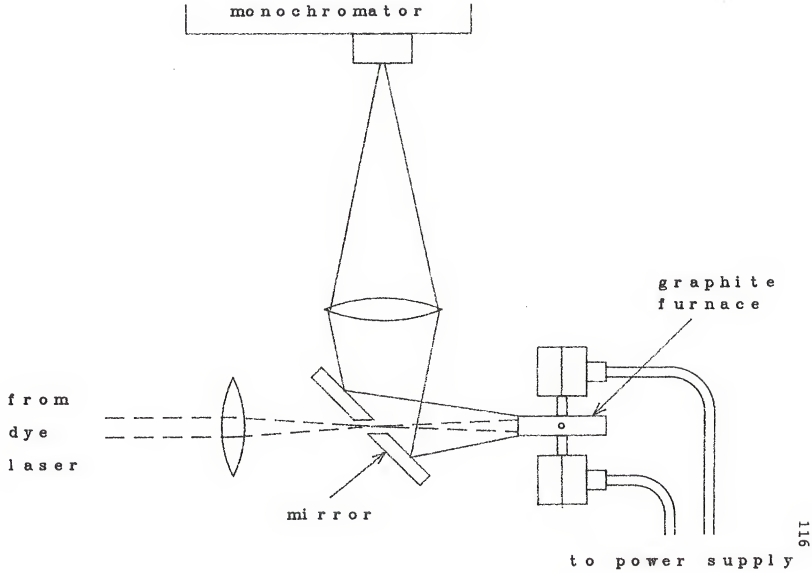
monochromator
graphite
furnace
from
dye
laser
mirror
to power supply

transitions from the laser excitation wavelengths. In order to keep stray light from entering the detection system (from sources other than the laser), all the experiments were performed at night and with all the room lights turned off until the end of the experiment.

One more additional detection system was utilized with the N_2 laser system. It consisted of a monochromatorless light collection apparatus designed by Bomen (Bomen, Quebec, Canada) (Figure 4-4) to be used in their Fourier Transform Interferometer as a collection accessory for Laser Raman Near-Infrared Fourier Transform Spectrometer. The main components of the collection optics accessory are an aluminum structure that holds a 90° off-axis ellipsoidal mirror, an aperture, and a filter holder. The off-axis ellipsoidal mirror has a hole (ϕ = 8 mm) drilled through the reflecting surface which is used to direct the laser beam after it passed through the graphite tube atomizer. The tube is imaged in front of the off-axis mirror in the axial direction which then transversally reflects and focuses this image on the aperture. By placing a narrow bandwidth interference filter ($\Delta\lambda \approx 10$ nm) (Schott, Opt. Glass, Duryea, PA) in front of the aperture, a fluorescence signal was detected when a photomultiplier tube housing (R955, Hamamatsu,

Figure 4-4. Schematic of the Non-Dispersive Optical Collection Apparatus.

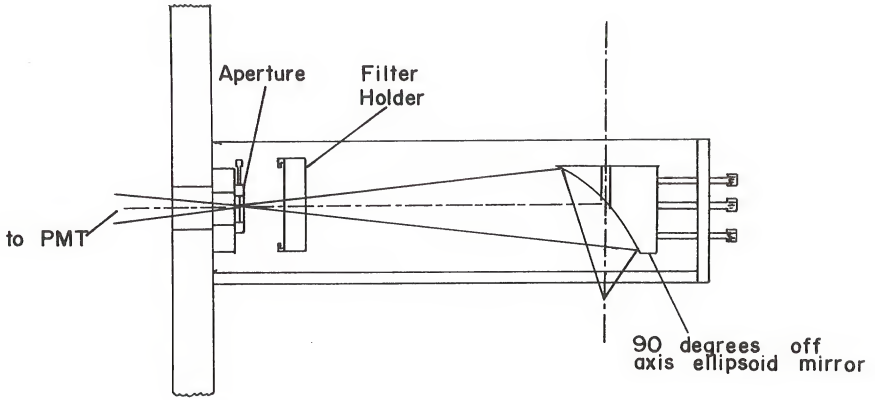

Bomem Collection Optics Accessory

Bridgewater, NJ) was attached after the aperture. All the detection electronics after the photomultiplier tube and the considerations on minimization of laser-induced scatter are similar to the ones described above (see Table 4-2).

Nd:YAG Pumped Dye Laser System

Laser System

A block diagram of the experimental setup is shown in Figure 4-5 and a detailed listing of the experimental components is described in Table 4-3. A frequency doubled ND:YAG laser (i.e., 532 nm) operated at 30 Hz was used as the pumping source for a dual dye laser system. The pump beam was split equally to pump each dye laser, though in this experiment only one dye laser head is used. Typical output energies from the frequency-doubled Nd:YAG laser was 250 mJ per pulse with a pulse duration of 12 ns. To obtain laser light at 283.306 nm for the Pb experiments a solution of Rhodamine 6G in methanol is continuously being flowed through the dye laser cuvettes. It is important to note that the dye concentration in the oscillator is different from the dye concentration in the amplifiers as recommended by the manufacturer [197]. After optimization, the visible laser light is passed through a KDP frequency doubling crystal where, with the use of an autotracking system, the

Figure 4-5. Block Diagram of the Nd:YAG Pumped Dye Laser System, Graphite Furnace, Atomic Fluorescence Spectrometer.

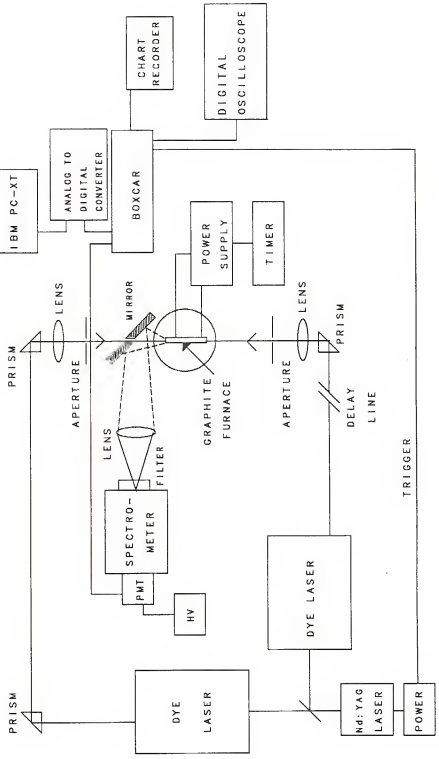
IBM PC-XT
ANALOG TO DIGITAL CONVERTER
BOXCAR
CHART RECORDER
DIGITAL OSCILLOSCOPE
POWER SUPPLY
TIMER
LENS
MIRROR
PRISM
APERTURE
LENS
FILTER
SPECTRO-METER
PMT
HV
GRAPHITE FURNACE
APERTURE
LENS
PRISM
DELAY LINE
TRIGGER
DYE LASER
DYE LASER
Nd:YAG LASER
POWER

TABLE 4-2. EXPERIMENTAL COMPONENTS FOR THE N_2 LASER PUMPED DYE LASER-GRAPHITE FURNACE ATOMIZER-ATOMIC FLUORESCENCE SPECTROMETER

Component	Model No.	Manufacturer
N_2 laser	UV-24	Molectron, Palo Alto, CA
Dye Laser	DL-II	Molectron, Pala Alto, CA
Frequency Doublers	562-126	INRAD, Northvale, NJ
Graphite Tube and Timing Furnace	--	Laboratory constructed
Furnace Power Supply	SCR 20-250	Electronics Measurements, Neptune, NJ
Graphite Furnace Atomizer	HGA-2200	Perkin-Elmer Corp., Norwalk, CT
Micropipette	--	Brinkmann Instrum. Co., Westbury, NY
Quartz Lenses	--	Esco Products, Inc., Oak Ridge, NJ
MgF_2 Lens	--	Optics for Research, Caldwell, NJ
0.35 m Monochromator	EU-70	McPherson, Acton, MA
Neutral Density Filters	--	Corion Corp., Holliston, MA
Color Glass Filters	WG-320 LG-370	Corion Corp., Holliston, MA

TABLE 4-2--continued

Component	Model No.	Manufacturer
Photomultiplier Tubes	R1414 R955	Hamamatsu Corp., Bridgewater, NJ
High Voltage Power Supply	226	Pacific, Concord, CA
Amplifier	4131	Evans Assoc., Berkeley, CA
Fast Amplifier	SR 240	Stanford Research Systems, Palo Alto, CA
Boxcar Averager Gated Integrator	SR 250	Stanford Research Systems, Palo Alto, CA
Computer Interface	SR 245	Stanford Research Systems, Palo, Alto, CA
Computer	PC-XT	IBM Corp., Boca Raton, FL
Oscilloscope	--	Tektronix, Inc., Beaverton, OR
Chart Recorder	D-5000	Houston Instruments, Austin, TX
Special Optics Collection Accesory	--	Bomem Quebec, Canada

TABLE 4-3. EXPERIMENTAL COMPONENTS FOR THE Nd:YAG LASER PUMPED DYE LASER-GRAPHITE FURNACE ATOMIZER-ATOMIC FLUORESCENCE SPECTROMETER

Component	Model No.	Manufacturer
Nd:YAG laser	YG 581-30	Quantel International, Santa Clara, CA
Dual Dye Laser	TDL 50	Quantel International, Santa Clara, CA
Frequency Doublers	HD 50	Quantel International, Santa Clara, CA
Graphite Tube and Timing Circuit	--	Laboratory constructed
Furnace Power Supply	SCR 20-250	Electronics Measurements, Neptune, NJ
Micropipette	--	Brinkmann Instrum. Co., Westbury, NY
90° Quartz Prisms and Quartz Lenses	--	Esco Products, Inc., Oak Ridge, NJ
0.22 m Double Monochromator and Scan Controller	1680 B CD2A	Spex Industries, Inc., Edison, NJ
Neutral Density Filters and Color Glass Filters	--	Corion Corp., Holliston, MA
Photomultiplier Tube	R955	Hamamatsu Corp., Bridgewater, NJ
High Voltage Power Supply	301	Bertan Assoc. Inc., Hicksville, NY
Amplifier	4131	Evans Association Berkeley, CA

TABLE 4-3--continued

Component	Model No.	Manufacturer
Boxcar Averager Gated Integrator	SR 250	Stanford Research Systems, Palo Alto, CA
Computer Interface	SR245	Stanford Research Systems, Palo Alto, CA
Computer	PC-XT	IBM Corp., Boca Raton, FL
Digital Oscilloscope	2430 A	Tektronix, Inc., Beaverton, OR
Chart Recorder	D-5000	Houston Instruments, Austin, TX

angle matching condition is achieved and the maximum UV (283.306 nm) output is obtained. The fundamental and the second harmonic waves are separated in this case by a dispersive Pellin-Broca quartz prism. The output energies at these wavelengths are of ~ 1 mJ per pulse. It is important to note that this system is a complete commercial unit, and it is operated according to the manufacturer's instructions; consequently, there has been no modifications made to this system.

Furnace System

The graphite tube atomizer system (Figure 4-6) was similar to the one designed by Molnar et al. [198] and then modified by Goforth and Winefordner [171]. The tube dimensions were 36 mm in length with an internal diameter of 4 mm. It consisted of two water-cooled brass blocks mounted on a bakelite support serving the purpose of holding the graphite tube and providing the necessary electrical contact with two stainless steel plates screwed into the top of the brass blocks. A flow of argon gas was maintained above and around the tube. In order to obtain a small gas flow inside the graphite tube, two small bore stainless steel tubes were positioned very close to each end of the tube. The flow rate was adjusted with calibrated flowmeters (Dwyer Instr.,

Figure 4-6. Schematic of Graphite Tube Electrothermal Atomizer.

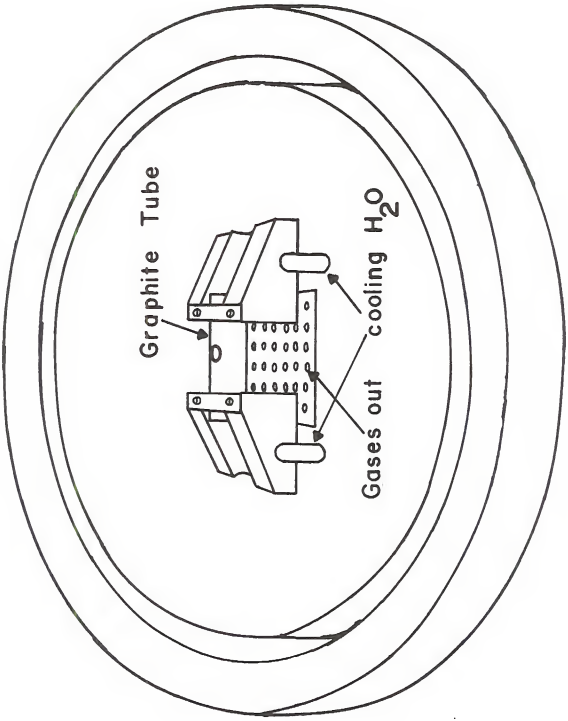
Graphite Tube
cooling H_2O
Gases out

Michigan City, IN). The heating rate and the final temperature were controlled in the same way as in the first furnace system described in the N_2 laser pumped dye laser system.

Detection System

The detection electronics for this system are basically identical to the ones already described with two exceptions. In this system, a 0.22 m double monochromator (Spex Industries, Inc., Edison, NJ) is used and as in the monochromatorless collection accessory the photomultiplier tube is a R955 (Hamamatsu Corp., Bridgewater, NJ).

Copper Vapor Pumped Dye Laser System

Laser System

The configuration of this system is similar to the previous two systems already described. A copper vapor laser (Model 251, Metalaser Tech, Pleasanton, CA) is used for another group of experiments. This pulsed laser operates at a 6kHz repetition rate with an average power of ~ 14-18 W. A dye laser (Molectron DL-II, Laser Photonics, Orlando, FL) equipped with a flowing dye, laser cuvettes system is pumped by the copper vapor laser. The fundamental (visible) laser output is frequency doubled to obtain the necessary transitions in the UV regions for the excitation of the elements being determined. The output energies per

pulse are typically 200-500 nJ, the pulsewidth is ~ 20 ns, and the spectral bandwidth is 0.02 nm.

Furnace System

The graphite tube atomizer system used with this laser system is a Varian CRA-90 (Varian Instrument Division, Palo Alto, CA). This commercial system has been described in the literature [199] and basically consists of a small graphite tube (18 mm length, 3 mm I.D.) mounted between two graphite contact electrodes set between two water-cooled stainless steel blocks. It presents the great advantage of allowing the analyst to utilize graphite tube, rod, and cup atomizers. In contrast to the commercial furnace described in a previous section, this model allows the use of different rates of atomization ($25^{\circ}C\ s^{-1}$ to $800^{\circ}C\ s^{-1}$). In addition, because of the small size of the graphite tube, during the ashing and atomization steps, this atomizer achieves the greatest level of isothermality; on the other hand, the size produces very short residence times for the atoms which in some cases can be a disadvantage.

Detection Electronics

In this system, all the components used for the detection of the atomic fluorescence are as described in the two previous sections with the exception of the fluorescence

monochromator. A Spex Minimate 0.25 m medium resolution monochromator is used. Because of the inability of the analog-to-digital converter (ADC) to digitize data at a rate faster than 1.2 kHz, it is necessary to divide the trigger digital signal (busy output) coming out of the boxcar integrator by a multiple of 10, in this manner, the ADC working at 600 Hz rate (6000/10) can transfer all the data points taken since this interface contains a buffer memory which accumulates untransferred data points. Accordingly, a simple ÷ 10 circuit is added to the detection electronics system. One more note about this system is that in order to alleviate the problem of radiofrequency interferences (RFI) produced by the Cu vapor laser the use of electronic RFI filters is necessary since due to the size of the laser enclosure and the constant need of opening it, it is impossible in this case to build a Faraday cage around the laser as we described for the N_2 laser (see Table 4-4).

Preparation of Solutions

Stock solutions of 1000 μg/mL for most elements were prepared from reagent grade chemicals in deionized water as described in [200, 201]. In other cases, the stock solutions were obtained from commercial sources (Spex Industries, Edison, NJ). Working solutions were prepared by

TABLE 4-4. EXPERIMENTAL COMPONENTS FOR THE CU VAPOR LASER PUMPED DYE LASER-GRAPHITE FURNACE ATOMIZER-ATOMIC FLUORESCENCE SPECTROMETER

Component	Model No.	Manufacturer
Cu Vapor Laser	251	Metalaser Tech., Pleasanton, CA
Dye Laser	DL-II	Laser Photonics, Orlando, FL
Frequency doubler	562-126	INRAD, Northvale, NJ
Graphite Tube Atomizer	CRA-90	Varian Instrum. Div., Palo Alto, CA
Micropipette	--	Brinkmann Instrum. Co., Westbury, NY
0.25m Monochromator	Minimate	Spex Industries, Edison, NJ
Color Glass and Neutral Density Filters	--	Corion Corp., Holliston, MA
Photomultiplier Tube	R955	Hamamatsu Corp., Bridgewater, NJ
High Voltage Power Supply		Laboratory constructed
Amplifier	4131	Evans Assoc., Berkeley, CA
Boxcar Averager Gated Integrator	SR 250	Stanford Research Systems, Palo Alto, CA
Computer Interface	SR 245	Stanford Research Systems, Palo Alto, CA

TABLE 4-4--continued

Component	Model No.	Manufacturer
Computer	PC-XT	IBM Corp., Boca Raton, FL
Oscilloscope	--	Tektronix, Inc., Beaverton, OR
Chart Recorder	D-5000	Houston Inst., Austin, TX

serial dilution from the stock solutions on a daily need basis. For some of the lead experiments we used ultrapure water (Seastar, Seattle, WA) to prepare a group of dilutions; otherwise, deionized (Barnstead, Newton, MA) water was used.

Cleaning of Glassware

All volumetric pipets were allowed to stand for 24 hours in a detergent solution; then, they were rinsed thoroughly with distilled water, concentrated nitric acid, and deionized water prior to their use. Volumetric flasks (10 mL) were allowed to stand in concentrated nitric acid (HNO_3, reagent grade) for 24 hours, then rinsed with distilled and finally deionized water.

CHAPTER 5
RESULTS AND DISCUSSION

Rationale

The first part of this work consisted of an extensive characterization of the Laser Atomic Fluorescence Spectrometry method when combined with electrothermal tube atomizers from the point of view of sensitivity and efficiency of signal detection. For this task, only single-step laser excitation was necessary and lead (Pb) which possesses a very sensitive direct line fluorescence detection scheme was selected as the best possible case. This scheme consists of excitation at 283.31 nm ($6p^2\ ^3P_0 \rightarrow 7s\ ^3P_1^\circ$) and the corresponding monitoring of fluorescence at 405.78 nm ($7s\ ^3P^\circ \rightarrow 6p^2\ ^3P_2$) (see Figure 5-1). As noted before, the use of a nonresonance transition will minimize the problem of laser scatter. Furthermore, at the excitation wavelength, the three laser systems used are able to operate very efficiently, (e.g., second harmonic generation is carried out under optimal conditions). Finally, lead is easily atomized in graphite tube furnaces at temperatures of about 1600°C,

Figure 5-1. Partial Grotrian Diagram for Lead.

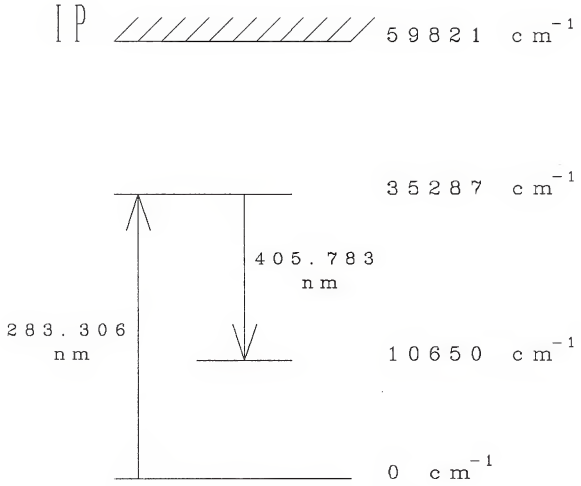

Lead

meaning that background emission at the emission wavelength produced by the hot graphite tube is significantly reduced.

One more consideration for the selection of lead is the current need for an ultrasensitive method to determine this element. Even in the early days of atomic fluorescence spectrometry, there were several reports dedicated solely to its determination [202, 203]. Today lead is recognized as a very important environmental pollutant [204]. Its toxicology is the object of a great deal of research [205] and the demand for methods of direct analysis at concentrations in the sub-parts per trillion range keeps increasing. A very good example of this need comes from the characterization of the concentration of lead in the Antarctic and Arctic circles [206-209]; such studies can give an estimate of the influence of industrial inputs as compared to the natural sources of atmospheric lead, such as continental dust, volcanoes, and sea spray. In the past, this type of work was carried out using graphite furnace atomic absorption spectrometry preceded by an extensive preconcentration step [210]. At this time, it is felt that the technique of laser excited atomic fluorescence spectrometry using electrothermal atomizers deserves to be considered as the method of

choice for such tasks. The discussion that follows will examine why this method presents such high expectations.

Preparation of Graphite Tubes and Electrodes

Since two of the furnace atomizers used were homemade, it was necessary to construct graphite tubes that will fit in them. All the tubes were made from Ringsdorff (Sigri Corp., Somerville, NJ) graphite tube stock. These tubes were cut to the specific length and a single hole was drilled on each of them to allow sample injection. The tubes used with the N_2 laser pumped dye laser system were 28 mm in length and their outer diameter was 6 mm (inner diameter 4 mm). The tubes used with the Nd:YAG laser pumped dye laser system were 34 mm in length and their outer diameter was also 6 mm (i.d., 4mm). The tubes used with the Cu vapor laser pumped dye laser system were obtained from a commercial source (Buck Scientific, Norwalk, CT). The tubes and electrodes used in this furnace are the ones recommended by the manufacturer. There tubes were 18 mm in length and 5 mm outer diameter (3 mm inner diameter).

It is important to note that all the graphite tubes used in these experiments were pyrolytically coated. The use of pyrolytically coated graphite presents a number of advantages over normal graphite, such as an increased

lifetime, low permeability, and a high resistance to oxidation [128, 130, 211]. It is also important to remark that contrary to some other recent works [36, 110, 162, 163], no additional holes were drilled on the graphite tubes to serve as ports for observation of fluorescence or to allow the passage of the laser radiation. Graphite tubes without modification produce a better atomization efficiency because there are no losses of mass due to the additional openings.

Heating Rates

The optimization of the heating rate is an important parameter leading to maximum sensitivity. For the lead case, it was found that the largest signals were obtained when a very high temperature (and hence a very fast heating rate) was set on the power supply of the electrothermal atomizer while a short amount of time was set on the timing circuit. In this way, a low atomization temperature became accessible with a high heating rate. This approach is certainly useful to improve the detection limit of readily volatile elements but it may not be practical for other elements or in the case of real samples where matrix interferences need to be minimized by maintaining a constant atomization temperature. The use of modern commercial furnace controllers is recommended since they are capable of

achieving fast heating rates over a large range of final temperatures [212-214].

A 2.5 s atomization time while using more than 200 A to heat the graphite tube proved to be the best conditions for our experiments. These conditions provided heating rates of $\sim 700^{\circ}C\ s^{-1}$ with final temperatures between 1600-1800°C for all the three furnace systems. Under these conditions the pyrolitic coating on the tubes proved to be very useful since about 75 atomizations were possible before replacement became necessary.

Imaging Considerations and Furnace Emission

The imaging of the fluorescence at the monochromator entrance slit was found to be of critical importance. By careful selection of the optical components, especially focusing lenses, it is possible to spatially resolve the blackbody emission from the atomic fluorescence signal. The image of the tube consisted of a bright ring surrounding a dark circle and the size of the ring depended on the positioning of the focusing lens. As stated in Chapter 4, in order to match the solid angles of the monochromator and the optical detection system, a slight magnification of the image was produced. The use of an iris diaphragm in front

of the entrance slit was used to mask the bright ring allowing the dark region to pass through the dispersive system.

Reduction of Laser Scatter

The use of a nonresonance transition like the one used in this work should initially guarantee almost complete elimination of source induced scatter. In the lead case, "environmental" (also known as "white") fluorescence becomes an important factor. Environmental fluorescence arises when ultraviolet light impinges on optical apparatuses, such as mirrors and lenses, which generate a large number of fluorescent photons in the region of 290-420 nm [215, 216]. Since the laser beam is directed through a very small hole drilled on a mirror even with the most careful alignment it was impossible to eliminate this problem. The use of glass filters certainly helped to minimize the influence of "white" fluorescence, but still at the analytical fluorescence wavelength [405.78 nm] a considerable scatter signal was measured.

Effect of the Monochromator Slit Width

The effect of the slit width on the fluorescence signal, background signal, and blank noise was studied for a 100 pg (10 mg/ml) of a lead standard. The signal-to-noise ratio decreased when the slits were decreased from 2 mm to

0.5 mm and also decreased when the slits were increased from 2 mm to 4 mm. These results were observed with the Nd:YAG laser pumped dye laser system where a 0.22 m double monochromator is used. In the other two systems, the slit widths used were 2 mm for the N_2 laser system and 1.25 mm for the Cu vapor laser system which maintains spectral bandpasses of 4 and 10 nm since the reciprocal linear dispersion on the spectrometers used were 2 nm/mm and 8 nm/mm, respectively. As observed by Michel et al. [110], the signal-to-noise ratio should be independent of the slit width and the observed degradation due to variations of the slit width could be attributed to a non-uniform intensity distribution of the furnace image in the plane of the entrance slit. All the detection limits reported, for the three systems, were determined with 2 mm slit width for the Nd:YAG and N_2 laser systems and a 1.25 mm slit width for the Cu vapor laser system.

Fluorescence Measurements

All measurements were carried out using the optical detection systems described in the previous chapter. The tuning of the laser to the 283.30 nm excitation line for lead was achieved by using an air-acetylene flame as described in the experimental section. The insertion of a

polypropylene pipet tip at the injection port of the graphite tube is used to scatter some laser light into the monochromator, and with the signal obtained, the gate on the boxcar integrator is optimized. Next, the laser beam is blocked and a measurement of the background is taken. This measurement is used to calculate an ideal detection limit where both furnace emission and laser induced scatter has been totally eliminated. For this measurement, the computer takes data during 2000 firings of the laser in the case of the N_2 and Nd:YAG lasers, and during 7000 firings of the Cu vapor laser. The laser beam is eventually allowed to pass through the furnace tube which leads to another measurement. Again the laser beam is blocked, and the furnace is then fired sixteen times and measurements including furnace emission are taken during the time the furnace is on. Now with the use of a 10 ng/mL Pb solution and a micropipette, 10 μl injections (5 μl into the Varian CRA-90) are introduced into the graphite tube and fluorescence measurements are obtained. The maximum signal is achieved when all the parameters, such as heating rate imaging on the monochromator slit, etc., are optimized. This set of measurements provides an estimation of the instrumental detection limit which can be limited either by laser scatter or background

furnace emission. To make sure that the 10 ppb standard solution has been prepared correctly, a comparison was made with an NBS standard certified to contain 24 ppb of Pb [217, 218].

A more conventional approach to obtain the instrumental detection limit is the calibration curve method. Here, a series of dilutions were prepared and measured in a similar fashion as described above. For lead due to environmental contamination, it is impossible to obtain a "clean" blank standard. The "off line" method for measuring the blank was used, which means that the dye laser is detuned by 0.1-0.2 nm away from the analytical wavelength when such measurements are performed. This assumes an ideal case where contamination is completely eliminated. When the analytical data is plotted, the curve was extrapolated to three times the standard deviation of the "off line" blank measurements and a detection limit is obtained [15, p. 79]. Using the same plot, an estimation of the analytical useful range (also known as linear dynamic range) was obtained.

In order to improve the signal-to-noise ratio, one should take advantage of saturation of the absorption transitions as stated in Chapter 3. From that discussion, it is important to note that when the saturation condition is

achieved the fluorescence signal does not increase any longer while the laser scatter keeps increasing linearly with a corresponding increase in laser irradiance. To obtain the optimum laser irradiance calibrated neutral density filters were used to produce a 10-fold or a 100-fold decrease when these filters were placed in front of the laser beam before it enters the atomization cell. By doing this, it is expected that the fluorescence signal will not decrease but laser scatter or at least the frequency of stray laser photons entering the detection system will be reduced by a factor of 10 or 100 depending on which filter is used. In the Nd:YAG laser pumped dye laser system, the results demonstrated that with a 10-fold reduction in laser irradiance, the fluorescence signal did not decrease and a considerable reduction in laser scatter occurred. With the N_2 laser pumped dye laser system, very similar results were obtained but in this case a very small decrease in the fluorescence signal was observed probably meaning that saturation with the 10-fold laser irradiance reduction was barely being approached. In both systems, the use of a 100-fold reduction decreased the signal by factors of $\sim$ 6 and $\sim$ 10 (Nd:YAG and N_2 lasers, respectively). When the same approach was tried with the Cu vapor laser pumped dye laser

system, the fluorescence signal decreased by a factor of ~ 4 when a 10-fold decrease in irradiance was applied.

During the lead experiments, the photomultiplier tubes were operated at ~ 900 V in order to maintain a gain of ~ 10^7. When a 100 pg (10 ng/ml) aliquot was injected in the atomizer, the corresponding fluorescence signal was so intense that the photomultiplier tube output gave a nearly flat response meaning that it was operating in a nonlinear region. The use of a calibrated neutral density filter to produce a 100-fold reduction in the number of photons entering the monochromator became imminent. Only in this way was it possible to operate the PMT in its normal linear region. To obtain a calibration curve for lead, the use of additional neutral density filters (e.g., 0.1%, 0.01% transmittance) was necessary when higher concentration standards were injected.

One final consideration observed while performing these measurements is the effect of signal averaging. Two different outputs can be acquired from the boxcar integrator; one of them evaluates every laser shot during the atomization interval and the other carries out an average of different numbers of laser pulses during the same atomization time. It was observed that the standard deviation of the

noise (laser scatter, furnace emission, etc.) was reduced by a factor of ~ 4 when the boxcar was set to average 10 laser pulses and its average output was sent to the computer.

Limits of Detection

Some of the typical experimental conditions under which the experiments were performed are given in Table 5-1. Here the probing efficiency is an estimate of the volume of the atomizer being probed divided by the volume of atomization defined by the dimensions of the graphite tube. In Table 5-2, signals are given for all the laser and spectrometer systems for excitation of 100 pg of lead (50 pg in the case of the Cu vapor laser) introduced into the furnace as well as the standard deviations calculated by running the furnace without any sample injections. The values used for the standard deviations assumed that laser-induced noise is the limiting noise in all our experimental setups.

In Figures 5-2 to 5-6, the boxcar outputs for lead injections into the furnace atomizers are shown. In Figure 5-7, the boxcar output obtained when a 5 μl aliquot of ultrapure water obtained from a commercial source (Seastar Chemical, Seattle, WA) was injected in the graphite atomizer (Cu vapor laser system) and demonstrates the extreme sensitivity of this method. Under clean room conditions, this

TABLE 5-1. TYPICAL EXPERIMENTAL CONDITIONS FOR ALL LASER SYSTEMS

Laser/Optical System	Repetition Rate (Hz)	Beam Diameter (mm)	Energy (mJ/p)	Probing Efficiency
Nitrogen pumped dye 0.35 m spectrometer	20	2	0.025	40%
Nitrogen pumped dye ellipsoidal mirror	20	2	0.025	40%
Nd:YAG pumped dye 0.22 m double spectrometer	30	2	1	55%
Cu vapor pumped dye 0.25 m spectrometer	6000	1	0.0004	25%

TABLE 5-2. PEAK FLUORESCENCE SIGNALS FOR LEAD AND NOISE-RELATED FIGURES[a]

System	Signal, mV		Std dev, mV	
	ND_1[b]	no ND filter[c]	ND_1[b]	no ND filter[c]
N_2 laser 0.35 spectrometer[d]	75,550	115,850	0.70	2.4
N_2 laser Bomem accessory[d]	45,200	107,900	2.75	9.4
Cu vapor laser 0.25 m spectrometer[e]	36,750	118,200	0.18	0.42
Nd:YAG laser 0.22 m spectrometer[d]	62,600	---	0.61	----

[a]Averaged output of the boxcar (10 pulses averaged).

[b]Neutral density filter (10% transmission) in front of the 283.306 nm laser beam.

[c]No neutral density filter in front of laser beam.

[d]100 pg samples.

[e]50 pg samples.

Figure 5-2. Temporal Behavior of the Atomization and Decay of 100 pg of Lead in the Furnace. N_2 Pumped Dye Laser System (0.35 m Spectrometer).

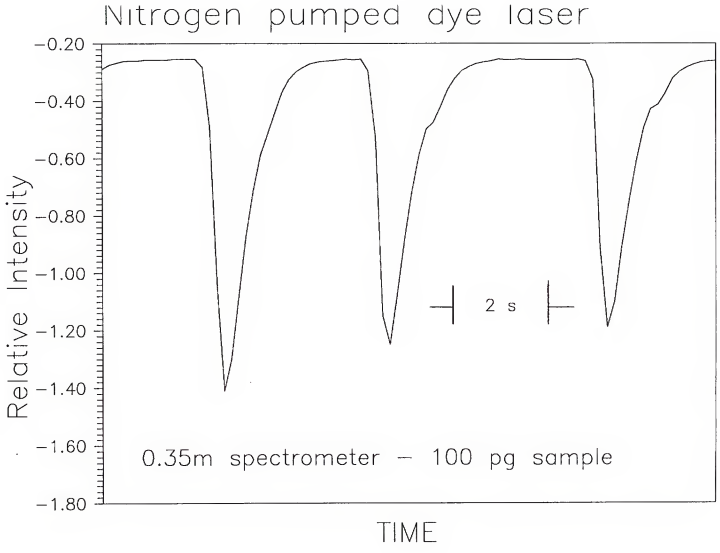
Nitrogen pumped dye laser
−0.20
−0.40
−0.60
−0.80
−1.00
−1.20
−1.40
−1.60
−1.80
Relative Intensity
2 s
0.35m spectrometer – 100 pg sample
TIME

Figure 5-3. Temporal Behavior of the Atomization and Decay of 100 pg of Lead in the Furnace. N_2 Pumped Dye Laser System (Non-Dispersive Optical Collection System.)

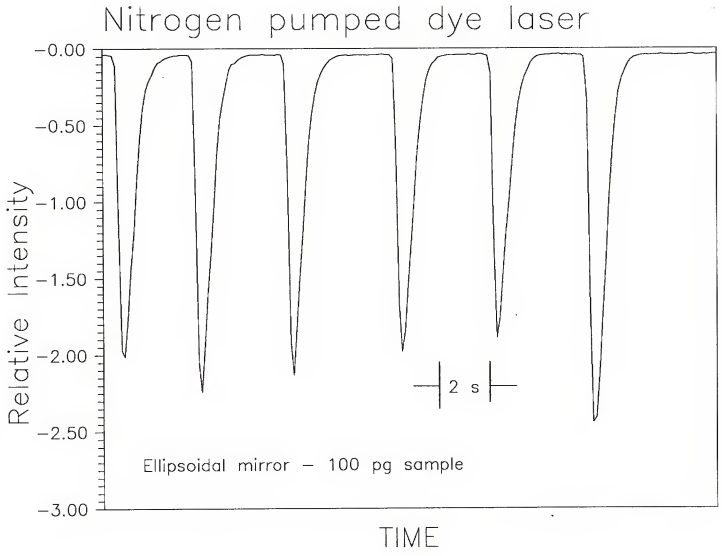
Nitrogen pumped dye laser
−0.00
−0.50
−1.00
−1.50
−2.00
−2.50
−3.00
Relative Intensity
2 s
Ellipsoidal mirror – 100 pg sample
TIME

Figure 5-4. Temporal Behavior of the Atomization and Decay of 100 pg of Lead in the Furnace. Nd:YAG Pumped Dye Laser System.

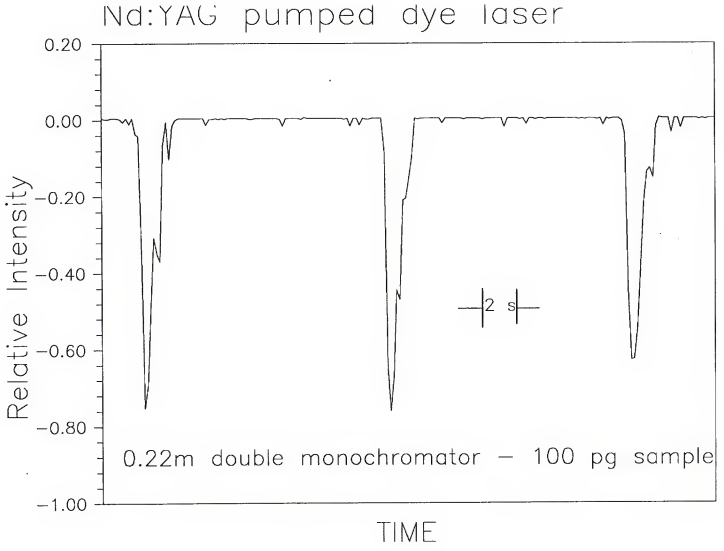
Nd:YAG pumped dye laser
0.20
0.00
−0.20
−0.40
−0.60
−0.80
−1.00
Relative Intensity
2 s
0.22m double monochromator – 100 pg sample
TIME

Figure 5-5. Temporal Behavior of the Atomization and Decay of 50 pg of Lead in the Furnace. Cu Vapor Pumped Dye Laser System (First Injection).

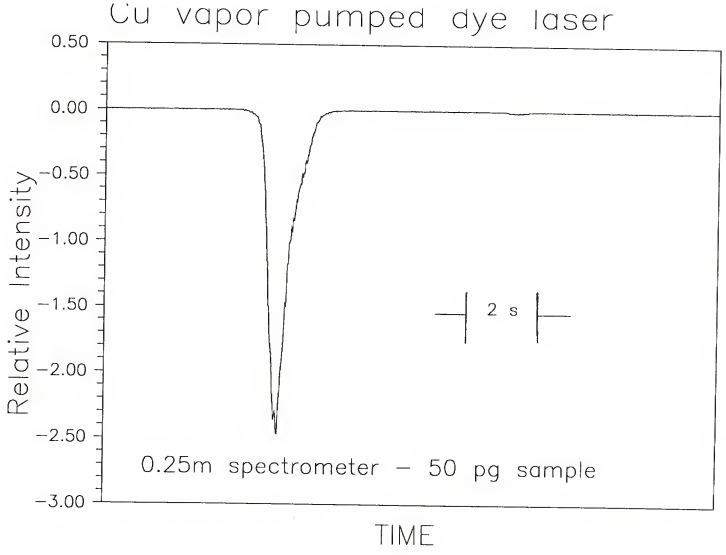
Cu vapor pumped dye laser
0.50
0.00
−0.50
−1.00
−1.50
−2.00
−2.50
−3.00
Relative Intensity
2 s
0.25m spectrometer – 50 pg sample
TIME

Figure 5-6. Temporal Behavior of the Atomization and Decay of 50 pg of Lead in the Furnace. Cu Vapor Pumped Dye Laser System (Second Injection).

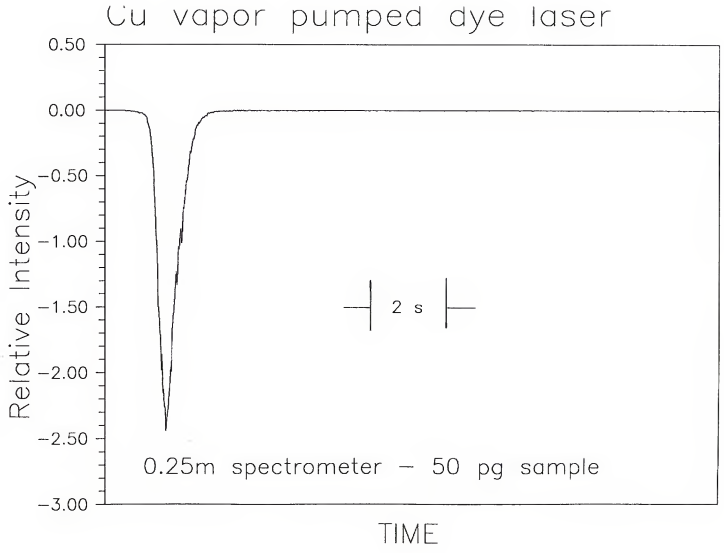
Cu vapor pumped dye laser
0.50
0.00
−0.50
−1.00
−1.50
−2.00
−2.50
−3.00
Relative Intensity
2 s
0.25m spectrometer – 50 pg sample
TIME

Figure 5-7. Temporal Behavior of the Atomization and Decay of a 5 μl Injection of Ultrapure Water. Cu Vapor Pumped Dye Laser System. Estimated Lead Concentration 250 fg.

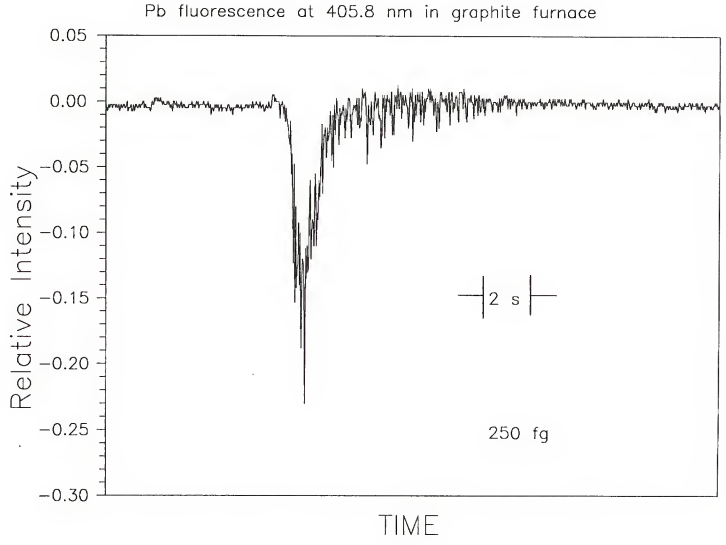
Pb fluorescence at 405.8 nm in graphite furnace
0.05
0.00
−0.05
−0.10
−0.15
−0.20
−0.25
−0.30
Relative Intensity
2 s
250 fg
TIME

water was supposed to contain no more than a few parts per trillion of lead. Once the container was opened in our non-controlled laboratory, several injections were made resulting in fluorescence signals with increasing intensity as time went by. Apparently, the lead present in the air started to contaminate the ultrapure water. It is estimated [219, 220] that the content of the lead in the air of an ordinary laboratory ranges from 0.1-0.5 $\mu g/m^3$. Comparing the signal strength given by the initial injection with the signal output of calibrated standards (higher concentration), it was estimated that the concentration of this water to be $\sim$ 250 fg. Every additional injection produced a larger signal until the signal level approached the one typically observed for the deionized water available in the laboratory.

In Table 5-3, the two groups of detection limits obtained for all the experimental systems are given. The first column contains the calculated instrumental detection limits that would be obtained if the limiting noise, laser induced noise, is completely eliminated. To achieve these ideal conditions, the use of baffles, light traps, and a more careful positioning and alignment of all the optical components will be necessary. These results indicate that

TABLE 5-3. ABSOLUTE DETECTION LIMITS AS OBTAINED BY SINGLE-STEP EXCITATION AT 283.306 NM AND FLUORESCENCE DETECTION AT 405.789 NM[a]

Experimental System	Detection Limits (fg) (b)	(c)
Cu vapor pumped dye laser, 0.25 m spectrometer[d]	0.08	0.5
Nd:YAG pumped dye laser, 0.22 m double spectrometer	0.2	3
Nitrogen pumped dye laser, 0.35 m spectrometer	0.2	3
Nitrogen pumped dye laser, off-axle ellipsoidal mirror	0.3	18

[a] S/N = 3, off line.

[b] Obtainable under ideal conditions.

[c] Obtained under our experimental conditions (laser irradiance attenuated 10X), laser scatter limited.

[d] No attenuation of laser irradiance.

it is possible to reach subfemtogram detection limits for all the experimental systems. The unprecedented sensitivity achieved with the high repetition dye laser system predicts that concentrations as low as 100 fg ml^{-1} could be determined. The second column presents the calculated instrumental detection limits when laser induced noise was considered as the limiting noise. Even in this case, all systems were able to achieve detection limits in the low femtogram range. Note that furnace blackbody emission was not considered in the noise figures mainly because of the low atomization temperature used and because it was possible to temporally distinguish between fluorescence signal and the background furnace emission signal when the boxcar output was sent to the computer.

Additional measurements were carried out to obtain a calibration curve (see Figure 5-8) for lead. In this case, the system that gave the best results in the previous set of measurements was used. As described before, the "off line" method was used to measure the blank signal. The detection limit obtained from extrapolation of the calibration curve plot to the blank level corroborates the results of the signal-noise measurements. If only measurements in the linear region (concentrations starting at 1 ng/ml) are taken

Figure 5-8. Analytical Calibration Curve for Lead. Cu Vapor Pumped Dye Laser System.

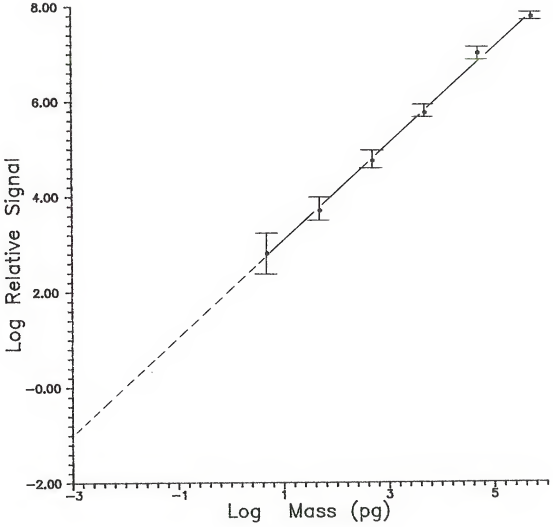
8.00
6.00
4.00
2.00
-0.00
-2.00
Log Relative Signal
-3
-1
1
3
5
Log Mass (pg)

into consideration, the analytically useful range (AUR) would be close to five orders of magnitude; otherwise, the AUR could be considered to be nine orders of magnitude. A recent report has demonstrated that working in the lower end of the curve can be achieved if clean room facilities and ultrapure reagents are used [170].

In Table 5-4, a comparison is given between the best detection limits so far achieved by other research groups. The outstanding results produced with the Cu vapor laser system confirms the discussion in Chapter 3, where a 10 times improvement in the LOD was predicted by increasing the laser repetition frequency to 100 kHz. In our case, an increase in repetition frequency up to 6 kHz produced a 6 times improvement in LOD.

Non-Dispersive Spectrometric System

The use of non-dispersive filter-type detection systems is not new to atomic fluorescence spectrometry. Several reports [221-227] have demonstrated their use especially when they are combined with a solar-blind photomultiplier tube. Their use in laser atomic fluorescence with graphite furnace atomizers has been limited to the works of Hohimer and Hargis [96, 158] and Miziolek and Willis [228] where combinations of interference and colored filters with a

TABLE 5-4. COMPARISON OF BEST ABSOLUTE DETECTION LIMITS FOR LEAD (fg)[e]

		Reference
This Work[a]	0.5	--
Dougherty et al.[b]	7	[36]
Bolshov et al.[c]	1.5	[97]
Dittrich et al.[b]	68	[162]
Falk et al.[c]	5	[34]
Omenetto et al.[d]	5	[112]

[a]Cu vapor laser system.

[b]Modified graphite tube atomizer.

[c]Graphite cup atomizer.

[d]Graphite tube unmodified atomizer.

[e]Best LOD using ETA-AAS is 2000 fg [212].

photomultiplier tube were used to determine elements, such as Tl, Cs and Pb. The greatest advantages of using a non-dispersive optical collection system is a higher energy throughput and simpler instrumentation but also the disadvantage of a lower rejection ratio for unwanted source scattered photons as compared with a dispersive system. In these experiments, an off-axis ellipsoidal mirror was used to collect the fluorescence emitted from the atomizer cell. This type of ellipsoidal mirror is considered to be one of the most elegant ways to produce a perfect image as described by James and Sternberg [229], a fact clearly observed during this work. Although the detection limits obtained for lead using this approach are only one order of magnitude higher than the results obtained with the other systems, it must be concluded that a non-dispersive system can only be used advantageously in the UV region where background blackbody emission is also reduced.

LEAFS-ETA for Other Elements

In Table 5-5 the detection limits obtained for a group of four different elements are presented; also included are the best results obtained by other workers. All the LOD's were calculated using the calibration curve method. As in the case of Pb, environmental contamination for Fe and Tl

TABLE 5-5. DETECTION LIMITS FOR OTHER ELEMENTS INVESTIGATED BY LEAFS-ETA

Experimental System	Element	λ_{exc}---λ_{fl} (nm)	Detection Limits (pg) This work	Other workers
Cu vapor pumped dye laser 0.25 m spectrometer	Fe	296.7 -- 373.5	0.5	0.1[a]
Cu vapor pumped dye laser 0.25 m spectrometer	Ga	287.4 -- 294.4	2	10[b]
Nitrogen pumped dye laser 0.35 m spectrometer	Tl	276.8 -- 352.9	0.007	0.002[c]
Nitrogen pumped dye laser 0.35 m spectrometer	Ir	295.1 -- 322.1	10	6[c]

[a]Bolshov, M.A. et al., SAB 36, 1143 (1981).

[b]Dittrich, K. et al., JAAS 2, 63 (1987).

[c]Omenetto, N. et al., JAAS 3, 231 (1988).

imposed the use of the "off line" measurement for the blanks. Meanwhile for Ga and Ir, the blank measurements were performed at the analytical wavelength.

In the case of the Cu vapor laser system, the detection limits obtained are not as impressive as in the lead case but still compare favorably with the results presented by other workers. Two factors that may hinder sensitivity in this system are low energy per pulse, which may not allow the approach of saturation, and the dimensions of the graphite tube atomizer. As described before, the tubes used in this system are only 1.8 cm in length; residence time of the atoms in the graphite tube is quadratically related to the atomizer length. Data obtained from L'Vov and Nikolaev [141] allow the calculation of the diffusion coefficients for Ga, Fe, and Pb at their corresponding atomization temperatures which then allows the estimation of the residence time of the atoms in the atomization volume. For Ga and Fe, the residence times calculated are of the order of 80-100 ms, while for lead the residence time approaches 300 ms. The effect of the residence time of the atoms on the sensitivity can be examined by using a longer tube atomizer which theoretically should increase the residence time of the atoms in the graphite cell.

The LOD's obtained with the N_2 laser system for Tl and Ir certainly compare favorably with the results of other workers. Thallium presents another example of excellent sensitivity (7 fg) for an element that presents similar conditions to the lead experiments; sensitive direct line fluorescence scheme, ease of atomization, etc. On the contrary, iridium is a noble metal with very low volatility which introduces the need for the use of a high atomization temperature in order to carry out absorption or fluorescence measurements [230-233]. The measurement of the blank immediately identified furnace blackbody emission as the source of the limiting noise for the determination or iridium. The best signal-to-noise ratio was obtained when the slit width was reduced to 250 μm. The LOD obtained in this work, and by Bolshov et al. [104], are at least more than two orders of magnitude better than the best LOD reported for atomic absorption spectrometry with furnace atomization (2 ng [230, 233]). Some improvement in sensitivity may be achieved by using a different excitation-fluorescence scheme where the fluorescence is measured in the region between 250-290 nm and the use of a solar-blind photomultiplier tube (see Figure 5-9).

Figure 5-9. Analytical Calibration Curve for Iridium. N_2 Pumped Dye Laser System.

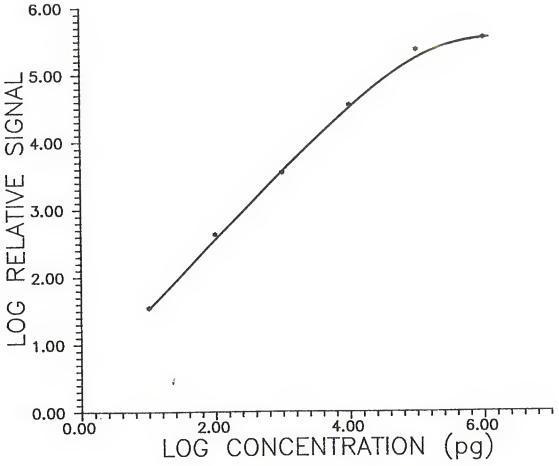
LOG RELATIVE SIGNAL
6.00
5.00
4.00
3.00
2.00
1.00
0.00
0.00
2.00
4.00
6.00
LOG CONCENTRATION (pg)

CHAPTER 6
HOW FAR FROM THE INTRINSIC DETECTION LIMIT?

This chapter is aimed toward a comparison between the experimental detection limits obtained for lead and the intrinsic detection limits, as defined by Alkemade [17, 18], which can be calculated assuming that the limiting error is that inherent in the signal, (i.e., caused by the statistical fluctuations in the number of atoms probed and in the detection process). Before this comparison is presented, a brief discussion on how low a concentration can be measured by laser excited fluorescence techniques is given. Refer to Figure 6-1.

LEAFS and Single Atom Detection

The fluorescence intensity that can be generated from an arbitrary sample can be described very simply if a number of assumptions is made. In this case, the signal intensity is described in terms of measurable experimental parameters and a simple model is adopted. Going back to the two energy levels case presented in Chapter 2, the following conditions are again valid: level 1 has a population of n_1 m^{-3} and is the ground state; level 2 has a population n_2 m^{-3}, a lifetime

Figure 6-1. Random Errors (Sources of Fluctuations).

Sources of Error

Extrinsic	Intrinsic
background	discrete nature of matter
matrix	analyte atoms in the sample
atomizer	*analyte atoms in the atomizer
scattering	*detection process is a chance process
laser power	
detector and amplifier	

* ULTIMATE L.O.D. if extrinsic fluctuations suppressed !

of τ_2 s, and a radiative quantum efficiency of Y and is the only excited state that can be populated. The possibility that atoms in level 2 can relax to levels other than the ground state is allowed, but it is assumed that these other levels decay so quickly to the ground state that their populations may be neglected. It is also assumed that the concentrations are too low to absorb the incoming photons or fluorescence photons (pre- and postfilter effects). The fraction of the total fluorescence from level 2 that occurs at the particular transition observed is designated by the branching ratio β. The spontaneous fluorescence produced by the sample at the transition observed is

$$S_{fluor} = \beta \, Y \, \tau_2^{-1} \, n_2 \, V \tag{6.1}$$

while the signal detected is

$$S_{out} = \beta \, Y \, \tau_2^{-1} \, n_2 \, V \, \Omega_{coll} \, \eta_{det} \tag{6.2}$$

where

S_{out} = output signal in counts/s

V = sample volume under observation, m^3

Ω_{coll} = efficiency of the optical system including monochromator and filters, sr

η_{det} = efficiency of detecting and counting fluorescence photons, counts sr^{-1}

Assuming the excitation intensity is not attenuated as it propagates through the sample, the rate of change of level 2 is

$$\frac{dn_2}{dt} = \frac{\sigma I}{h\nu}(n_1 - n_2) - \tau_2^{-1} n_2 \qquad (6.3)$$

where

σ = optical cross section for the transition, (m^2)

I = laser intensity (W/m^2)

$h\nu$ = energy of a laser photon (J)

The first term represents the laser excitation rate from the ground state (the difference $n_1 - n_2$ is required to account for stimulated emission), while the second term represents all the radiative and nonradiative relaxation processes that depopulate the excited level. Assuming that the population level 2 reaches a steady-state value (e.g.,

$dn_2/dt = 0$), and that $n_T = n_1 + n_2$, then Equation 6.3 can be solved for n_2

$$n_2 = \frac{\sigma I n_T}{2 \sigma I + h\nu \tau_2^{-1}} \tag{6.4}$$

Substitution of Equation 6.4 into 6.2 gives

$$S_{out} = \frac{\beta \eta \tau_2^{-1} \sigma I n_T V \Omega_{coll} \eta_{det}}{2 \sigma I + h\nu \tau_2^{-1}} \tag{6.5}$$

Now there are two important limiting cases for this expression as already seen in Chapters 2 and 3. At low excitation intensities, the expression becomes

$$S_{out}^{low} = \frac{\beta \eta \sigma P n_T l \Omega_{coll} \eta_{det}}{h\nu} \qquad (6.6)$$

where

P = laser flux (W)

l = path length (m)

This last expression is the familiar one applicable to conventional fluorescence spectroscopy [63].

The second limiting case occurs at very high excitation intensities, where the rate of stimulated emission exceeds the normal excited state relaxation rate ($2\sigma I >> h\nu \tau_2^{-1}$). Then

$$S_{out}^{high} = \frac{\beta \tau_{rad}^{-1} n_T V \Omega_{coll} \eta_{det}}{2} \qquad (6.7)$$

where τ_{rad}^{-1} = lifetime or natural lifetime of level 2 (= $\eta \tau_2^{-1}$. This equation expresses the saturation condition where the output signal reaches its highest possible value.

To easily visualize the extreme sensitivity that laser excited fluorescence techniques provide, an experiment performed by Fairbank et al. [101] will be considered. These researchers measured absolute Na concentrations of 100 atoms/cm^3 using resonance fluorescence in a Na vapor cell. One should be reminded that when working at saturation, the intensity of scattered light keeps increasing linearly with a corresponding increase in laser irradiance. So when resonance fluorescence is being monitored, the benefits of saturation are offset because the S/N ratio is degraded. Consequently, these workers attenuated their dye laser by using neutral density filters in order to avoid saturation. A power of 3 μ W (9×10^{12} photons/s) was used to excite Na vapor over a 2 cm path length in a cell that was well baffled to eliminate scattered light. An f/1.8 optical system (collection efficiency of about 2%) imaged the fluorescence onto a photomultiplier tube (quantum efficiency $\sim$ 10%). The Na D line has an optical cross section of 8.3×10^{-12} cm^2 and the quantum efficiency is assumed to be unity. If these values are substituted into Equation 6.6, the following expression is obtained

$$S_{out}^{low} = 0.3\ n_T \qquad (6.8)$$

The minimum detectable concentration depends on how low an output signal can be measured in the presence of the scattered light (limiting noise). The scattering at the PMT in this experiment was reduced by 3×10^{-10} from the incident light intensity (2.7×10^{3} photons/s). Fairbank and co-workers were able to get a factor of 30 lower than the scattered light by wavelength modulation of the laser at 1.5 Hz and by using a lock-in amplifier. By doing this a lower limit of 90 photons/s was reached which converts to 9 photoelectron/s. Substitution into Equation 6.8, demonstrates the possibility of observing 30 atoms/cm^3, a value close to the 100 atoms/cm^3, observed in Fairbank's experiment. This value of 100 atoms/cm^3 corresponds to 1.7×10^{-19} moles/liter.

Other workers have been able to improve considerably the lower limit obtained by Fairbank et al. For example Balykin et al. [234] by using extensive baffling and the use of two detectors operating in a coincidence configuration obtained a 10^{14} rejection of laser light, which permitted the detection of a single Na atom. More recently, several research groups have performed a similar task with the use of the photon burst correlation technique [235-238]. Alkemade [17] had developed a statistical approach aimed to

improve the efficiency of detecting small numbers of atoms by using the so-called single atom detection techniques (SAD). A brief discussion of this approach is given in the next section.

Detection Efficiency

All the experiments mentioned in the previous section require the production of an event in the detector which carries information about its own appearance in the volume being probed. In laser excited fluorescence spectrometry, the event may be the emission of a single photoelectron or a burst of photoelectrons in one photodetector, or it may be the coincidence between such emissions in two photodetectors.

After internal and/or external amplification, the event is registered as a count or current pulse. The total number of events, N_e, occurring in a single probing with probing time T can be found by accumulating the counts, or by integrating the current pulses. If T is long, the count rate or the detector output current can also be recorded as a function of time, smoothed by the recorder time constant. Integration over T then yields a measure for N_e. The statistical errors can be improved if one repeats the probing R

times. The total time taken for R repeated probings is called the (total) measurement time, t_m.

With a pulsed laser, the probing time T is determined by the pulse duration or the width of the time gate, whichever is shorter. Multiple probings are obtained by firing laser shots at a repetition frequency, f_{rep}. By means of a boxcar integrator and a smoothing circuit, the count rate or output current can then be recorded as a function of time and averaged or integrated over t_m.

The probe volume V_p is determined by the geometry of the laser beam (s) and by the part of the irradiated region that is "seen" by the detector. When the radiant energy density of the laser beam or the efficiency of detecting a fluorescence photon varies with position inside V_p, the term effective probe volume must be used.

Before a relationship between N_e and the number, N_p, of atoms in V_p is established, a distinction between two extreme probing conditions needs to be presented: the (quasi)-stationary and the nonstationary case. Usually V_p is a small part of the atomizer volume V_a and atoms move in and out of V_p freely and independently. Let τ be the (mean) residence or transit time of an atom in V_p. The (quasi)-stationary case (a) is found if τ is much larger than the

probing time T; the nonstationary case (b) occurs if $\tau << T$. In the former case, the number, N_p, of atoms in V_p does, virtually, not vary in a time interval of length T, whereas N_p varies stochastically in the latter case.

Since in the experiments performed during this work, the prevalent case is the stationary one, from now on only equations pertaining to this condition will be presented.

The relationship between N_e and N_p can be expressed as

$$\bar{N}_e = \epsilon_d \bar{N}_p \tag{6.9}$$

Where ϵ_d is the detection efficiency ($0 \leq \epsilon_d \leq 1$). In laser excited fluorescence, ϵ_d depends on the rate of photoexcitation, the solid angle of observation, the quantum efficiency of the photocathode, and so on. The probability that an event remains unobserved because it is concealed by background or electronic noise is not included in ϵ_d.

If $\bar{N}_e << 1$, it should be interpreted as the possibility that one event occurs during T. Similarly, if $\bar{N}_p << 1$, it represents the probability of finding one atom in V_p at an arbitrary moment. The probability of finding two atoms in V_p is then $(\bar{N}_p)^2$ and so on. For a statistically stationary stochastic system, the bar on N_e and N_p relates to the

average over an ensemble of similar systems at any moment as well as to the time average for one system.

Overall Efficiency of Counting Atoms

The overall efficiency ϵ_o of a laser spectrometer to count atoms in the sample is given as the probability that a given atom in the sample produces an event in a single probing interval, and is expressed as

$$\epsilon_o \equiv \frac{N_e}{N_s} \tag{6.10}$$

where N_s is defined as the number at analyte entities in a consumed sample (one free atom derives from one entity). The overall efficiency, ϵ_o, can be decomposed into a product of partial efficiencies, namely the atomization efficiency ϵ_a, the probing efficiency ϵ_p, and the detection efficiency ϵ_d (see Figure 6-2).

$$\epsilon_o = \epsilon_a \cdot \epsilon_p \cdot \epsilon_d \tag{6.11}$$

Figure 6-2. Schematic Layout of a Laser-Based Spectrometer. (Redraw from [18].)

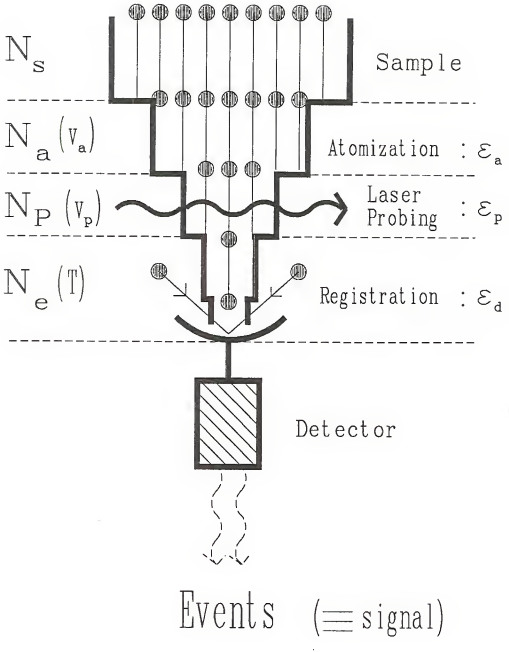
N_s
Sample
$N_a\,(V_a)$
Atomization : ε_a
$N_P\,(V_p)$
Laser Probing : ε_P
$N_e\,(T)$
Registration : ε_d
Detector
Events (≡ signal)

The number density, n_a, of free atoms in a closed atomizer with volume V_a containing N_a free atoms is determined by

$$N_a = n_a \cdot V_a \tag{6.12}$$

With an assumed uniform atom distribution, the mean number, $\bar{N}_p$, of atoms in the probe volume V_p can be expressed as

$$\bar{N}_p = n_a V_p = N_a \frac{V_p}{V_a} \tag{6.13}$$

In the case of stationary probing, by using Equation 6.13 a definition for ϵ_p, can be obtained

$$\epsilon_p = \frac{\bar{N}_p}{N_a} = \frac{V_p}{V_a} \tag{6.14}$$

Statistical Expressions

The analytical limit of detection (LOD) is defined as the concentration, c_m, or quantity, q_m, in the sample, which produces a mean signal equal to k times the root-mean-square (rms) random error [239-242]. The statistical confidence factor k is usually taken as 3 [243, 244]. Two different categories of random errors can be distinguished, as was shown in Figure 6-1. On one side, there are errors arising from extrinsic sources of fluctuations, such as fluctuations in the background, fluctuations in the laser power or in the efficiency of atomization, and detector or amplifier noise. On the other side, there is an intrinsic error in the signal itself, arising from the discrete nature of matter. First, the number of analyte atoms found in the sample or atomizer will fluctuate around a mean value in a manner described by Poisson statistics. Second, the detection process is a chance process. The resulting error which becomes relatively more important for smaller numbers of atoms and detected photons determines the intrinsic limit of detection. This is the ultimate LOD obtainable when all extrinsic fluctuations are suppressed.

When small numbers of atoms are to be counted, it is appropriate to consider the number of events, N_s, counted in

a single probing interval T, as the signal. The minimum detectable signal is therefore

$$(\bar{N}_e)_m = k \cdot \tilde{N}_e \qquad (6.15)$$

where $\tilde{N}_e \equiv \sqrt{(\overline{\Delta \tilde{N}_e})^2}$ is the rms intrinsic error in N_e.

It is necessary to derive a statistical expression for ϵ_d, being the probability of an event occurring in a single probing when one atom is present in V_p. Let ϕ be the constant probability per second that a photoelectron is generated as long as there is one atom in V_p. If the atom generates at most one photoelectron during its stay in V_p, each photoelectron generated counts as one event. Then

$$\epsilon_d = \phi \cdot T \quad (\text{ if } \phi \cdot T \ll 1) \qquad (6.16)$$

Assuming Poisson statistics again, the relative standard deviation or the precision in a single probing can be given by

$$\frac{\tilde{N}_e}{\bar{N}_e} = (\tilde{N}_e)^{-1/2} \tag{6.17}$$

The final precision obtained with R repeated probings is expressed by

$$\frac{\tilde{N}_e}{\bar{N}_e} = (\tilde{N}_e\ R)^{-1/2} \tag{6.18}$$

Using Equations 6.15 and 6.18, an expression for $(\tilde{N}_e)_m$ when the probings are repeated R times is obtained

$$(\tilde{N}_e)_m = k^2/R \tag{6.19}$$

Recalling Equation 6.9 and combining it with Equation 6.19 gives the minimum value $\bar{N}_p$ that can be determined

$$(\tilde{N}_p)_m = \frac{k^2}{\epsilon_d R} \tag{6.20}$$

If Equation 6.16 is now used, the following expression results

$$(\bar{N}_p)_m = \frac{k^2}{\phi\ T\ R} \tag{6.21}$$

For the analytical detection limit, it is not so much $\bar{N}_p$ but rather $n_a \equiv \bar{N}_p/V_p$ that is relevant, since the latter is directly related to the sample concentration independently of the magnitude of V_p. The corresponding expression for $(n_a)_m$ is given as

$$(n_a)_m = k^2/\phi\ T\ V_p\ R \tag{6.22}$$

Intrinsic Detection Limits for All Lead Experiments

In the lead experiments carried out during this work, a direct line fluorescence transition is monitored which terminates on a metastable level, as already established in Chapter 3. In this case, the time-integrated parameter ϕ can be evaluated by the following expression

$$\phi = \eta_s \cdot \eta_m \cdot \frac{\Omega_F}{4\pi} \cdot \eta_o \, \eta_p \cdot A_{um} \qquad (6.23)$$

where η_s is the "saturation factor" which indicates the efficiency of the excitation process, η_m is a factor taking into account the loss of atoms due to their accumulation into the metastable level during laser probing time, $(\Omega_F/4\pi)$ is the fraction of solid angle observed, assuming isotropic fluorescence emission, η_o is the overall optical transmission factors of the system, η_p is the quantum efficiency of the photomultiplier, and A_{um} is the transition probability, of the fluorescence monitored between the upper level u and the metastable level m.

The saturation factor can be calculated according to the following expression

$$\eta_s = \left\langle \frac{g_u}{g_u + g_l} \right\rangle \cdot \left\langle \frac{1}{1 + \frac{E_\nu(\nu_{lu})}{E_\nu^s(\nu_{lu})}} \right\rangle \qquad (6.24)$$

where g_u and g_l are the statistical weights of the upper, u, and lower, l, levels connected by the excitation transition, $E_\nu(\nu_{lu})$ is the spectral irradiance of the laser at the excitation transition and $E_\nu^s(\nu_{lu})$ is the saturation spectral irradiance.

Since the metastable level can act as a trap for the atoms during the interaction time with the laser pulse, one should take into account a loss factor since the atoms accumulating in the trap will not be available again for the excitation process. This factor is evaluated by solving the rate equations 3-level or 4-level systems where the laser excitation saturates the lower and upper levels and fluorescence is observed between the upper level and one of the two metastable levels indicated as m and m' [24, 187]. When the fluorescence pulse is integrated over a rectangular laser pulse of duration T, the following expression is obtained

(6.25)

$$F_{T_l} = \frac{C \cdot n_T}{A_{um} + A_{um'}} (1 - \exp[\eta_s \cdot (A_{um} + A_{um'}) \cdot T])$$

Where F_T is the integrated fluorescence pulse, C is a constant of proportionality, n_T is the total number density

of the atoms between the 3 levels, and $(A_{um} + A_{um'})$ is the sum of the spontaneous transition probabilities between the upper level and the metastable levels [245]. In the above equation, the collisional quenching rates between levels have been neglected in comparison with the radiative rates since the atoms are present in a pure argon atmosphere. It can be seen that, for $[(A_{um} + A_{um'}) \cdot T] \ll 1$, the maximum fluorescence signal will be given by

$$F_{T_2} = C \cdot n_T(\eta_s \cdot T) \tag{6.26}$$

The term η is defined as

$$\eta_m = F_{T_1}/F_{T_2} \tag{6.27}$$

The residence time, T, for atoms within the furnace is given by

$$T = l^2/8D \tag{6.28}$$

where l is the effective length (furnace) over which atoms diffuse and D is the diffusion coefficient of the atomic vapor.

All the parameters and the characteristics of the experimental detection systems are collected in Tables 6-1 and 6-2. The experimental absolute detection limits given in Chapter 5 are converted into numbers of atoms in the probe volume by assuming the atomization efficiency measured, for Pb, for graphite tube atomization by Falk and Tilch [189]. Also, shown in Table 6-2 are the obtainable detection limits for lead which can be obtained in the case where laser scatter noise, environmental fluorescence and furnace emission noise are completely eliminated, (i.e., detector noise limited).

Several considerations can be made, if the results presented in Table 6-2 are examined:

1. The detection efficiency, ϵ_d, is exceedingly small. This is due to the poor collection efficiency of the optics and to the short interaction time resulting from the use of pulsed lasers with pulse durations not exceeding 20 ns. Since, according to Alkemade [18], a necessary condition for the existence of SAD is $\epsilon_d = 1$, it is clear that this condition will never be met by the experimental laser systems considered here, even if the best possible experimental values are assumed in the calculations of ϕ, (e.g., $\eta_s = 0.75$, $\eta_a = 1$,

TABLE 6-1. EXPERIMENTAL AND CALCULATED CHARACTERISTICS OF THE EXCITATION-DETECTION SYSTEM (Pb) FLUORESCENCE

System	Pulse Rate	$\frac{\Omega_F}{4\pi}$	$\eta_o \eta_p$	η_s	η_m
Nd:YAG dye laser	30	3.09×10^{-3}	0.0154	0.750	0.600
Nitrogen dye laser	20	5.92×10^{-3}	0.0231	0.732	0.821
Cu vapor dye laser	6000	1.10×10^{-2}	0.0432	0.563	0.541

η_o = Overall transmission factor of the system.

η_p = Quantum efficiency of the photomultiplier tube.

η_s = "Saturation factor," efficiency of excitation process.

η_m = Accounts for loss of atoms into metastable level.

TABLE 6-2. EXPERIMENTAL AND CALCULATED MINIMUM DETECTABLE NUMBER OF ATOMS IN THE PROBE VOLUME FOR DIFFERENT LASER SYSTEMS

Laser System	T (s)	τ (s)	V_a (cm^3)	V_p (cm^3)	ϵ_d	R
Nd:YAG dye laser	1.2×10^{-8}	0.48	0.452	0.251	2.32×10^{-5}	11
Nitrogen dye laser	5.0×10^{-9}	0.25	0.327	0.126	3.66×10^{-5}	8
Cu vapor dye laser	2.0×10^{-8}	0.03	0.064	0.015	2.58×10^{-4}	1800

T = Probing time (laser pulse).

τ = Atomization time.

V_a = Atomization volume.

V_p = Probing volume.

ϵ = Detection efficiency

R = Number of repetitions.

TABLE 6-2--continued

Laser System	$(N_p)_m$ Exp (Exp)	$(N_p)_m$ Calc.	ψ ($\frac{\text{Exp}}{\text{calc}}$)
Nd:YAG dye laser	3.49×10^6 (2.33×10^5)	3.53×10^4	99 (7)
Nitrogen dye laser	2.42×10^6 (1.61×10^5)	3.08×10^4	79 (5)
Cu vapor dye laser	2.47×10^5 (3.95×10^4)	19	1.3×10^4 (2.1×10^3)

$(N_p)_m$ = Number of atoms being probed during each measurement.

ψ = Ratio of $(N_p)_m$ obtained experimentally and $(N_p)_m$ calculated.

($\Omega_z/4\pi$) = 0.5, A = 10^8 s^{-1} and $\eta_o \cdot \eta_p$ = 0.2). Only when longer laser pulses are used, such as with flashlamp pumped dye lasers or CW lasers which are also capable of saturation, will ϵ_d reach unity. While this is certainly true for a simple two-level system, it must be pointed out that the benefit of a longer duration pulse will not apply to the case of lead, as well as to similar other three-level and four-level systems. In the lead case, the accumulation losses into the metastable trap will be severe (i.e., η_m = 0.01), and as discussed in Chapter 3 an optimum value for the duration of the laser pulse will be of the orders of 7 ns.

2. The low value of ϵ_d will cause the mean number of events, $\bar{N}_e$, in Equation 6.9 to fluctuate even for large values of $\bar{N}_p$, since now the occurrence of an event is a chance process [18]. The resulting intrinsic detection limit given by Equation 6.20 can, therefore, still be reached in the experimental situations described in this work, provided that any extrinsic causes of noise are eliminated.

3. As seen from Equation 6.20 and 6.22, a very important role is played by the number of probings, R, which is

dictated by the repetition frequency of the laser and by the overall measuring time of the experiment. Again, it is necessary to point out that in the case of lead, the optimum repetition rate should be equal to the reciprocal lifetime of the metastable level, (i.e., 10^5 Hz [97, 246].

4. The experimental LOD's obtained with the different laser systems reported in Table 6-2 are seen to exceed the calculated intrinsic LOD's by a factor ranging from 79 to 1.3×10^4 in the case of the N_2 pumped dye laser system and the Cu vapor pumped dye laser system, respectively. Environmental fluorescence and laser induced stray light in the detection system were the major causes of extrinsic errors which were not eliminated in these experiments, as described in Chapter 5. In the case of the Cu vapor dye laser system, even though the best experimental detection limit was achieved, the discrepancy between the calculated and observed LOD is significant, indicating that some other limiting noise (s) must have been present. However, it can also be seen from Table 6-2 that in the case of the N_2 pumped and Nd:YAG pumped dye laser systems, the estimated obtainable experimental LOD differs from the

intrinsic LOD by a factor of only 5 and 7, respectively.

General Conclusions

Two types of general conclusions apply to the results described in this chapter. The first is that not only could SAD not be reached for Pb but also the intrinsic detection limit could not be closely approached for the experimental conditions reported for the different laser and atomization systems used. As a result, in order to approach the intrinsic LOD, the experimental set-up needs to be improved by achieving a much better rejection of scattered laser photons into the monochromator-detection apparatus and in minimizing the noise due to furnace emission.

The achievement of this goal is a very difficult task that requires an increased effort in keeping stray light at a minimum level. It would also help to measure the fluorescence in the ultraviolet region, where the emission from the hot furnace is negligible [247].

The second conclusion is that the experiment needs to be optimized in order to decrease the intrinsic detection limit obtainable. One way would be to increase the efficiency of the fluorescence light collection. However, since in all the cases considered, the fluorescence was excited

and collected longitudinally along the axis of the atomizer, this improvement can hardly be better than a factor of 2, since the fluorescence solid angle will always be dictated by the internal diameter of the graphite tube which will act as a limiting aperture. Another way is to increase the number of probings, R. In this respect, the Cu vapor pumped dye laser represents a good choice, even though the optimum repetition frequency in the case of lead would be 10^5 Hz. A third way is to match as closely as possible the atomizer volume with the probe volume, for example, by enlarging the laser size at the atomizer while still maintaining saturated conditions and correspondingly assuring that the entire volume of excitation is seen by the detector. A final ideal way would be to produce a burst of atoms (with unity atomization efficiency) in a time equal to the probing time, (i.e., of the same order of duration as the laser pulse).

CHAPTER 7
FINAL COMMENTS

Summary

This work has demonstrated that laser excited atomic fluorescence combined with an electrothermal graphite tube atomizer can provide the extreme sensitivity needed for the analysis of trace elements in areas such as the semiconductor industry, biomedical laboratories, and many others. In addition, by careful optimization of the analytical laser spectrometer system, it was shown that three different types of laser systems can provide detection limits in the low femtogram range and even lower in the case of high repetition rate, Cu vapor laser. The use of graphite tube atomizers needs to be stressed because now the possibility of performing analytical determinations of samples with complicated matrices is a possibility due to the enhanced atomization efficiency [188, 192, 193] which in many cases can avoid the need for vacuum atomization [248]. Finally, it was also shown that very good sensitivity can be achieved for a number of other elements for which the atomization parameters differed somewhat from the ones used for lead.

The detection limits obtained for lead were compared to the intrinsic detection limits calculated according to the statistical expressions developed by Alkemade [18]. It was concluded that the experimental LOD's were still far from the intrinsic LOD's and that the possibility of single atom detection with our experimental setups is still remote.

Future Work

Some suggestions need to be made about the selection of appropriate graphite tube atomizers. First, the use of commercial models is a must, mainly because with the development of graphite furnace atomic absorption spectrometry the instruments available today are as good as the best designed homemade models and sometimes even better. The selection of a commercial graphite furnace atomizer still needs much consideration as to which laser system is going to be used. Optimization of the probing efficiency should be the most important parameter to be considered.

The initial experiments with the off-axis ellipsoidal mirror should be continued, but in this case, fluorescence should be measured preferably in the ultraviolet region and the use of solar-blind photomultiplier tubes and narrow band interference filters would help very much in this approach. With the use of stepwise excitation (double resonance), a

large number of optical transitions become available for almost every element, which enhances the possibility of monitoring atomic fluorescence in this part of the spectrum (UV) and bringing upon the laser method, a very large increase in selectivity [249].

REFERENCES

1. J.R. Davis, Jr., A. Rohatgi, R. H. Hopkins, P.D. Blais, P. Rai-Choudhury, J.R. McCormick and H.C. Mollenkopf, IEEE Trans. Electron Devices, ED-27, 677 (1980).

2. H.J. Graf and W.L. Reynolds, Solid State Technol., 28(3), 141 (1985).

3. P. Murugaiyan, Pure & Appl. Chem., 54, 835 (1982).

4. T.Y. Kometani, Anal. Chem., 49, 2289 (1977).

5. M.S. Leloux, At. Spectrosc., 8, 71 (1987).

6. J.D. Winefordner, European Spectroscopy News, 79, 24 (1988).

7. G.H. Morrison, CRC Crit. Rev. Anal. Chem., 8, 287 (1979).

8. G. Tölg, Analyst, 112, 365 (1987).

9. J.A.C. Broekaert and G. Tölg, Fresenius Z. Anal. Chem., 326, 495 (1987).

10. J.A.C. Broekaert, Anal. Chim. Acta, 196, 1 (1987).

11. R.S. Houk, Anal. Chem., 58, 97A (1986).

12. D.J. Douglas and R.S. Houk, Prog. Analyt. Atom. Spectrosc., 8, 1 (1985).

13. M.H. Nayfeh, American Scientist, 67, 204, March-April (1979).

14. G.M. Hieftje, J. Chem. Ed., 59, 900 (1982).

15. V.S. Letokhov, Ed., "Lasers Analytical Spectrochemistry," Adam Hilger, Bristol, UK (1985).

16. E.H. Piepmeier, Ed., "Analytical Applications of Lasers," Wiley Interscience, New York, NY (1986).

17. C. Th. J. Alkemade, Appl. Spectrosc., 35, 1 (1981).

18. C. Th. J. Alkemade, in "Analytical Applications of Lasers," Chapter 4, E.H. Piepmeier, Ed., Wiley Interscience, New York, NY (1986).

19. V.S. Letokhov, "Laser Selective Detection of Single Atoms" in C. Bradley-Moore, Ed., Chemical and Biochemical Applications of Lasers, Academic Press, New York, NY (1980).

20. V.I. Balykin, G.I. Bekov, V.S. Letokhov, and V.I. Mishin, Usp. Fiz. Nauk, 132, 293 (1980) [Sov. Phys. Usp., 23, 651 (1980)].

21. V.P. Zharov and V.S. Letokhov, "Laser Optoacoustic Spectoscopy," Springer-Verlag, Berlin, Heidelberg (1986).

22. J.C. Travis, G.C. Turk, J.R. DeVoe, P.K. Schenk, and C.A. van Dijk, Prog. Analyt. Atom. Spectrosc., 7, 199 (1984).

23. N. B. Zorov, Yu. Ya. Kuzyakov, and O.I. Matveev, Zh. Anal. Khim., 37, 520 (1982) [J. Anal. Chem. U.S.S.R., 37, 400 (1982)].

24. N. Omenetto, B.W. Smith, and L.P. Hart, Fresenius Z. Anal. Chem., 324, 683, (1986).

25. P. Camus (Ed.), "Optogalvanic Spectroscopy and Its Applications," J. Phys. 44, Coll C7, Suppl. 11 (1983).

26. I. Magnusson, Spectrochim. Acta, 43 B, 727, (1988).

27. V.S. Letokhov, "Laser Photoionization Spectroscopy," Academic Press, Orlando, FL (1987).

28. V.S. Letokhov, Scientific American, p. 54, Sept. (1988).

29. G.S. Hurst and M.G. Payne, Spectrochim. Acta, 43B, 715 (1988).

30. T.J. Whitaker, B.A. Bushaw, and B.D. Cannon, Laser Focus/Electro-Optics, 24, 88 February (1988).

31. B.A. Bushaw and G.K. Gerken, "Trace Isotopic Analysis by Double-Resonance Ionization with cw-lasers and Graphite Furnace Atomization," presented at 4th Int. Symp. RIS & Its Applications, Gaithersburg, Maryland, U.S.A., April 10-15 (1988).

32. N. Omenetto, Appl. Phys. B, 46, 209 (1988).

33. N.V. Bodrov, T.E. Dobrova, A.M. Nemets, S.V. Oshemkov, and A.A. Petrov, Zh. Prikl Spektrosk., 47, 563 (1987) [J. Appl. Spectrosc. U.S.S.R., 47, 996 (1987)].

34. H. Falk, H.J. Paetzold, K.P. Schmidt, and J. Tilch, Spectrochim. Acta, 43B, 1101 (1988).

35. M.A. Bolshov, A.V. Zybin, V.G. Koloshnikov, and I.I. Smirenkina, Spectrochim. Acta, 43B, 519 (1988).

36. J.P. Dougherty, F.R. Preli, Jr., and R.G. Michel, J. Anal. At. Spectrom., 2, 429 (1987).

37. R.W. Wood, Phil. Mag., 10, 513 (1905).

38. R.W. Wood, "Physical Optics," Dover Publications, New York, NY (1934).

39. A.C.G. Mitchell and M.W. Zemansky, "Resonance Radiation and Excited Atoms," Cambridge Univ. Press, London, UK (1971).

40. P. Pringsheim, "Fluorescence and Phosphorescence," Interscience, New York, NY (1949).

41. E.L. Nichols and H.L. Howes, Phys. Rev., 22, 425 (1923).

42. E.L. Nichols and H.L. Howes, Phys. Rev., 23, 472 (1924).

43. R.M. Badger, Z. Phys., 55, 56 (1929).

44. R. Mannkopff, Verhandl. d. Deutsch. Phys. Ges., 14, 16 (1933).

45. A.L. Boers, C. Th. J. Alkemade, and J.A. Smit, Physica, 22, 358 (1956).

46. C. Th. J. Alkemade, "Proceedings of the Xth Colloquium Spectroscopicum International," E.R. Lippincott, M. Margoshes, Eds., pp. 143-170, Spartan Books, Washington, DC (1963).

47. J.D. Winefordner and T.J. Vickers, Anal. Chem., 36, 161 (1964).

48. J.D. Winefordner and R.A. Staab, Anal. Chem., 36, 165 (1964).

49. J.D. Winefordner and R.A. Staab, Anal. Chem., 36, 1367 (1964).

50. J.D. Winefordner, S.G. Schulman, and T.C. O'Haver, "Luminescence Spectrometry in Analytical Chemistry," John Wiley, New York, NY (1973).

51. V. Sychra, V. Svoboda, and I. Rubeska, "Atomic Fluorescence Spectroscopy," Van Nostrand Reinhold Co., London (1975).

52. G.F. Kirkbright and M. Sargent, "Atomic Absorption and Fluorescence Spectroscopy," Academic Press, London, UK (1974).

53. J.D. Winefordner and J.M. Mansfield Jr., Appl. Spectrosc. Rev., 1, 1 (1967).

54. J.D. Winefordner and J.M. Mansfield in "Fluorescence," Chapter 13, G.G. Guilbault, Ed., Dekker, New York, NY (1967).

55. J.D. Winefordner, V. Svoboda, and L.J. Cline, CRC Crit. Rev. Anal. Chem., 1, 233 (1970).

56. A. Syty, in "Flame Emission and Atomic Absorption Spectrometry," Vol. 2, J.A. Dean and T.C. Rains, Eds., Chapter 8, pp. 197-233, Marcel Dekker, New York, NY (1971).

57. T.S. West and M.S. Cresser, Appl. Spectrosc. Rev., 7, 79 (1973).

58. J.D. Winefordner, Rec. Chem. Prog., 29, 24 (1968).

59. M.S. Cresser and P.N. Keliher, Caribbean J. Sci. Math., 2, 1 (1972).

60. G.F. Kirkbright and T.S. West, Chem. Brit., 8, 428 (1972).

61. T.S. West, Analyst, 99, 886 (1974).

62. R.F. Browner, Analyst, 99, 617 (1974).

63. N. Omenetto and J.D. Winefordner, Prog. Analyt. Atom. Spectrosc., 2, 1 (1979).

64. J.D. Winefordner and R.C. Elser, Anal. Chem., 43(4), 24A (1971).

65. J.D. Winefordner, Accounts Chem. Res., 4, 259 (1971).

66. J.D. Winefordner, J. Chem. Ed., 55, 72 (1978).

67. J.D. Windfordner, Chemtech, p. 123, February (1975).

68. D.J. Butcher, J.P. Dougherty, J.T. McCaffrey, F.R. Preli, Jr., A.P. Walton, and R.G. Michel, Prog. Analyt. Spectrosc., 10, 359 (1987).

69. J.D. Winefordner, in "Recent Advances in Analytical Spectroscopy," K. Fuwa, Ed., pp. 151-164, Pergamon Press, Oxford, UK (1982).

70. B.V. L'Vov, "Atomic Absorption Spectrochemical Analysis," Hilger, London, UK (1970).

71. E.H. Piepmeier, in "Analytical Laser Spectroscopy," N. Omenetto, Ed., Chapter 3, pp. 119-166, Wiley, New York, NY (1979).

72. C. Th. Alkemade, Tj. Hollander, W. Snelleman, and P.J. Th. Zeegers, "Metal Vapours in Flames," Pergamon Press, Oxford, UK (1982).

73. N. Omenetto and J.D. Winefordner, Appl. Spectrosc., 26, 555 (1972).

74. C. Th. J. Alkemade and P.J. Th. Zeegers in "Spectrochemical Methods of Analysis," J.D. Winefordner, Ed., Chapter 1, pp. 3-125, John Wiley, New York, NY (1971).

75. E.H. Piepmeier, Spectrochim. Acta, 27B, 431 (1972).

76. E.H. Piepmeier, Spectrochim. Acta, 27B, 445 (1972).

77. B.A. Lengyel, "Introduction to Laser Physics," John Wiley, New York, NY (1966).

78. C.A. Sacchi and O. Svelto, in "Analytical Laser Spectroscopy," N. Omenetto, Ed., Chapter 1, pp. 1-46, John Wiley, New York, NY (1979).

79. O. Svelto, "Principles of Lasers," Plenum Press, New York, NY (1982).

80. W. Demtröder, "Laser Spectroscopy," Springer Verlag, Berlin (1982).

81. A.E. Siegman, "Lasers," Univ. Sci. Books, Mill Valley, CA, U.S.A. (1986).

82. R.L. Byer and R.L. Herbst, Laser-Focus, 14, 48, July (1978).

83. C.K. Rhodes, Ed., "Excimer Lasers, Topics in Applied Physics," Vol. 30, Springer-Verlag, Berlin, Heidelberg (1979).

84. F.P. Schafer, Ed., "Dye Lasers," Topic in Applied Physics, Vol. 1, Springer-Verlag, Berlin, Heidelberg (1973).

85. T.F. Johnson, Jr. "Tunable Dye Lasers" in "Encyclopedia of Phys. Sci. and Technol," Vol. 14, pp. 96-141, Academic Press, Orlando, FL (1987).

86. G.K. Klauminzer, Technical Note No. 8, Questek Inc., Billerica, MA, U.S.A. (1987).

87. F.J. Duarte, Lasers & Optronics, 7, 41, February (1988).

88. D.R. Crosley, Ed., "Laser Probes for Combustion Chemistry," ACS Symposium Series 134, American Chemical Society, Washington, DC (1980).

89. M.B. Denton and H.V. Malmstadt, Appl. Phys. Lett., 18, 485 (1971).

90. L.M. Fraser and J.D. Winefordner, Anal. Chem., 43, 1693 (1971).

91. L.M. Fraser and J.D. Winefordner, Anal. Chem., 44, 1444 (1972).

92. N. Omenetto, N.N. Hatch, L.M. Fraser, and J.D. Winefordner, Spectrochim. Acta, 28B, 65 (1973).

93. S.J. Weeks, H. Haraguchi, amd J.D. Winefordner, Anal. Chem., 50, 360 (1978).

94. J.A. Gelbwachs, C.F. Klein, and J.E. Wessel, Appl. Phys. Lett., 30, 489 (1977).

95. S. Neumann and M. Kriese, Spectrochim. Acta, 29B, 127 (1974).

96. J.P. Hohimer and P.J. Hargis, Jr., Appl. Phys. Lett., 30, 344 (1977).

97. M.A. Bolshov, A.V. Zybin, V.G. Koloshnivov, and M.V. Vasnetsov, Spectrochim. Acta, 36B, 345 (1981).

98. M.S. Epstein, S. Nikdel, J.D. Bradshaw, M.A. Kosinski, J.N. Bower, and J.D. Winefordner, Anal. Chim. Acta, 113, 221 (1980).

99. H. Uchida, M.A. Kosinki, and J.D. Winefordner, Spectrochim. Acta, 38B, 5 (1983).

100. N. Omenetto, H.G.C. Human, D. Cavalli, and G. Rossi, Spectrochim Acta, 39B, 115 (1984).

101. W.M. Fairbank, Jr., T.W. Haensch, and A.L. Schawlow, J. Opt. Soc. Am., 65, 199 (1975).

102. E. Miron, R. David, G. Erez, S. Lavi, and L.A. Levin, Appl. Phys. Lett., 35, 737 (1979).

103. M.A. Bolshov, A.V Zybin and I.I. Smirenkina, Spectrochim. Acta, 36B, 1143 (1981).

104. M.A. Bolshov, A.V. Zybin, L.N. Kolonina, I.A. Maiorov, I.I. Smirenkina, and O.A. Shiryaeva, Zh. Anal. Khim., 39, 320 (1984) [J. Anal. Chem. U.S.S.R., 39, 253 (1984)].

105. M.A. Bolshov, A.V. Zybin, V.G. Koloshnikov, I.I. Smirenkina, A.M. Artyushin, Yu. R. Kolomiiskii, Yu. M. Loginov, A.P. Osipov, S.G. Samokhavalov, and Yu. V. Frolov, Agrokhimiya, 22, 105 (1985) [CA 104: 17250v].

106. M.A. Bolshov, A.V. Zybin, V.G. Koloshnikov, I.A. Maiorov, and I.I. Smirenkina, Spectrochim. Acta, 41B, 487 (1986).

107. J. Tilch, H. Falk, H.J. Paetzold, P.G. Mon, and K.P. Schmidt, Colloq. Spectrosc. Internat. XXIV, Paper 067, Garmisch-Partenkirken, FRG, September (1985).

108. R. Konig, S. Mory, A. Rosenfeld, J. Tilch, and J. Lademann, Z. Chem., 22, 288 (1982).

109. F.R. Preli, Jr., J.P. Dougherty, and R.G. Michel, Spectrochim. Acta, 43B, 501 (1988).

110. F.R. Preli, Jr., J.P. Dougherty, and R.G. Michel, Anal. Chem., 59, 1784 (1987).

111. J.P. Dougherty, F.R. Preli, Jr., J.T. McCaffrey, M.D. Seltzer, and R.G. Michel, Anal. Chem., 59, 1112 (1987).

112. N. Omenetto, P. Cavalli, M. Broglia, P. Qi, and G. Rossi, J. Anal. At. Spectrosc., 3, 231 (1988).

113. M. Leong, J. Vera, B.W. Smith, N. Omenetto, and J.D. Winefordner, Anal. Chem., 60, 1605 (1988).

114. N. Omenetto and H.G.C. Human, Spectrochim. Acta, 39B, 1333 (1984).

115. H.G.C. Human, N. Omenetto, P. Cavalli, and G. Rossi, Spectrochim. Acta, 39B, 1345 (1984).

116. A. Walsh, Spectrochim. Acta, 7, 108 (1955).

117. C. Th. J. Alkemade and J.M.W. Milatz, J. Opt. Soc. Am., 45, 583 (1955).

118. C. Th. J. Alkemade and J.M.W. Milatz, Appl. Sci. Res., 4B, 289 (1955).

119. B.V. L'Vov, Inzh. Fiz. Zh., 2, 44 (1959) [English Translation, Spectrochim. Acta, 39B, 159 (1984)].

120. B.V. L'Vov, Spectrochim. Acta, 17, 761 (1961).

121. B.V. L'Vov, Spectrochim. Acta, 24B, 53 (1969).

122. B.V. L'Vov, Zh. Anal. Khim., 35, 1575 (1980) [J. Anal. Chem. U.S.S.R., 35, 1024 (1980)]

123. R.E. Sturgeon, Anal. Chem., 49, 1255A (1977).

124. B.V. L'Vov, Spectrochim. Acta, 33B, 153 (1978).

125. G. Lundgren, L. Lundmark, and G. Johansson, Anal. Chem., 46, 1028 (1974).

126. N.G. Zhou, W. Frech, and L. de Galan, Spectrochim. Acta, 39B, 225 (1984).

127. C.L. Chakrabarti, S. Wu, and P.C. Bertels, Spectrochim. Acta, 38B, 1041 (1983).

128. W. Huettner and C. Busche, Fresenius Z. Anal. Chem., 323, 674 (1986).

129. A.A. Brown and M. Lee, Fresenius Z. Anal. Chem., 323, 697 (1986).

130. G. Schlemmer and B. Welz, Fresenius Z. Anal. Chem., 323, 703 (1986).

131. S.R. Lawson, F.G. Dewalt, and R. Woodriff, Prog. Analyt. Atom. Spectrosc., 6, 1 (1983).

132. J.A. Holcombe and G.D. Rayson, Prog. Analyt. Atom Spectrosc., 6, 225 (1983).

133. W. Frech, N.G. Zhou, and E. Lundberg, Spectrochim. Acta, 37B, 691 (1982).

134. W. Frech, A.O. Lindberg, E. Lundberg, and A. Cedergren, Fresenius Z. Anal. Chem., 323, 716 (1986).

135. W. Pingxin and L. Tiezheng, Spectrochim. Acta, 41B, 1225 (1986).

136. R.E. Sturgeon, C.L. Chakrabarti, and C.H. Langford, Anal. Chem., 48, 1792 (1976).

137. M.K. Conley, J.J. Sotera, and H.L. Kahn, Instrumentation Laboratory, Aid Report No. 149, Wilmington, MA (1981).

138. N. Zhe-Ming and S. Xiao-Quan, Spectrochim. Acta, 42B, 937 (1987).

139. W. Frech, J.A. Persson, and A. Cedergren, Prog. Analyt. Atom. Spectrosc., 3, 279 (1980).

140. H. Falk, Spectrochim. Acta, 33B, 695 (1978).

141. B.V. L'Vov and V.G. Nikolaev, Zh. Prikl. Spectrosk. 46, 7 (1987) [J. Appl. Spectrosc. U.S.S.R., 46, 1 (1987)].

142. I.L. Grinshtein, L.A. Vasil'eva, and D.A. Katsov, Zh. Prikl. Spektrosk., 46, 13 (1987) [J. Appl. Spectrosc. U.S.S.R., 46, 6 (1987)].

143. B.V. L'Vov and G.N. Ryabchuk, Spectrochim. Acta, 37B, 673 (1982).

144. B.V. L'Vov, P.A. Bayunov, and G.N. Ryabchuk, Spectrochim. Acta, 36B, 397 (1981).

145. Wim M.G.T. van den Broek and L. de Galan, Anal. Chem., 49, 2176 (1977).

146. R. Woodriff, M. Marinkovic, R.A. Howald, and I. Eliezer, Anal. Chem., 49, 2008 (1977).

147. R.E. Sturgeon and C.L. Chakrabarti, Anal. Chem., 49, 1100 (1977).

148. J.D. Winefordner, in "Atomic Absorption Spectroscopy," R.M. Dagnall and G.F. Kirkbright, Eds., pp. 35-49, Butterworths, London, UK (1970).

149. A.G. Gaydon and H.G. Wolfhard, "Flames, Their Structure, Radiation and Temperature," 4th ed., Chapman and Hall, London, UK (1979).

150. M. Hoenig and R. Wollast, Spectrochim. Acta, 37B, 399 (1982).

151. H.J.T. Ellingham, J. Soc. Chem. Ind., 63, 125 (1944).

152. C.W. Fuller, Analyst, 99, 739 (1974).

153. H. Massmann, Spectrochim. Acta, 23B, 215 (1968).

154. T.S. West and X.K. Williams, Anal. Chim. Acta, 45, 27 (1969).

155. M.P. Bratzel, Jr., R.M. Dagnall, and J.D. Winefordner, Anal. Chim. Acta, 48, 197 (1969).

156. M.P. Bratzel, Jr., R.M. Dagnall, and J.D. Winefordner, Appl. Spectrosc., 24, 518 (1970).

157. M.D. Amos, P.A. Bennet, K.G. Brodie, P.W.Y. Lung, and J.P. Matousek, Anal. Chem., 43, 211 (1971).

158. J.P. Hohimer and P.J. Hargis, Jr., Anal. Chim. Acta, 97, 43 (1978).

159. M.A. Bolshov, A.V. Zybin, L.A. Zybina, V.G. Koloshnikov and I.A. Maiorov Spectrochim. Acta, 31B, 493 (1976).

160. M.A. Bolshov, A.V. Zybin, V.G. Koloshnikov, A.V. Pisarskii, and A.N. Smirnov, Zh. Prikl. Spektrosk., 28, 45 (1978) [J. Appl. Spectrosc. U.S.S.R., 28, 31 (1978)].

161. M.A. Bolshov, in "Laser Analytical Spectrochemistry," Chapter 2, V.S. Letokhov, Ed., pp. 52-97, Adam Hilger, Bristol, UK (1985).

162. K. Dittrich and H.J. Stark, J. Anal. At. Spectrom., 1, 237 (1986).

163. K. Dittrich and H.J. Stark, J. Anal. At. Spectrom., 2, 63 (1987).

164. D. Goforth and J.D. Winefordner, Talanta, 34, 290 (1987).

165. M.A. Bolshov, A.V. Zybin, Yu. R. Kolomiiskii, V.G. Koloshnikov, Yu M. Loginov, and I.I. Smirenkina, Zh. Anal. Khim., 41, 402 (1986). [J. Anal. Chem. U.S.S.R., 41, 313 (1986)].

166. M.A. Bolshov, S.A. Dashin, A.V. Zybin, V.G. Koloshnikov, M.A. Maiorov, and I.I. Smirenkina, Zh. Anal. Khim., 41, 1862 (1986) [J. Anal. Chem. U.S.S.R., 41, 1301 (1986)].

167. M.A. Bolshov, I.B. Gornushkin, Kh. I Zil'bershtein, A.V. Zybin, Yu. B. Kiselev, and I.I. Smirenkina, Zh. Anal. Khim., 42, 312 (1987) [J. Anal. Chem. U.S.S.R., 42, 253 (1987)].

168. M.A. Bolshov, A.B. Zybin, V.G. Koloshnikov, and I.I. Smirenkina, Acta Phys. Hung., 61, 119 (1987).

169. S.A. Dashin and I.A. Maiorov, Zavod. Lab., 53, 27 (1987) [Industrial Laboratory, 53, 1031 (1987)].

170. V.M. Apatin, B.V. Arkhangel'skii, M. A. Bolshov, V.V. Ermolov, V.G. Koloshnikov, O.N. Kompanetz, N.I. Kuznetzov, E.L. Mikhailov, V.S. Shishkovskii, and C.F. Boutron, submitted to Spectrochimica Acta B.

171. D. Goforth and J.D. Winefordner, Anal. Chem., 58, 2598 (1986).

172. J.P. Dougherty, J.A. Costello, and R.G. Michel, Anal. Chem., 60, 336 (1988).

173. J.W. Daily, Appl. Opt., 16, 568 (1977).

174. G.D. Boutilier, M.B. Blackburn, J.M. Mermet, S.J. Weeks, H. Haraguchi, J.D. Winefordner, and N. Omenetto, Appl. Opt., 17, 2291 (1978).

175. M.A. Bolshov, A.V. Zybin, V.G. Koloshnikov, and K.N. Koshelev, Spectrochim. Acta, 32B, 279 (1977).

176. D.R. Olivares and G.M. Hieftje, Spectrochim. Acta, 33B, 79 (1978).

177. G. Zizak, J.D. Bradshaw, and J.D. Winefordner, Appl. Opt., 19, 3631 (1980).

178. C.A. van Dijk, N. Omenetto, and J.D. Winefordner, Appl. Spectrosc., 35, 389 (1981).

179. N. Omenetto, C.A. van Dijk, and J.D. Winefordner, Spectrochim. Acta, 37B, 703 (1982).

180. K.G. Muller and M. Stania, J. Appl. Phys., 49, 5801 (1978).

181. M. Mailander, J. Appl. Phys., 49, 1256 (1978).

182. J.J. Deakin and D. Husain, J. Chem. Soc. Faraday Trans. II, 68, 1603 (1966).

183. C.H. Corliss and W.R. Bozman, "Experimental Transition Probabilities," NBS Monograph 53, Washington, DC (1962).

184. N. Omenetto and J.D. Winefordner, CRC Crit. Rev. Anal. Chem., 13, 59 (1981).

185. G.D. Boutilier, J.D. Bradshaw, S.J. Weeks, and J.D. Winefordner, Appl. Spectrosc., 31, 307 (1977).

186. O.I. Matveev, Zh. Prikl. Spektrosk., 39, 709 (1983) [J. Appl Spectrosc. U.S.S.R., 39, 1213, (1983)].

187. C. Th. J. Alkemade, Spectrochim. Acta, 40B, 1331 (1985).

188. H. Falk, CRC Crit. Rev. Anal. Chem., 19, 29 (1988).

189. H. Falk and J. Tilch, J. Anal. At. Spectrom., 2, 527 (1987).

190. B.V. L'Vov, V.G. Nikolaev, E.A. Norman, L.K. Polzik and M. Mojica, Spectrochim. Acta, 41B, 1043 (1986).

191. W. Slavin and G.R. Carnrick, Spectrochim. Acta, 39B, 271 (1984).

192. C.L. Chakrabarti, D. Ferrarotto, S.J. Cathum, and C.J. Rademeyer, Can. J. Chem., 65, 1079 (1987).

193. R.E. Sturgeon and S.S. Berman, Anal. Chem., 55, 190 (1983).

194. R.E. Drullinger, Optics Comm., 39, 263 (1981).

195. D. Goforth, Ph.D. thesis, University of Florida, Gainesville, FL (1986).

196. F.J. Fernandez and J. Iannarone, At. Absorpt. Newsl., 17, 117 (1978).

197. Quantel International, Santa Clara, CA (1985).

198. C.J. Molnar, R.D. Reeves, J.D. Winefordner, M.T. Glenn, J.R. Ahlstrom and J. Savory, Appl. Spectrosc., 26, 606, (1972).

199. "Analytical Methods For Carbon Rod Atomizers," Varian Instruments, Palo Alto, CA (1980).

200. B.W. Smith and M.L. Parsons, J. Chem. Ed., 50, 679 (1973).

201. J.A. Dean and T.C. Rains, in "Flame Emissions and Atomic Absorption Spectrometry," Vol. 2, J.A. Dean and T.C. Rains, Eds., Chapter 13, pp. 327-339, Marcel Dekker, New York, NY (1971).

202. R.F. Browner, R.M. Dagnall, and T.S. West, Anal. Chim. Acta, 50, 375 (1970).

203. V. Sychra and J. Matousek, Talanta, 17, 363 (1970).

204. R.E. Lee, Jr., and V. Duffield, in "Ultratrace Metal Analysis in Biological Sciences and Environment," T.H. Risby, Ed., Chapter 11, pp. 146-171, Am. Chem. Soc., Washington, DC (1979).

205. G.N. Biddle, J. Assoc. Off. Anal. Chem., 65, 947 (1982).

206. C. Boutron, Anal. Chim. Acta, 106, 127 (1979).

207. C. Boutron, M. Leclerc, and N. Risler, Atmospheric Environment, 18, 1947 (1984).

208. C.F. Boutron and C.C. Patterson, Geochim. Cosmochim. Acta, 47, 1355 (1983).

209. J. Volkening and K.G. Heumann, Fresenius Z. Anal. Chem., 331, 174 (1988).

210. C. Boutron and S. Martin, Anal. Chem., 51, 140 (1979).

211. H.M. Ortner, W. Birzer, B. Welz, G. Schlemmer, J.A. Curtius, W. Wegscheider, and V. Sychra, Fresenius Z. Anal. Chem., 323, 681 (1986).

212. W. Slavin, Trends. Anal. Chem., 6, 194 (1987).

213. S. R. Koirtyohann and M.L. Kaiser, Anal. Chem., 54, 1515A, (1982).

214. S.R. Koirtyohann, Anal. Chem., 52, 736A (1980).

215. J.D. Bradshaw and D.D. Davis, Opt. Lett., 7, 224 (1982).

216. J.D. Bradshaw, M.O. Rodgers, and D.D. Davis, Appl. Opt., 21, 2493 (1982).

217. R. Alvarez, S.D. Rasberry and G.A. Uriano, Anal. Chem., 54, 1226A (1982).

218. Standard Reference Material 1643b, "Trace Elements in Water," Department of Commerce, National Bureau of Standards, Washington, DC.

219. R.K. Skogerboe, J. Assoc. Off. Anal. Chem., 65, 957 (1982).

220. T.J. Murphy, in "Accuracy in Trace Analysis", Vol. 1, P. LaFleur, Ed., National Bureau of Standards Special Publication No. 422, U.S. Department of Commerce, Washington, DC, pp. 509-537 (1976).

221. L. Dunkelman, W.B. Fowler and J. Hennes, Appl. Opt., 1, 695, (1962).

222. P.L. Larkins, R.M. Lowe, J.V. Sullivan, and A. Walsh, Spectrochim. Acta, 24B, 187 (1969).

223. P.L. Larkins, Spectrochim. Acta, 26B, 477 (1971).

224. P.L. Larkins and J.B. Willis, Spectrochim. Acta, 26B, 491 (1971).

225. K. Braun, W. Slavin, and A. Walsh, Spectrochim. Acta, 37B, 721 (1982).

226. H. Bubert, Spectrochim. Acta, 39B, 1377 (1984).

227. M.L. Wright, in "Feasibility Study of In-Situ Source Monitoring of Particulate Composition by Raman or Fluorescence Scatter," Environmental Protection Agency, Report No. EPA-R2-73-219, Washington, DC (1973).

228. A.W. Miziolek and R.J. Willis, Opt. Lett., 6, 528 (1981).

229. J.F. James and R.S. Sternberg, "The Design of Optical Spectrometers," p. 174, Chapman and Hall, London, UK (1969).

230. E. Adriaenssens and P. Knoop, Anal. Chim. Acta, 68, 37 (1973).

231. A.N. Savel'eva and N.P. Khairulina, Zh. Anal. Khim., 33, 1380 (1978) [J. Anal. Chem. U. S. S. R., 33, 1081 (1978)].

232. W.B. Rowston and J.M. Ottaway, Analyst, 104, 645 (1979).

233. K. Brajter, K. Slonawska, and Z. Vorbrodt, Chem. Anal., 27, 239 (1982).

234. V.I. Balykin, V.S. Letokhov, V.I. Mishin, and V.A. Semchishen, JETP Lett., 26, 357 (1977).

235. D.A. Lewis, J.F. Tonn, S.L. Kaufman, and G.W. Greenlees, Phys. Rev. A, 19, 1580 (1979).

236. R.A. Keller and J.J. Snyder, Laser Focus/Electro-Optics, 22, 86, March (1986).

237. B.A. Bushaw, T.J. Whitaker, B.D. Cannon, and R.A. Warner, J. Opt. Soc. Am. B, 2, 1547 (1985).

238. C.Y. She and W.M. Fairbank, Jr., in "Laser-Based Ultrasensitive Spectroscopy and Detection V", pp. 49-54, R.A. Keller, Ed., SPIE, Bellingham, WA (1983).

239. H. Kaiser, Anal. Chem., 42, No. 2, 24A (1970).

240. H. Kaiser, Anal. Chem., 42, No. 4, 26A (1970).

241. H. Kaiser, Pure & Appl. Chem., 34, 35 (1973).

242. M.L. Parsons, J. Chem. Ed., 46, 290 (1969).

243. G.L. Long and J.D. Winefordner, Anal. Chem., 55, 712A (1983).

244. M.S. Epstein, in "Detection in Analytical Chemistry," L.A. Currie, Ed., Chapter 6, pp. 109-125, Am. Chem. Soc., Washington, DC (1988).

245. J. Reader, C.H. Corliss, W.L. Wiese, and G.A. Martin: "Wavelength and Transition Probabilities for Atoms and Atomic Ions," NSRDS-NBS 68, Washington, DC (1980).

246. M.A. Bolshov, A.V. Zybin, and V.G. Koloshnikov, Sov. J. Quantum. Electron., 10, 1042 (1980).

247. J.C. Wright in "Applications of Lasers to Chemical Problems," T.R. Evans, Ed., Chapter 2, pp. 35-179, John Wiley, New York, NY (1982).

248. G.I. Bekov and V.S. Letokhov, in "Laser Analytical Spectrochemistry," V.S. Letokhov, Ed., Chapter 3, pp. 98-151, Adam Hilger, Bristol, UK (1985).

249. J.A. Vera, C. Stevenson, G. Petrucci, N. Omenetto, and J.D. Winefordner, in preparation.

BIOGRAPHICAL SKETCH

Jorge A. Vera was born in Ponce, Puerto Rico, on October 11, 1956. In May, 1974, he graduated from Escuela Superior Trina Padilla de Sanz in Arecibo, P. R. In May, 1981, he graduated from the Catholic University of P. R. in Ponce, P. R., with a Bachelor of Science degree in chemistry. In August, 1982, he entered the Graduate School at the University of Florida in Gainesville, Florida.

He is a member of the Optical Society of America and the Society for Applied Spectroscopy.

I certify that I have read this study and that in my opinion it conforms to acceptable standards of scholarly presentation and is fully adequate, in scope and quality, as a dissertation for the degree of Doctor of Philosophy.

James D. Winefordner, Chairman
Graduate Research Professor of
Chemistry

I certify that I have read this study and that in my opinion it conforms to acceptable standards of scholarly presentation and is fully adequate, in scope and quality, as a dissertation for the degree of Doctor of Philosophy.

Gerhard M. Schmid
Associate Professor of
Chemistry

I certify that I have read this study and that in my opinion it conforms to acceptable standards of scholarly presentation and is fully adequate, in scope and quality, as a dissertation for the degree of Doctor of Philosophy.

Richard A. Yost
Associate Professor of
Chemistry

I certify that I have read this study and that in my opinion it conforms to acceptable standards of scholarly presentation and is fully adequate, in scope and quality, as a dissertation for the degree of Doctor of Philosophy.

A. Brajter-Toth

Anna F. Brajter-Toth
Associate Professor of
Chemistry

I certify that I have read this study and that in my opinion it conforms to acceptable standards of scholarly presentation and is fully adequate, in scope and quality, as a dissertation for the degree of Doctor of Philosophy.

Alex E. Green

Alex E. Green
Graduate Research Professor of
Astronomy

This dissertation was submitted to the Graduate Faculty of the Department of Chemistry in the College of Liberal Arts and Sciences and to the Graduate School and was accepted as partial fulfillment of the requirements for the degree of Doctor of Philosophy.

May, 1989

Dean, Graduate School